COUPLED MODELING OF DYNAMIC RESERVOIR/WELL INTERACTIONS UNDER LIQUID-LOADING CONDITIONS

A Dissertation

by

AKKHARACHAI LIMPASURAT

Submitted to the Office of Graduate and Professional Studies of
Texas A&M University
in partial fulfillment of the requirements for the degree of

DOCTOR OF PHILOSOPHY

Chair of Committee,	Peter P. Valko
Co-Chair of Committee,	Gioia Falcone
Committee Members,	Catalin Teodoriu
	Maria A. Barrufet
Head of Department,	Dan Hill

December 2013

Major Subject: Petroleum Engineering

ABSTRACT

Liquid loading in a gas well occurs when the upward gas flow rate is insufficient to lift the coproduced liquid to the surface, which results in an accumulation of liquid at the bottom of the well. The liquid column in the tubing creates backpressure on the formation, which decreases the gas production rate and may stop the well from flowing. To model these phenomena, the dynamic interaction between the reservoir and the wellbore must be characterized. Due to wellbore phase re-distribution and potential phase-reinjection into the reservoir, the boundary conditions must be able to handle changing flow direction through the connections between the two subsystems.

This study presents a new formulation of the wellbore boundary condition used in reservoir simulators. The boundary condition uses the new state variable, the multiphase zero flow pressure (*MPZFP,* p^0), to determine flow direction in the connection grid block. If the wellbore pressure is less than the p^0, the connection is producing; otherwise, it is injecting. The volumetric proportion of the flow is always determined by the upstream side.

The new reservoir simulator is used in coupled modeling associated with liquid loading phenomena. The metastable condition can be modeled in a simple manner without any limiting assumptions and numerical stability problems.

We also applied this simulator for history matching of a gas well flowing with an intermittent production strategy. A basic transient wellbore model was developed for this

purpose. The long-term tubinghead pressure (THP) history can be traced by our coupled simulation.

Our modeling examples indicated that, the new wellbore boundary condition is suitable in modeling the dynamic interactions between reservoir and wellbore subsystems during liquid loading. The flow direction through the connection grid block can be automatically detected by our boundary condition without numerical difficulty during the course of the simulation. In addition, the capillary pressure can be accounted at the connection grid blocks when applying our new formulation in the reservoir simulator.

DEDICATION

To my parents.

ACKNOWLEDGEMENTS

My sincere gratitude goes to my advisor, Dr. Peter P. Valko, who provided continuous support and rightful advice for my research. His enthusiasm and broad knowledge on this aspect have brought me forward throughout the last year of my study. His contributions to this project have made my research life very enjoyable and rewarding.

I also would like to thank my co-advisor, Dr. Gioia Falcone, for her continuous support throughout my graduate program. I am greatly indebted for her persuasion to pursue my PhD degree, which has brought me great opportunities to learn and develop myself both academically and intellectually. The achievement in my research would not be possible without her effortless advice and generous help.

I thank Dr. Catalin Teodoriu and Dr. Maria A. Barrufet for helping in evaluation of this work as committee members.

Last but not the least, I would like to thank all of my friends in College Station for bringing me happiness during my time at Texas A&M.

NOMENCLATURE

A	Interface area, wellbore area, ft
B	Formation volume factor, res-bbl/Stb, res-bbl/Scf
d	Diameter, ft
f	Settled water fraction, dimensionless
F	Inter-block flow rate, Stb/d, Scf/d
g	Gravitational constant, 32.17 lb_m-ft/lb_f-s^2
h	Height, ft
k	Permeability, mD
m	Phase mass in wellbore, lb_m
M	Accumulation term, gas molecular weight
P	Pressure, psia
PI	Productivity index, mD-m
q	Sink/source rate, Stb/d, Scf/d
r	Radius, ft
R	Residual term; gas constant, 10.732 ft^3-psi/(R-lb_mmol)
S	Phase saturation, dimensionless
t	Time, day
V	Volume, ft^3
X	Primary variables
z	Gas compressibility factor, dimensionless

α	Scaling parameter, dimensionless
β	Transmissivity conversion factor to field unit, 1.127E-3
μ	Viscosity, cP
ρ	Density, lb_m/ft^3
ϕ	Porosity, dimensionless

Subscripts

ave	Average
c	Capillary; critical
eq	Equivalent
F	Frictional term
g	Gas
H	Horizontal
n,m	Grid-block number
p	Iteration step
r	Relative
T	Total
TH	Tubing head
W	Water
wf	Well flowing
β	Fluid phase

Superscripts

k	Time step

TABLE OF CONTENTS

Page

Page

LIST OF FIGURES

Page

Page

Page

Page

Page

LIST OF TABLES

CHAPTER I

INTRODUCTION

Problem Statement

Most gas wells producing some liquid experience challenges in production losses due to liquid loading, which occurs when the gas rate is insufficient to carry coproduced liquid to the surface. Some liquids will flow counter-current to the gas and accumulate in the bottom of the well, creating backpressure on the formation. This results in a sharp reduction in the gas production rate, and in the worst case, the well ceases flowing.

Liquid loading phenomena are believed to be initiated inside the wellbore when the liquid film at the tube wall flows downward. The accumulation of the liquid at the bottom of the well increases the backpressure at the near-wellbore region. Reinjection of the liquid can take place if an immediate bottomhole pressure is greater than the reservoir pressure in the near-wellbore region. If the reservoir pressure from the far region is able to replenish flow to the wellbore, gas and water can push some of the reinjected water back to the wellbore.

Another possible situation is that, at the lower part of the well, which has more pressure than the upper one, the liquid is reinjected into the reservoir while the gas and water are still flowing at the upper part of the reservoir during the liquid loading. All of these are transient behaviors that typically occur in liquid loading wells, which make modeling of the liquid loading problem complex.

The petroleum industry has recognized the importance of the liquid loading problem in gas wells and paid attention to various alleviating techniques for years. These include velocity string installation, plunger lifts, foam injections, downhole pump, etc. Since each of the remedial options has its own technical characteristics, their applicability varies depending on the characteristics and the conditions of the well.

Although remedial measures exist, the predictive tools for this particular problem are still not reliable. The existing industry efforts have been made to predict flowing conditions that remain out of the liquid loading regime, using the so-called “Turner’s criteria." This is the first step toward modeling of the rich group of transient flow conditions both in the reservoir and in the wellbore.

The complexity of developing a good model for predicting the liquid loading phenomena is mainly due to the dynamic interaction between the two subsystems. Both submodels must be able to capture transient flow conditions involved during the liquid loading on their own. In addition, the integrating model should allow implicit coupling.

The well model should be able to describe multiphase flow along the tubing during liquid loading. In essence, it must account for phase redistribution resulted in variations of phase composition at shared interfaces.

The near-well reservoir model must be able to identify flow directions and its associated phase flow rates as a result of immediate pressure differences between the two subsystems. These changes in flow directions can happen as frequently as minutes or months. In addition, the reservoir model must be able to couple and simulate without numerical stability during the course of the simulation. Most numerical difficulty in the

reservoir model happens at the grid block locating a connection between the reservoir and the wellbore. Thus, this requires a special attention in formulating the wellbore boundary condition, particularly in the liquid loading problems

At present, the models used to predict and diagnose the liquid loading problem are based on steady-state analysis, thus overlooking the transient feature particular to liquid loading. Several researchers have put efforts into modeling this problem to link the well dynamics to the well. However, even when the transient multiphase well model is used, the reservoir model is simply characterized by the steady-state IPR . Consequently, the transient phenomena during liquid loading may be lost and some observations may be difficult to simulate.

This study addresses the importance of formulation of the wellbore boundary conditions in the reservoir simulation. The new boundary condition is suitable for the coupled modeling between the reservoir and the wellbore model as it can automatically predict the flow direction at the wellbore boundary. This particular feature is an important requirement in modeling the complex phenomena in the liquid loading problem.

In fact this work is a part of the Joint Industry Project (JIP) on “Liquid Loading in the Operation of Gas Fields: Mechanisms, Prediction and Reservoir Response.” This project addresses the industry problem in a broader aspect, both theoretically and practically. The project concerning the impact of liquid loading both in the wellbore and the near-well region has been in progress since 2009.

Within the framework of this JIP, Zhang et al. (2009) developed a near-wellbore reservoir simulator to identify U-shaped pressure curves in the near-wellbore region caused by the liquid reinjection. They indicated that the traditional Inflow Performance Relationship describing the flow from the reservoir is not appropriate to capture this phenomenon and suggested to use the numerical approach instead.

Fernandez et al. (2010) presented a design of a flow loop attached to the porous medium to experimentally mimic liquid loading conditions in the integrated wellbore/reservoir system.

Waltrich et al. (2011) built this flow loop facility and performed a validation on transient wellbore simulators against the experimental investigation. They identified limitations in those simulators for evaluating liquid loading phenomena. Those limitations were related to transitions between flow regimes and liquid holdup modeling.

Alves et al. (2012) developed a numerical model addressing the flow pattern transition between churn and annular flow regimes.

In this study, we developed a new version a reservoir simulator that further investigates transient flow conditions in the near-wellbore region. We proposed a new wellbore boundary condition that is suitable for modeling back flow and related phenomena. It can be applied to determine crossflow of the liquid phase during liquid loading. In addition, the new reservoir model enables integrated reservoir/wellbore modeling to understand the system behavior under the liquid loading phenomena.

Objectives

The objectives of this study are summarized as follows:

1. Develop a numerical reservoir model that is capable of simulating two phase (gas and water), two- dimensional (radial/vertical directions), isothermal systems. This reservoir model will be used for modeling the onset of liquid loading phenomena.
2. Formulate the wellbore boundary conditions that are capable of predicting backflow situations during the liquid load-up in the wellbore.
3. Validate and identify differences in simulation results against a commercial reservoir package.
4. Model dynamic interaction between the reservoir and the wellbore under liquid loading conditions.
5. Validate experimental results on the investigation of a U-shaped pressure profile in the gas system.

Importance

To characterize transient flow behaviors during liquid loading, it is important to model dynamic interaction in the reservoir and the wellbore. Most existing integrated modeling tends to analyze this problem based on steady-state analysis. Even when the transient multiphase wellbore models are used, the problem is still incorrectly defined because a steady-state inflow performance relationship (IPR) is used to characterize the

reservoir, which involves the wrong boundary condition between the well and the reservoir.

The wellbore boundary condition plays an important role in integrated reservoir/wellbore modeling. For the liquid loading problem, the boundary condition must be formulated in such a way that it can predict backflow at the interface between the reservoir and the wellbore, depending on the pressure differences of the two subsystems. Moreover, the effect of capillary pressure should be incorporated in the flow across the boundary without causing numerical instability issues. Most commercial software ignores the capillary effect at the well block in order to accommodate robustness in the simulation.

Although the prediction of onset of the liquid loading is expected to rely on Turner's critical criteria with some modification, the modeling of dynamic interaction between the reservoir and the wellbore will help operators understand the system behavior during liquid loading and know how to design the production system more realistically to extend the life of the gas well.

Structure of the Dissertation

Chapter II gives details of existing modeling approaches in predicting the onset of the liquid loading problem. It also discusses attempts in integrated reservoir/wellbore modeling to analyze production behavior under the liquid loading effect. None of them have mentioned the wellbore boundary conditions appropriate for this problem. In

addition, this chapter provides a literature search of wellbore boundary modeling for some specific problems, which we can apply in the area of liquid loading problems.

Chapter III describes the numerical formulation for our reservoir simulation. Moreover, the formulation of the wellbore boundary condition for modeling liquid loading phenomena is presented.

Chapter IV presents the comparison of the reservoir simulation results against that generated from the model previously developed by Zhang et al. (2009). The result comparison of the well block indicates that numerical errors in the solution are propagated by using Zhang et al. model while the numerical issues are not observed when using our numerical simulation. Moreover, the validation of the simulation results against commercial software, ECLIPSE, shows the difference when predicting the backflow situation. Our simulation can predict switching back and forth in flow directions, thanks to the wellbore boundary condition, while ECLIPSE cannot identify that behavior, which is important in modeling the liquid loading. In addition, we show the simulation results in the near-wellbore region under the imposed oscillating bottomhole pressure. Those simulation results indicate the U-shaped pressure profiles during the liquid reinjection, similar to what was addressed by Zhang et al. (2009). Lastly, we show the use of our numerical simulation to validate the experimental investigation on the U-shaped pressure profiles in the near-wellbore region. The differences between numerical and experimental solutions were used to adjust experimental setup to obtain and analyze transient flow in the near-wellbore region more rigorously.

Chapter V gives the analysis of the metastable flow condition, which is the common production behavior effect of liquid loading. The modeling of the metastable flow condition is associated with dynamic interaction between the reservoir and the wellbore model. Dousi et al. (2006) proposed a modeling approach for this particular problem using the steady-state IPR as the reservoir model and the empirical wellbore model. We show that our reservoir simulation can substitute the IPR model, giving some insights about the near-wellbore region in the metastable regimes.

Chapter VI presents an integrated reservoir/wellbore modeling approach for history matching the wellhead performance history of a liquid-loaded gas well. This gas well has been experiencing the usual symptoms of liquid loading from the start. The strategy of intermittent production cycles has been implemented to recover gas production for over 25 years. We applied our reservoir simulation together with our developed wellbore model to reproduce the main characteristics of the tubinghead pressure history, which identified how the reservoir and the well interact during repetitive production cycles.

Chapter VII gives a summary of the conclusions from this work and suggests future works toward understanding liquid loading phenomena.

CHAPTER II

LITERATURE REVIEW

Introduction

During the life of gas wells, there is a stage where the gas flow rate is insufficient to carry coproduced liquid to the surface. Once this condition is reached, some fraction of the produced liquid will flow counter-current to the gas and accumulate in the bottom of the well. As liquid accumulates, it increases backpressure on the formation. Some accumulated liquid can re-enter the near-wellbore region, depending on the pressure difference at the connection interface (perforations). The increase in backpressure results in reduction of the gas production rate, and in some cases, it kills the well. This is a typical liquid loading problem.

The liquid loading problem often occurs at later life of the gas wells, where the reservoir pressure decreases, as well as at the early life of the gas wells with high liquid/gas ratios. The sources of liquid in the wellbore can be from condensation of water vapor along the well, drop-out condensate in the near-wellbore region, or connate formation water and ingress of water influx from aquifers into the well as pressure and temperature decrease. Mostly liquid water originates from condensed water vapor; however, in some gas wells, inflow of formation water may be more significant (Veeken et al. 2009).

Diagnosing the liquid loading problem is complex because its phenomena include flow instabilities in the well, and are further affected by flow instabilities in the

near-wellbore region. Thus, to model the liquid loading problem, it is necessary to understand how the multiphase flow in the well and the multiphase flow in the reservoir dynamically interact with each other.

A number of industry efforts have been made to predict the flowing conditions such that the well remains out of the liquid loading regime, using the so-called "Turner's criteria." These criteria are usually used by operators to design the production system to ensure that the well can flow at gas rates capable of removing liquid out of the well. However, they cannot be used to capture the transient features, such as wellbore phase redistribution and phase reinjection into the reservoir, which typically occur in the liquid loading regime.

To characterize mechanisms behind the liquid loading phenomena, it is important to understand the flow regime (patterns) in the well, which describes how multiphase fluid interact to each other, according to forces acting at the interior of each phase and at the interfaces of the multiphase fluid. The flow regimes are typically classified by the phase composition of the multiphase flow. **Fig. 2.1** depicts the flow regime map developed by Hewitt and Roberts (1969).

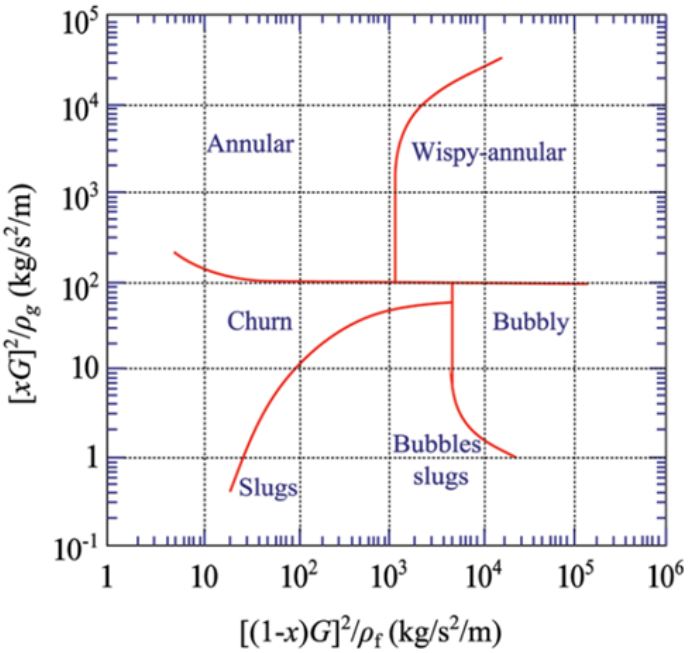

Fig. 2.1 – Flow regime map by Hewitt and Roberts (1969)

In the early life of the gas well, the annular flow or wispy annular flow is typically experienced during normal operations. Liquids can be transported as a film along the walls of the tubing, but also be entrained in the main gas flow in the form of droplets. **Fig. 2.2** presents the distribution of liquid forms in the annular flow.

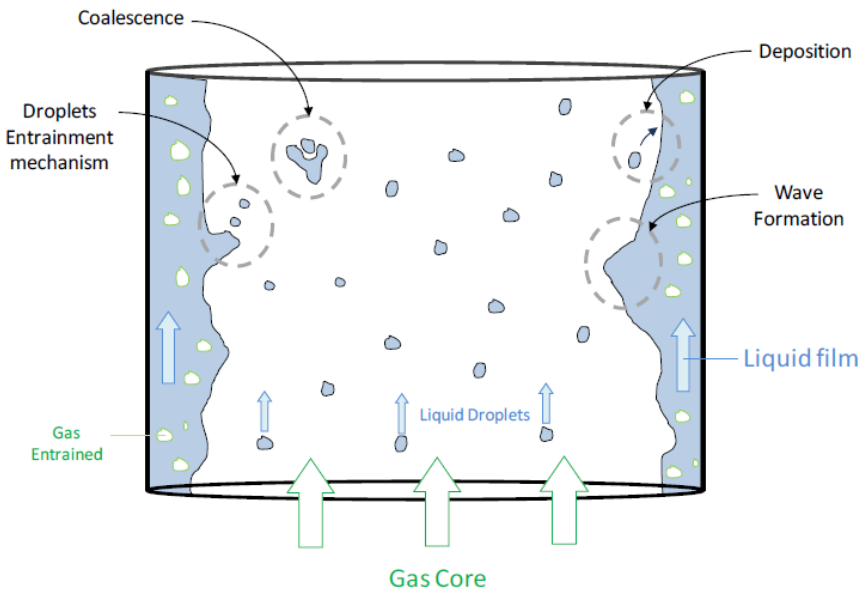

Fig. 2.2 – Schematic representation of liquid forms distribution in the annular flow (Waltrich, 2012)

As the gas velocity decrease, the ability of the gas to transport the liquid film reduces. It starts to thicken. The inner parts closed to the tubing wall starts to flow downward, while the droplets are still produced upward. This is defined as the onset of liquid loading. In the recent studies, it was proven that the annular flow is transitioning into churn flow at this moment (Westende et al., 2007; Schiferli et al., 2010; Yusuf et al., 2010; Waltrich, et al., 2011; Daas and Golczynski, 2012). Although some part of liquid films are flowing downward, the inner part is still forced upward by the gas core. As the gas velocity decreases even more, it reduced the ability of the gas core to drag the liquid film upward. This process continues until the net flow is downward and the well completely dies.

At the late life of the gas wells, the liquid loading is nearly inevitable. The depletion in the reservoir pressure, causing a decrease in the gas velocity, increases chances of a liquid column accumulating at the bottom of the well. The increase in backpressure on the formation can cause reinjection of the liquid to the reservoir or stack to reduce the gas rates even more. As a consequence, the well is unable to flow and requires more frequent shut-ins to build up reservoir pressure. The heavier phase (liquid) is accumulated at the bottom of the well and completely segregated from the lighter phase (gas) because of the gravitational force. Some liquids may be reinjected into the reservoir and worsen the gas mobility around the wellbore (J. Wang, 2012).

To prevent and alleviate the liquid loading problem, it is important to have a better understanding of when and how liquid loading occurs. In essence, this understanding requires accurate predictions of the critical gas flow rates and its associated phenomena.

In the following, we discuss industry efforts in modeling liquid loading problems to address the complexity in multiphase flow in the well. In addition, we present dynamic wellbore/reservoir models used in the liquid loading problems. None of those has addressed the importance of wellbore boundary conditions suitable for this particular problem. We discuss the general approach in modeling the wellbore boundary condition embedded in most commercial software. Then we introduce some existing alternative methods of the wellbore boundary condition which can be adapted for modeling in our specific simulator.

Prediction of the Onset of the Liquid Loading Problem

In the field, typical symptoms that indicate the well is undergoing liquid loading include erratic production and increase in decline rate, tubing pressure decreasing as casing pressure increases, annular heading, cessation of liquid production, and presence of loading recorded through pressure spikes at the gas measuring device (Lea et al., 2003). **Fig. 2.3** shows a plot of well performance data indicating the occurrence of liquid loading.

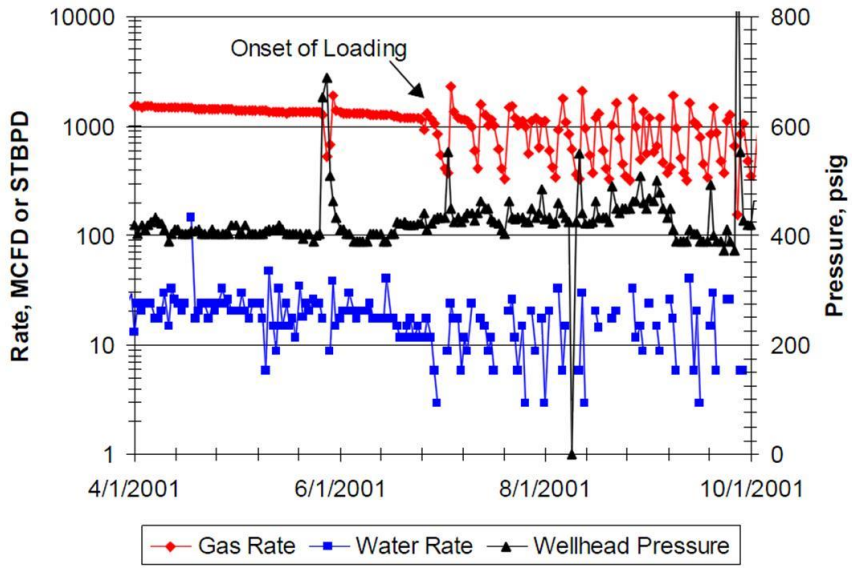

Fig. 2.3 – Well performance data indicates liquid loading (Sutton et al., 2003)

Many remedial techniques have been developed to alleviate liquid loading problems. Velocity strings, plunger lifts, and foam injections can be applied relying on natural energy of the system. Downhole pumps and gas lift provide extra energy to the

system (Dunham et al. 2008). Oyewole and Lea (2008) provides comprehensive comparisons of advantages and disadvantages of remedial techniques to remove liquids from the liquid loaded gas wells. In general, these techniques should be applied before the problem becomes too severe.

An intermittent production strategy can also alleviate the liquid loading problem (Whitson et al. 2012). It can be achieved by ensuring that the gas wells are produced above the liquid loading criteria of their own field production history. Once the liquid loading rates are reached, the wells must be shut-in for a short period, letting the near-well regions build up pressure. The production/shut-in cycle continues until the well can no longer produce at an economic rate.

Industry efforts have emphasized the models to predict the onset of the liquid loading problem in order to guarantee the stable operating conditions and to be far from those liquid loading regimes.

The most notable model was developed by Turner et al. (1969). Their model is based on the force balances in the largest droplet entrained in the gas core, which determine the drag force exerted by the gas core and the buoyancy force on the droplet (**Fig. 2.4**). From this force balance, Turner et al. were able to calculate minimum gas velocity required to ensure suspension of liquid droplets in the gas core. The equation to calculate "Turner's velocity" in oilfield units is expressed as:

$$v_c = 1.8949 \left[\frac{\sigma(\rho_l - \rho_g)}{\rho_g^2}\right]^{0.25} \quad (2.1)$$

where v_c is Turner velocity in ft/s, σ is interfacial tension in dynes/cm, ρ_l is liquid density in lbm/ft^3, and ρ_g is gas density in lbm/ft^3.

The coefficient in **Eq. 2.1** was already increased to 20% of its original value to match their database. This increase can be viewed as a safety factor to ensure the well is unloaded. Turner et al. suggested evaluating the velocity using fluid properties at the wellhead condition. The Turner et al. model has been widely used to predict the critical gas rate in the fields because the fluid properties at the wellhead conditions can be easily evaluated.

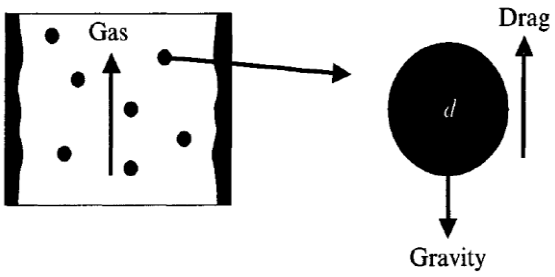

Fig. 2.4 – Liquid droplet transported in a vertical gas stream (Lea et al., 2003).

Coleman et al. (1991) suggested that the 20% adjustment in the Turner et al. equation was not required in their field data. They also pointed out that gas gravity, interfacial tension, and temperature have little impact on the accuracy of the Turner's rate calculation, whereas the wellbore diameter and pressure have more impact.

Guo et al. (2006) revisited the droplet model proposed by Turner et al. (1969). They proposed a kinetic-based method to determine the minimum velocity, which is higher than that predicted by Turner et al model. They also indicated that the conditions at the bottomhole control transport of droplets up the well, contradicting what Turner et al. suggested.

Zhou and Yaun (2009) revised Turner's droplet model to account for liquid droplet coalescence in the gas core. They pointed out that the liquid droplet concentration controls the chances of droplet coalescences along the tubing. The liquid holdup can be applied to represent the liquid droplet concentration in the gas well. Thus, they proposed the new correlation as:

$$v_{c,N} = v_{c,T} + \ln\frac{H_l}{\beta} + \alpha \tag{2.2}$$

where $v_{c,N}$ is critical velocity from the Zhou and Yaun model; $v_{c,T}$ is critical velocity from the Turner et al. model; H_l is the liquid holdup; β and α are threshold values for liquid droplet concentration. According to Zhou and Yaun, $\alpha = 0.6$ and $\beta = 0.01$ if evaluated using the data set from Turner et al. (1969).

Zhou and Yaun stated that if the liquid holdup is equal or less than β, the critical velocity is equal to what predicted by the Turner et al. model; otherwise, the new model is applied.

Westende et al. (2007) studied liquid transport under churn and annular flow regimes in a vertical tube. They did not observe the droplet flow reversal at the Turner criteria. Only a few droplets (0.4%) were found to have velocities close to zero. In

addition, the maximum droplet size was much smaller than that postulated by Turner et al. (1969). They concluded that the droplet flow reversal has a weak impact factor on the onset of the liquid loading problem. The liquid film reversal seemed to be the root cause of liquid loading.

Veeken et al. (2009) applied OLGA simulation to conduct a parametric study on the liquid loading problem. They stated that OLGA, which accounted for liquid film modeling, yielded a better match of minimum stability in their field data set than that predicted by the original Turner et al. expression.

Sutton et al. (2010) found that Turner's criteria should be evaluated at the bottomhole conditions if the wellhead pressure is lower than 1,000 psia or if the well is producing free water. They also recommended using the more rigorous pressure/volume/temperature (PVT) correlations to evaluate the Turner velocity, rather than the simple expressions suggested by Turner et al. (1969).

Waltrich et al. (2011) compared experimental results against three different transient wellbore simulations. They believed that the onset of the liquid loading is related to the liquid film reversal and associated with the transition from annular to churn flow regime. They pointed out that simulated pressure waves maybe important to stabilities of the liquid film in the annular flow regime.

Although there are a number of indications that the onset of the liquid loading problem is caused by the liquid film reversal, rather than the droplet flow reversal, it is still expected that the Turner's criteria with some modifications will remain applicable in

the field. This doesn't come as surprise because the onset of film reversal is governed by the same balance between drag and gravitational forces (Veeken and Belfroid, 2011).

Importance of Dynamic Modeling for the Liquid Loading Problem

The conventional way to analyze dynamic interaction between the reservoir and well is to combine the inflow performance relationship from the reservoir and the outflow performance relationship, typically called *nodal analysis*. These two curves determine flow rates from the subsystem associated with a given pressure drop at the point of consideration (nodal point). The intersection of the inflow and the outflow curves is the predicted operating point for the integrated system. **Fig. 2.5** illustrates the typical inflow and outflow performance relationships.

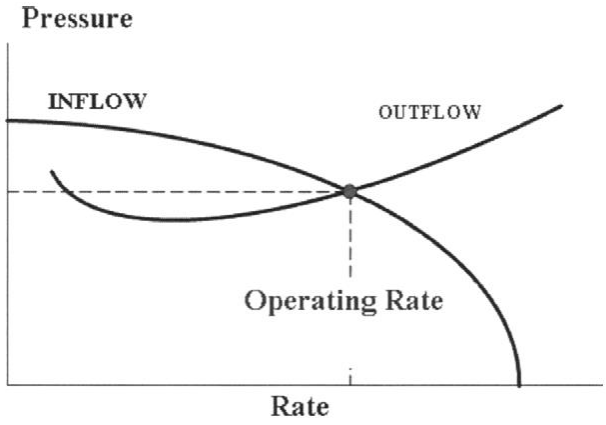

Fig. 2.5 – The operating point of the integrated system determined from the intersection of the inflow and outflow curves (Lea et al., 2003).

If the operating gas rate determined from this approach corresponds to the critical gas velocity, it can be considered as the onset of the liquid loading problem.

The outflow performance relationships are typically constructed by summing the hydrostatic pressure and the frictional pressure loss from the nodal point toward the wellhead. The IPR may be constructed using the simplified backpressure equation, of which the flow rate is proportional to the pressure difference between the average reservoir pressure and the bottomhole pressure (Lea et al. 2003). This backpressure equation is given by:

$$q_{sc} = C\left(p_r^2 - p_{wf}^2\right)^n \tag{2.3}$$

where q_{sc} is the gas flow rate, p_r is the average reservoir pressure, p_{wf} is the flowing wellbore pressure, and C and n are constants determined from well test data.

Eq. 2.3 is developed for analyzing the multirate well testing based on an assumption that the reservoir is in semisteady- or steady-state conditions (Dake 1978).

Although this diagnostic approach is useful to analyze the effects of liquid loading on gas wells, it omits transient features in the well and those in the near-wellbore region which are important to understanding the onset of the liquid loading problem. Realistic transient boundary conditions at the interface between the reservoir and the wellbore must be defined to couple the two subsystems while capturing the intermittent features of liquid loading (Solomon et al. 2008).

Belfroid et al. (2008) analyzed the effect of reservoir permeability on an ability to restart liquid-load gas wells, using the nodal analysis approach. They used a modified form of **Eq. 2.3,** which is based on the steady-state assumption. They pointed out that in

high-permeability reservoirs, stable production is difficult to restart because the reservoir is more sensitive to pressure drop than in low-permeability reservoirs.

Dousi et al. (2006) introduced a numerical approach to explain a frequently observed phenomenon where gas wells are able to produce at a relatively constant but significantly reduced rate after the onset of the liquid loading. This particular condition was referred as a *metastable* condition. This condition is attained at the equilibrium between the produced liquid falling downward and the liquid injected into the reservoir. To mimic the gas metastable condition, the integrated model comprises a two-layer reservoir and a wellbore model. Both submodels were based on the steady-state assumption. The detail of Dousi et al. model will be discussed later in this dissertation.

Gool and Currie (2007) improved the Dousi et al. model by increasing the number of layers in the reservoir model, as opposed to the two-layer reservoir. They pointed out that the new model slowed down to reach the metastable condition and slowed the reduction in gas flow rate when liquid loading starts.

Sagen et al. (2007) developed the semi-implicit coupling scheme for plugging the near-wellbore reservoir model into the transient wellbore model. The reservoir model solves the fluid transport through porous media and returns the pressure and saturations in time and space. The wellbore model provides the pressure boundary for the reservoir model, while the reservoir model provides flow rates into the wellbore.

The outline of the semi-implicit coupling scheme is described as follows:

1. At time step $n+1$, the wellbore model requests the sensitivity coefficients a_p^n and b_p^n in the relation:

$$M_P^{n+1} = a_P^n p_P^{n+1} + b_P^n \tag{2.4}$$

where $a_P^n = \frac{dM_P^n}{dP_P^n}$ (2.5)

and $b_P^n = M_P^n - a_P^n p_P^n$ (2.6)

M_P is the mass flow rate of each phase. p_P is the pressure at the interface boundary in the wellbore model. M_P^n and p_P^n are calculated at the timestep n.

2. Run the wellbore model using **Eq. 2.4** as the boundary condition. Then, the wellbore model will send p_P^{n+1} and M_P^{n+1} to the reservoir model.
3. Run the reservoir simulation to timestep n+1, using the wellbore supply boundary conditions.

Chupin et al. (2007) used the integrated reservoir-wellbore model to simulate the metastable condition of the liquid-loaded gas wells, which were proposed by Dousi et al. (2006). Chupin et al. applied a coupling scheme similar to that developed by Sagen et al. (2007). They presented the numerical solutions of the flow rate, liquid holdup, and water saturation at the reservoir/wellbore interface in the metastable regime. However, we believe that high-frequency oscillations in their presented numerical solutions are potentially associated with numerical difficulties in the simulation.

Hu et al. (2010) applied an updated version of the model used by Chupin et al. (2007) to investigate the intermittent production strategy in the gas wells to prevent liquid loading. They pointed out the well should be shut-in before the liquid accumulates in the well to avoid gas rate reduction in the next cycle.Both Chupin et al. (2007) and Hu et al. (2010) assumed no capillary pressure in the reservoir.

Schiferli et al. (2010) conducted coupled wellbore/reservoir modeling to optimize intermittent production using the OLGA software. In their model, the optimum shut-in period is 2 hr every 12 hr of production time. They also indicated the more water is reinjected into the reservoir if the shut-in time is longer.

Pourafshary et al. (2009) introduced a method to determine the amount of liquid accumulation at the bottom of the reservoir and applied it in their coupled wellbore/reservoir model. However, they did not provide details of the model and the solution procedure. They indicated that for the gas wells producing with low drawdown pressure, high liquid accumulation is expected.

Zhang et al. (2009) developed a numerical reservoir model to describe possible reinjection in the near-well region during liquid loading. They identified the U-shaped pressure profile in the near-wellbore reservoir by imposing an oscillating bottomhole pressure from the inner boundary. **Fig. 2.6** illustrates the U-shaped pressure profile in the near-wellbore region. A sensitivity analysis was performed to evaluate the length of the disturbed distance from the wellbore. They pointed out that the high oscillation frequency, high fluid compressibility, and low permeability led to a short length of the U-shaped pressure profile.

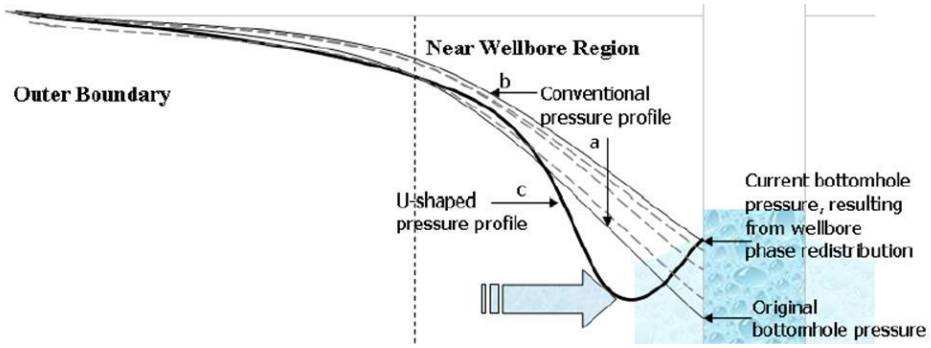

Fig. 2.6 - U-shaped pressure profile in the near-wellbore region explains possible reinjection during liquid loading (Zhang et al. 2010)

Zhang et al. (2010) investigated the effect of relative permeability hysteresis to the U-shaped pressure profile. They indicated that in the high oscillation frequency in bottomhole pressure, the disturbed distance from the wellbore changes very little.

Y. Wang (2012) conducted an experimental study on the transient flow condition in the near-wellbore region. He confirmed from a dry-gas experiment that the U-shaped pressure curves exist as a result of backflow from the wellbore, as proposed by Zhang et al.(2009).

J. Wang (2012) performed a numerical reservoir simulation to study the effect of liquid loading in the near-wellbore region. He indicated that the near-wellbore damage, including scale deposition, clay swelling, and sand production, caused by the liquid loading decrease the gas recovery by several folds, even after the effective deliquification is applied to the well.

Waltrich (2012) investigated the onset of liquid accumulation at the bottom of the vertical tube under conditions corresponding to both regions of several liquid loading

criteria. He indicated from the experimental results that the liquid accumulation at the bottom of the tube could not be initiated by the wellbore alone. According to his opinion, the pseudo-porous medium representing the near-wellbore region may be important to trigger this onset of the liquid accumulation.

The Need for a New Formulation of the Wellbore Boundary Condition for the Liquid Loading Problem

In order to simulate the transient flow conditions in the coupled wellbore/reservoir models during liquid loading, it is important to define realistic boundary conditions at the interface between the reservoir and the wellbore model. The wellbore boundary condition must be presented in such a way that it can predict liquid backflow into the reservoir and include effects of capillary pressure at the boundary.

The conventional method of presenting a well in a reservoir simulator is to define a sink/source term, described by a form of IPR. Individual phase fluxes are implicitly evaluated, corresponding to the phase potential difference between the grid-block and the wellbore. This formulation is embedded in most commercial numerical simulators. In multiphase reservoir simulation, the treatment of wells always presents a numerical challenge. Usually, the maximum changes in the primary variables happen at grid blocks directly connected to the well. Thus, the maximum allowed time step and the number of internal iterations required in a given time step are both significantly affected by the well block(s).

In order to accommodate robustness in commercial software, additional assumptions are often incorporated into the schedule set up. Those include negligible capillary pressure at the well block and a priori flow direction defined by the user. Even in purpose-built simulators, when the direction of the flow is calculated, such as in cross-flow investigations, most authors suggest compromising the capillary pressure in the well block to attain numerical stability.

For the investigation of specific problems, such as the liquid loading phenomena of wells producing from tight-gas formations, capillary pressure cannot be neglected. In addition, flow direction (production/injection) through a connection is unknown, as the wellbore conditions are rapidly changing. Therefore, representing sink/source terms requires special attention.

Coats et al. (2003) provided the treatment to the wellbore boundary condition for an integrated subsurface-surface framework. The equation is generalized such that it can automatically predict cross-flow situations based on the potential difference, assuming co-current phase flows in each individual connection. They suggested that gradients are weighted by fluid saturation, or motilities in the grid blocks. However, they neglected capillary pressure in the formulation.

Investigating a fractured, geothermal reservoir, Wu (2000) incorporated the capillary pressure in the pseudo well model. According to his experience, the apparent volume of the wellbore must be increased by 100 to 1000 folds to avoid convergence problems during the simulation.

Conclusion

The literature review presents modeling efforts towards characterization of dynamic interaction between the reservoir and the wellbore during liquid loading. Some of the dynamic modeling is subject to steady-state assumptions either in the wellbore or in the reservoir, or in both subsystems. Those modeling techniques require a rigorous characterization of the wellbore boundary condition that can capture transient behaviors at the boundary.

Although the petroleum industry has paid much attention to the predictive models for the onset of the liquid loading problems, a fundamental understanding in the mechanism during liquid loading is crucial. The modeling of the dynamic interaction between the two subsystems must be accurately described in order to identify the real cause of the liquid loading and suggest the appropriate design of the production system to extend the life of the gas well.

CHAPTER III

GOVERNING EQUATIONS AND FORMULATION OF NUMERICAL RESERVOIR SIMULATION

Introduction

The original aim of this study was to enhance simulation capability of the Zhang et al. (2009) work. The new numerical reservoir simulation is able not only to capture the U-shaped pressure profile in the near-wellbore region as previously presented by Zhang et al., but also to simulate flow in vertical direction due to gravity. This adds the benefit of being able to investigate crossflow between formations during liquid loading.

In addition to enhancing simulation dimensionality, this study gives a new formulation of the wellbore boundary condition that is suitable for dynamic modeling of the liquid loading problem. This new boundary condition includes the effect of capillary pressure at the boundary and predicts flow direction at the connection(s) between the two subsystems. Numerical instability was not observed during the course of the simulation when the new wellbore boundary condition was applied.

This chapter provides details of formulation of the numerical reservoir simulation. It enlists the governing equations and describes the discretization method using a fully implicit scheme. In addition, it presents a derivation of the new wellbore boundary condition applied in this study.

It should be noted that even though the governing equations in this work are similar to those applied in Zhang et al., we used a different numerical discretization

scheme. Zhang et al. used the implicit pressure explicit saturation (IMPEZ) method, which is conditionally stable as suggested by Peaceman (1977):

$$\frac{\Delta t}{\Delta x^2} < 6.23 \times 10^{-5} \ \frac{\text{day}}{\text{ft}^2} \tag{3.1}$$

where Δt is timestep size in the simulation and Δx is the size of the grid block in the direction to the flow.

Governing Equations and Numerical Formulation

To model liquid loading, a purpose-built numerical reservoir simulation was developed to handle gas and water phase flows in an isothermal porous medium. The simulator is adapted from an open source educational code called "FTSim" (Moridis, 2009). In terms of concepts, approaches, and architectures, the FTSim is based on TOUGH+, the suite of software codes developed at the Lawrence Berkeley National Laboratory (Moridis et al. 2008).

In the two-phase system, an underlying equation obeys conservation of mass, which can be expressed as:

$$\frac{\partial}{\partial t}(M_\beta) = -\nabla \cdot (\rho_\beta \boldsymbol{V}_\beta) + q_\beta \tag{3.2}$$

where M_β is the mass accumulation term of phase β ($\beta = w$ for water; $\beta = g$ for gas); ρ_β is the density of phase β under reservoir conditions; q_β is the sink/source term of phase β per unit volume, which determines phase fluxes at the connection to the well node. We will discuss more details in the next chapter regarding the new wellbore boundary condition for the liquid loading problem; V_β is the Darcy velocity of phase β.

The mass accumulation term of phaseβ is given by;

$$M_\beta = \phi S_\beta \rho_\beta \tag{3.3}$$

where ϕ is the effective porosity of the formation; S_β is the saturation of phase β.

Darcy's velocity is defined by:

$$V_\beta = -\frac{k k_{r\beta}}{\mu_\beta}\left(\nabla p_\beta - \rho_\beta g\right) \tag{3.4}$$

Where k is the absolute permeability of the formation; $k_{r\beta}$is the relative permeability to phaseβ; $\mu_\beta$is the viscosity of phase β; $p_\beta$is the pressure of phase β; and g is gravitational constant.

Two constitutive equations are required, in addition to **Eq. 3.2** to express all secondary variables and parameters as a function of a set of primary variables of interest. The following relationships are given as:

$$S_w + S_g = 1 \tag{3.5}$$

and $$p_g = p_w + p_c(S_w) \tag{3.6}$$

Where $p_c$is the capillary pressure, which is assumed to be a function of fluid saturation.

The relative permeabilities are assumed to be functions of fluid saturation. The porosities are assumed to be functions of fluid pressure. Fluid properties are assumed to be functions of pressure and temperature. Details of the formula employed in this simulation will be discussed in Appendix A.

Eq 3.2 can be discretized using the finite volume method. For gridblock *n*, **Eq 3.2** can be expressed by a set of first-order ordinary differential equations in time as:

$$\frac{dM_{\beta,n}}{dt} = \frac{1}{V_n}\sum_m A_{nm}V_{\beta,nm} + q_{\beta,n} \tag{3.7}$$

where $V_{\beta,nm}$ is the average value of Darcy velocity of phase β over gridblock interface A_{nm}between block V_n and V_m. The discretized flux $V_{\beta,nm}$expressed in terms of average values over parameters is given by:

$$V_{\beta,nm} = -\left[\frac{kk_{r\beta}}{\mu_\beta}\right]_{nm}\left[\frac{p_{\beta,n} - p_{\beta,m}}{D_{nm}} - \rho_{\beta,nm}g\right] \tag{3.8}$$

For this equation, suitable averaging methods are required for representing properties of each parameter at the interface between gridblocks *n* and *m*. $D_{nm}$is the distance between centerpoints *n* and *m*.

The time discretization is carried out with a first-order finite-difference scheme. The flux and sink/source terms in **Eq 3.7** are evaluated at the new time level,$t^{k+1} = t^k + \Delta t$, known as a fully implicit treatment, to obtain the numerical stability needed for a strongly nonlinear problem. Following time discretization scheme, **Eq 3.7** can be expressed as:

$$R_{\beta,n}^{k+1} = V_n\left(M_{\beta,n}^{k+1} - M_{\beta,n}^{k}\right) - \Delta t\left(\sum_m A_{nm}V_{\beta,nm}^{k+1} + q_{\beta,n}^{k+1}\right) = 0 \tag{3.9}$$

where $R_{\beta,n}^{k+1}$ is the residual of **Eq 3.9** of phase β in gridblock *n* at time level *k*+1. By convention in the petroleum industry, **Eq 3.9** can be rewritten in volumetric terms at standard condition as:

$$R_{\beta,n}^{k+1} = V_n\left[\left(\frac{\phi S_\beta}{B_\beta}\right)_n^{k+1} - \left(\frac{\phi S_\beta}{B_\beta}\right)_n^{k}\right] - \Delta t\left(\sum_m A_{nm}V_{\beta,nm}^{k+1} + q_{\beta,n}^{k+1}\right) = 0 \tag{3.10}$$

where $B_\beta$is the formation volume factor of phaseβ; $q_\beta$is the volumetric flow rate of phase β at standard condition. The Darcy's velocity is then rewritten as:

$$V_{\beta,nm} = -\left[\frac{kk_{r\beta}}{\mu_\beta B_\beta}\right]_{nm}\left[\frac{P_{\beta,n} - P_{\beta,m}}{D_{nm}} - \gamma_{\beta,nm}\right] \tag{3.11}$$

where $\gamma_{\beta,nm}$is the specific weight of phase β at interface A_{nm}in psi/ft.

For each gridblock, two equations describe the primary variables: pressure and saturation. In the gas/water system discretized into *N* gridblocks, **Eq 3.10** represents a set of 2*N* algebraic equations. The unknown, x_i (i = 1,2,3…2*N*), are 2*N* primary variables, which can completely define the state of the system at new time level t^{k+1}. These sets of equation are solved by Newton-Raphson iterations. This can be done by approximating **Eq 3.10** by the first-order Taylor expansion of the 2*N* linear equations.

$$R_{\beta,n}^{k+1}(x_{i,p+1}) \approx R_{\beta,n}^{k+1}(x_{i,p}) + \sum_i \left.\frac{\partial R_{\beta,n}^{k+1}}{\partial x_i}\right|_p (x_{i,p+1} - x_{i,p}) \approx 0 \tag{3.12}$$

$$-\sum_i \left.\frac{\partial R_{\beta,n}^{k+1}}{\partial x_i}\right|_p (x_{i,p+1} - x_{i,p}) = R_{\beta,n}^{k+1}(x_{i,p}) \tag{3.13}$$

where subscripts *p* denote iteration index at time level t^{k+1}. All terms $\frac{\partial R_{\beta,n}}{\partial x_i}$, called the Jacobian matrix, can be evaluated by numerical differentiation. **Eq 3.13** is solved by a precondition-conjugated gradient method. The iteration is continued until the residual $R_{\beta,n}^{k+1}$are reduced below a preset convergence tolerance.

Wellbore Boundary Formulation

Fig.3.1 presents a schematic of a gas/water system comprising one formation grid block and one well node. The pressure on the wellbore side is denoted by p_{wf} and the local volumetric ratio of the liquid phase inside the wellbore is denoted by S_{wwf}. This will play a role only if the flow direction is from the wellbore to the reservoir. Since the connection is horizontal, the flow through the connection is solely pressure driven, and hence must be of the same direction for both phases. (This condition is valid for *reservoir* simulation. For simulation of laboratory experiments, other conditions may apply.)

The conventional wellbore boundary condition states that the volumetric flow of each phase across the connection is given by:

$$q_{w,i} = \mathrm{PI}_i \left(\frac{k_{rw,i}}{\mu_{w,i}} \right) (p_{w,i} - p_{wf}) \tag{3.14}$$

$$q_{g,i} = \mathrm{PI}_i \left(\frac{k_{rg,i}}{\mu_{g,i}} \right) (p_{g,i} - p_{wf}) \tag{3.15}$$

where PI_i is the well-block productivity (or injectivity) index in grid block i. p_{wf} is the wellbore flowing pressure at the well side of the connection.

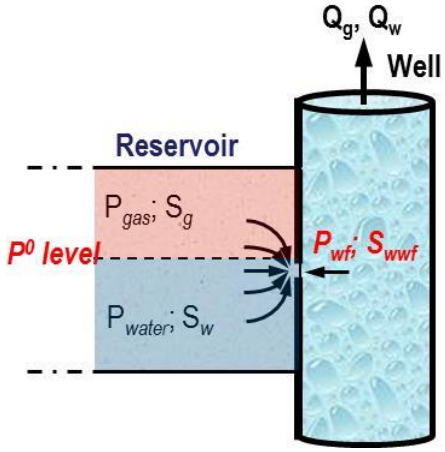

Fig.3.1 – Schematic illustration of p^0 concept for a representation of the wellbore model in the single-layer grid-block reservoir.

The productivity/injectivity index, PI_i, is the common property of the wellbore node and the grid-block, given by:

$$PI_i = \frac{2\pi k_H \Delta z_i}{ln\frac{r_e^*}{r_w}} \tag{3.16}$$

where r_e^* is the equivalent wellbore radius and k_H is the horizontal permeability. In most reservoir simulators, Peaceman's (1983) approach is used to evaluate these parameters and it is used in our new formulation. While this well index has been derived assuming single-phase, steady-state, incompressible flow and may require modifications for fast transients in multiphase flow problems, it is still appropriate for the scope of this work.

From **Eq. 3.14** and **Eq. 3.15**, the net volumetric flow rate at the connection equals zero when the magnitudes of the phase flows are equal with difference in signs.

This "happens" at a specific wellbore flowing pressure that we call multiphase zero-flow pressure (*MPZFP*), or "p^0":

$$q_{T,i} = \mathrm{PI}_i \left(\frac{k_{rw,i}}{\mu_{w,i}}\right)(p_{w,i} - p_i^0) + \mathrm{PI}_i \left(\frac{k_{rg,i}}{\mu_{g,i}}\right)(p_{g,i} - p_i^0) = 0 \tag{3.17}$$

$$p_i^0 = \frac{\left(\frac{k_{rw,i}}{\mu_{w,i}}\right)p_{w,i} + \left(\frac{k_{rg,i}}{\mu_{g,i}}\right)p_{g,i}}{\left(\frac{k_{rw,i}}{\mu_{w,i}}\right) + \left(\frac{k_{rg,i}}{\mu_{g,i}}\right)} \tag{3.18}$$

While the expression for p^0 is derived from a hypothetical counter-current flow situation that is — according to our basic assumption — not allowed in a single well-node/reservoir grid-block connection, it will still be used in the formulation of the new boundary condition as the means to determine the *common flow direction* of the two phases. At a given time, through a given connection, there will be only either production or injection for all phases, but cross-flow can happen from and to a well, via multiple connections, similarly to what was suggested by Holmes et al. (1998) and Coats et al. (2003).

Moreover, we require that the actual phase composition of the flow in the connection be determined by the upstream phase composition. The boundary condition satisfying the above criteria is depicted in **Fig. 3.2.**

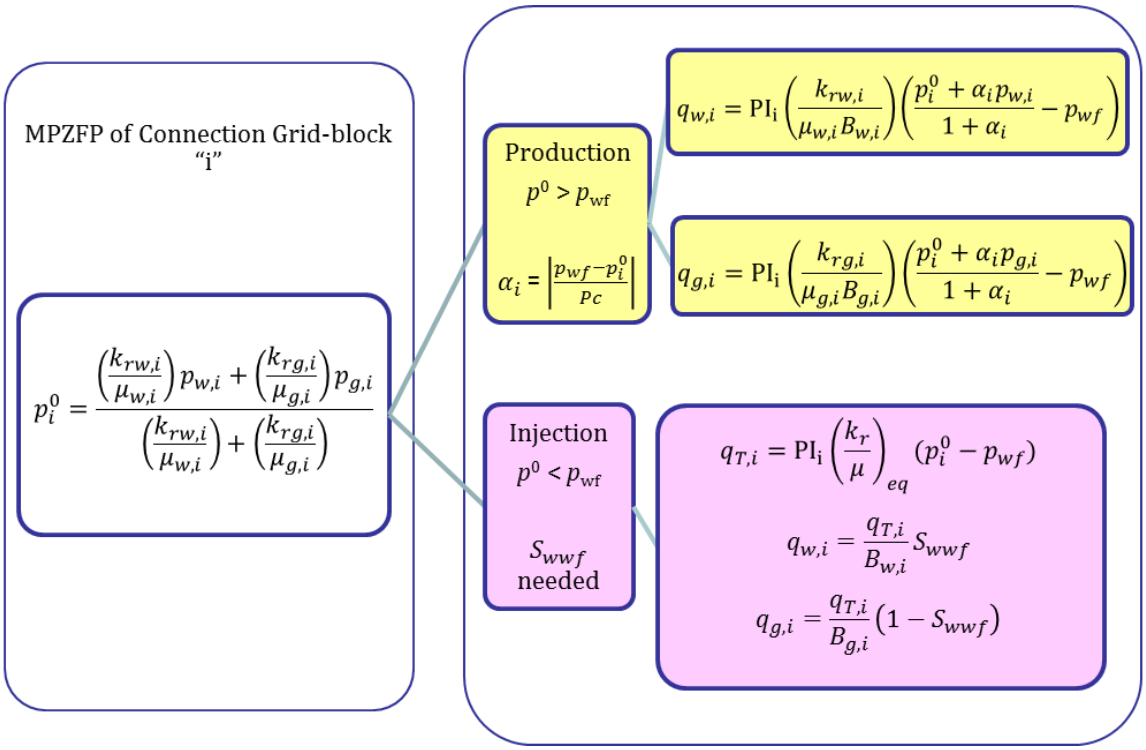

Fig. 3.2 - Wellbore boundary condition using the p^0 concept

In fact, the boundary condition has a state-dependent structure. As shown in **Fig. 3.2**, the flow direction is determined from the sign of the difference between p^0 (a state property of the grid-block) and p_{wf} (a state property of the wellbore side of the connection). The phase composition of the flow through the interface is determined from the upstream condition. Therefore, S_{wwf} (the liquid saturation on the wellbore side of the connection) is necessary to know in the case of injection, when the $\left(\frac{k_r}{\mu}\right)_{eq}$ term should also be a function of S_{wwf} and its particular form will be discussed later.

The scaling parameter, α, is introduced to measure how far we are from the switching condition, where "far" is measured in terms of the capillary pressure.

$$\alpha_i = \frac{\left|p_i^0 - p_{wf}\right|}{p_c} \tag{3.19}$$

At large pressure difference between wellbore and p^0 (relative to the capillary pressure), the scaling parameter will assure that the new boundary conditions tend to **Eq. 3.9** and **Eq. 3.10**. Thus, the algorithm depicted on **Fig. 3.2** will reproduce the results obtained with traditional wellbore boundary conditions. Moreover, if the capillary pressure is neglected in the connection grid-block, the traditional boundary conditions (**Eq. 3.14-3.15**) are again recovered.

This boundary condition can be used during production, shut-in, or injection at the wellhead, but that does not necessarily imply the actual flow directions through the individual connections. In fact, the actual direction of flow can change from time step to time step (even iteration to iteration), depending on the instantaneous state on the two sides of the connection. The approach can be easily generalized to any number of phases.

From the point of view of the following applications, it is important that, when the wellbore flowing pressure is varying continuously in time and happens to cross the p^0 of the grid-block, the source/sink terms for each phase go through zero in a smooth and synchronized manner.

External Boundary Conditions

The external boundary condition can mimic the effect from the far region of the reservoir in near-wellbore modeling. It can reduce memory requirements in term of integrating reservoir/wellbore modeling, of which the computation of both subsystems is intensively substantial. One alternative for modeling of the external boundary condition is by describing the flux terms onto the outermost grid block, assuming that pressure and phase saturation at the external boundary are time-invariant. In the near-wellbore modeling accounting for reservoir pressure depletion, we apply a constant pressure decline rate deducted to initial pressure at the boundary over time.

Initial Vertical Equilibrium

The initial condition in the multiphase flow system requires the definition of phase pressures and saturations in every gridblock at the beginning of the simulation. This specification can possibly be achieved by allowing flows in the vertical direction according difference in phase gravities and capillary forces until the reservoir reaches gravity/capillary equilibrium (Ertekin et al. 2001). For gas/water systems, three different zones are possible: the gas-cap zone, gas/water continuous zone, and water zone. For the scope in this study, only the gas/water continuous zone is present in the reservoir.

Conclusion

The new reservoir simulation has been formulated. Its derivation has been made for gas/water flow through isothermal porous media. The underlying diffusivity equation

is based on conservation of mass in the multiphase flow system. The solution of the differential equation is then solved by the finite-volume method for space discretization and the first-order finite difference method.

The formulation of the wellbore boundary condition has been presented. It was derived from the conventional wellbore boundary conditions of the multiphase flows which can detach between the phases considered. For the lateral connection between the reservoir and the vertical well, the flow through the connection is solely pressure driven, and hence must be of the same direction for both phases.

We determine the "multi-phase zero-flow pressure" or p^0 to calculate the direction and its magnitudes of the phase flows at the connection. The phase composition is determined by the upstream saturation condition. The boundary condition can be used during the production, shut-in, or injection at the wellhead. The actual direction of the flow can change from time step to time step, depending on the instantaneous state on the two sides of the connection.

CHAPTER IV

EVALUATION OF THE NUMERICAL RESERVOIR SIMULATION: COMPARISON AGAINST PREVIOUS CODES, VALIDATION WITH COMMERCIAL SOFTWARE, AND RESERVOIR SIMULATION DURING LIQUID LOADING*

Introduction

In this chapter, we used our developed reservoir simulator associated with the new wellbore boundary condition to model a simple loading case and compare the results with those from the Zhang et al. (2009) simulator. We focused on simulation results at the grid block where we applied the wellbore boundary condition (wellblock). This comparison indicated numerical instabilities in the Zhang et al. simulator, which may associated with an inappropriate wellbore boundary condition.

Moreover, we presented the comparison of the simulation results against a commercial reservoir package to identify differences in numerical results at the wellblock, under near-switching flow directions. With the new formulation of the wellbore boundary condition, the simulator can predict flow directions at the boundary depending on immediate pressure difference between the bottomhole and the reservoir, while the commercial package will command to shut the well if the

---

* Part of this chapter is taken from "Experimental and Numerical Investigation of Transient Gas Flow through Porous Media – Back Pressure Effects" by Liu et al., 2013. It is in preparation for publication in 2013- 2014.

downstream pressure is higher that the upstream one according to flow directions specified by users. This offers a great advantage when investigating the liquid loading conditions, of which the flow directions can be switching frequently depending on pressure fluctuation at the bottomhole.

We also presented the simulation results in the near-wellbore region when imposing an oscillating bottomhole pressure at the inner reservoir boundary. The results show the presence of U-shaped pressure profiles as a result of reinjection of the heavier phase, as indicated by Zhang et al. (2009).

In addition, we also applied this reservoir simulator to validate the experimental investigation of U-shaped pressure profiles in a single-phase gas experiment conducted at Clausthal University of Technology, Germany. This experiment is a subproject of our joint industry project on the liquid loading problem. Thus, the solutions from the experiment should be able to be interpreted by the simulator, and vice versa.

Comparison Simulation Results from the Developed Numerical Simulator against Zhang et al. (2010)

The synthetic two-phase case presented by Zhang et al. (2010) was chosen for this comparison. We refer to the Zhang et al. model as Sim1 and our model as Sim2. The radial geometry is described on one layer. The external radius is 4,000 ft. In the Sim1 model, the near-wellbore region is divided into 10 grid blocks, each 10 ft long, followed by 10 logarithmically distributed grid blocks reaching 1,000 feet from the wellbore, followed by 10 evenly distributed grid blocks of 300 ft each (total reservoir

radius measured from the wellbore equals 4,000 ft). In the Sim2 model, an even grid size is assigned on 200 blocks; each block has a length of 20 ft. The reservoir thickness is 100 ft. **Table 4.1** summarizes the key parameters used in this comparison exercise. Relative permeability and capillary pressure curves are shown in **Fig. 4.1**.

Table 4.1 – Key simulation parameters for result comparison against Zhang et al. (2010)

Reservoir Parameters	
Fluid type in the reservoir	Gas (C1) and Water
porosity	12.15 %
Absolute permeability	1 md
Initial reservoir pressure	4500 psia
Reservoir temperature	260 deg F
Initial water saturation	12%
Well Parameters	
Well radius	0.328 ft

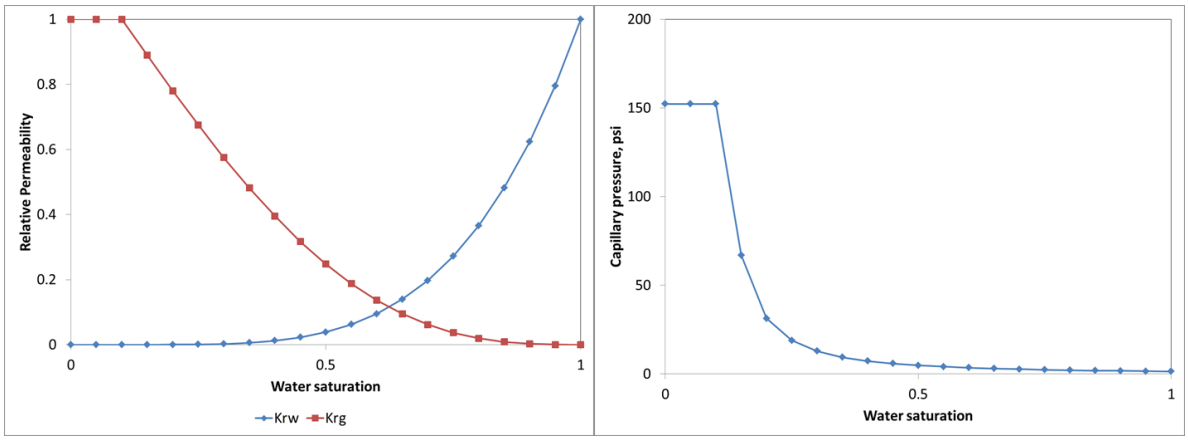

Fig. 4.1 – The relative permeability curves (left) and the capillary pressure curve (right) from an example problem shown by Zhang et al. (2010)

In the original model presented by Zhang et al. (2010), they applied a Leverett J-function to determine the capillary pressure, whereas the Corey function is used in our model.

Zhang et al. illustrated that the U-shaped pressure profile in the near-wellbore region is developed when imposing the oscillating bottomhole pressure at the wellbore boundary. **Fig 4.2** illustrates amplitudes of bottomhole pressure perturbation (step-wise) after stabilized flow of 30 Mscf/d for 55 days. The period of oscillation lasts 36 minutes, followed by a constant bottomhole pressure of the last perturbed value.

In addition, they indicated that both gas and water phases are reinjected during the period of pressure oscillation, leading to a U-shaped pressured profile in both phases. After the oscillation period, the U-shaped pressure in the water phase persists in the near-wellbore region and the water phase is still reinjected into the reservoir, while the gas phase is produced from the reservoir. They concluded that the counter-current flow

of the gas/water system exists in the one-layer model after bottomhole pressure oscillation.

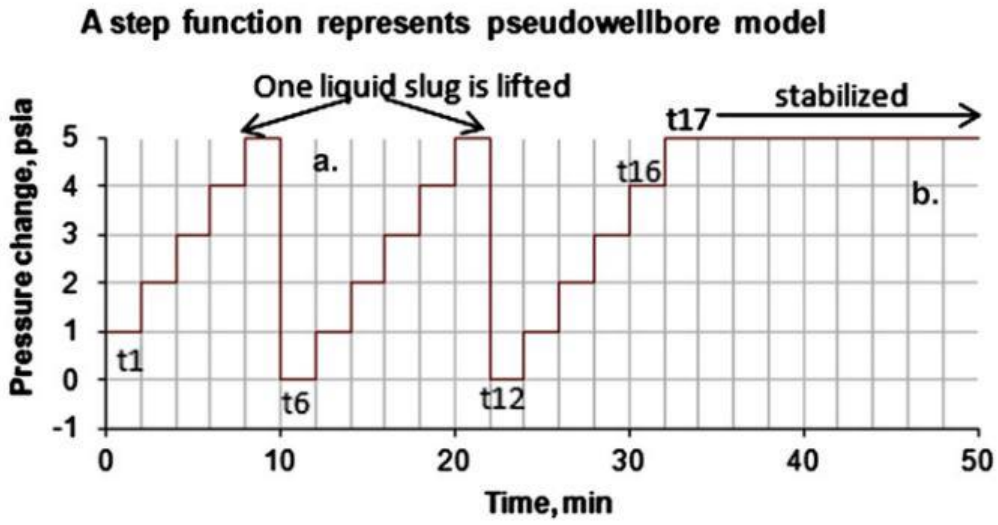

Fig. 4.2 – A step function pressure profile applied during the transient condition (Zhang et al. 2010)

A similar production schedule was applied in our model. **Fig. 4.3** shows the comparison of water and gas phase pressure at the well block during the first production period of 55 days. The pressure solutions from both models are nearly similar in this period even though the wellbore boundary condition is different.

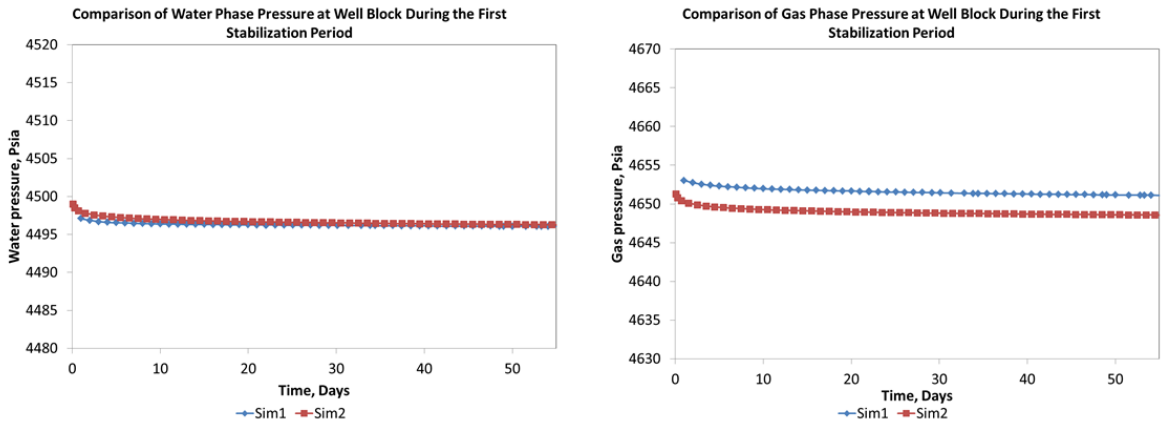

Fig. 4.3 – Comparison of the water phase pressure (left) and gas phase pressure (right) at the wellblock during 55 days (stabilization period)

However, during the pressure oscillation period, the pressure and rate solution generated from our model indicated that the well is steadily producing gas and no reinjection is taking place, as opposed to that from the Zhang et al. model (**Fig. 4.4(e)** and **Fig. 4.4(f)**). From the Sim1 model, the U-shaped pressure profiles in water and gas phases are observed in the near-wellbore region as shown in **Fig. 4.4(a)** and **Fig. 4.4(b)**; while from the Sim2 model, the pressure profiles in the near-wellbore indicate that both gas and water phases flow to the wellbore (**Fig. 4.4(c)** and **Fig. 4.4(d)**). This is contradictory to each other. We observed that the numerical errors in the gas rate occur over the period of pressure oscillation as shown in **Fig. 4.4(e)**. These numerical errors are also seen in interblock flow rate profiles presented by Zhang et al. (2010) since the gas and water rates between two adjacent grid blocks oscillate as shown in **Fig. 4.5**.

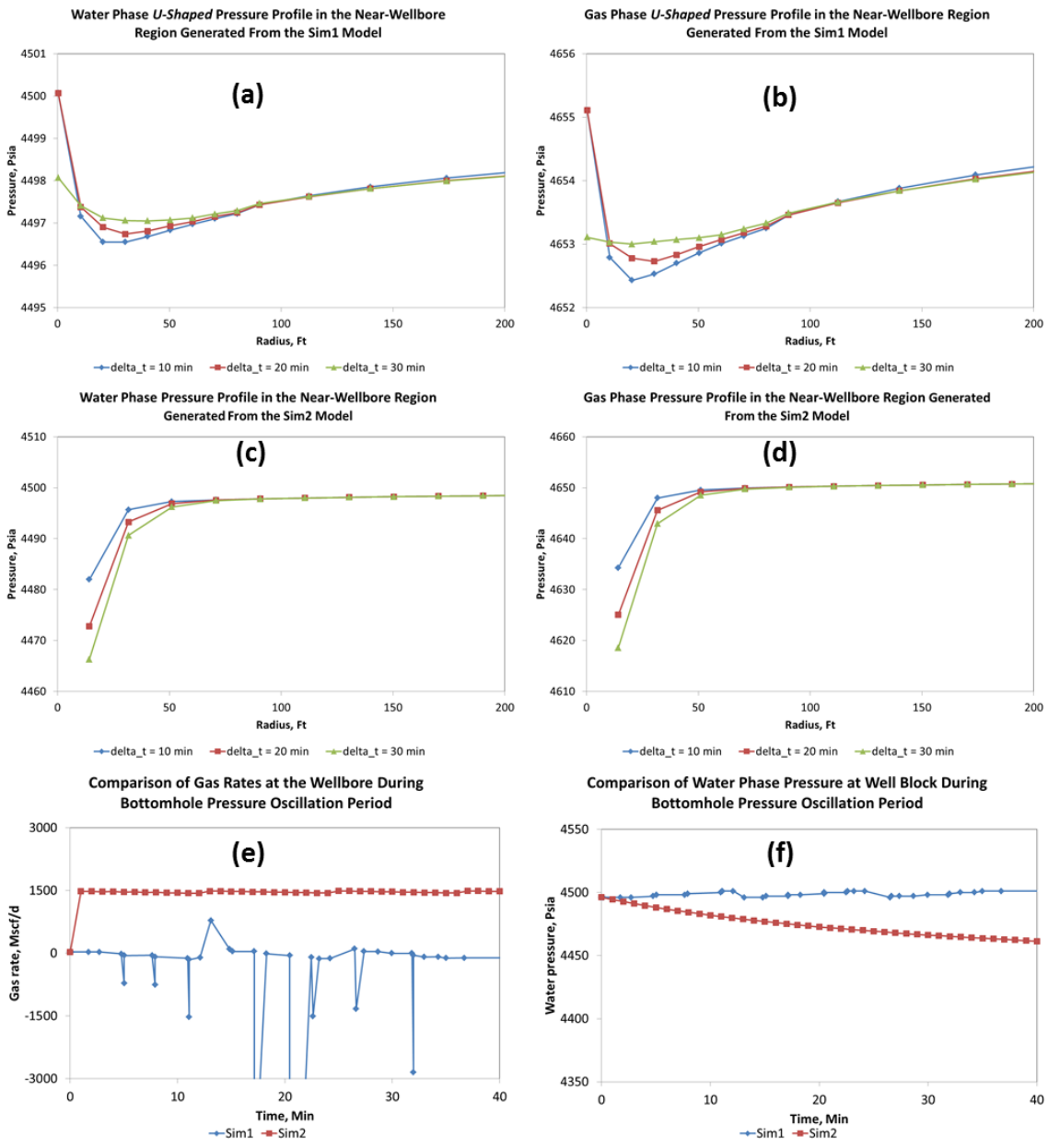

Fig. 4.4 – Comparison of the simulation results during the pressure oscillation period: (a) Water-phase U-shaped pressure profiles generated from the Sim1 model; (b) Gas-phase U-shaped pressure profiles generated from the Sim1 model; (c) Water-phase drawdown pressure profiles generated from the Sim2 model; (d) Gas-phase drawdown pressure profiles generated from the Sim2 model; (e) Comparison of gas rate results at the well block; (f) Comparison of water-phase pressure at the well block.

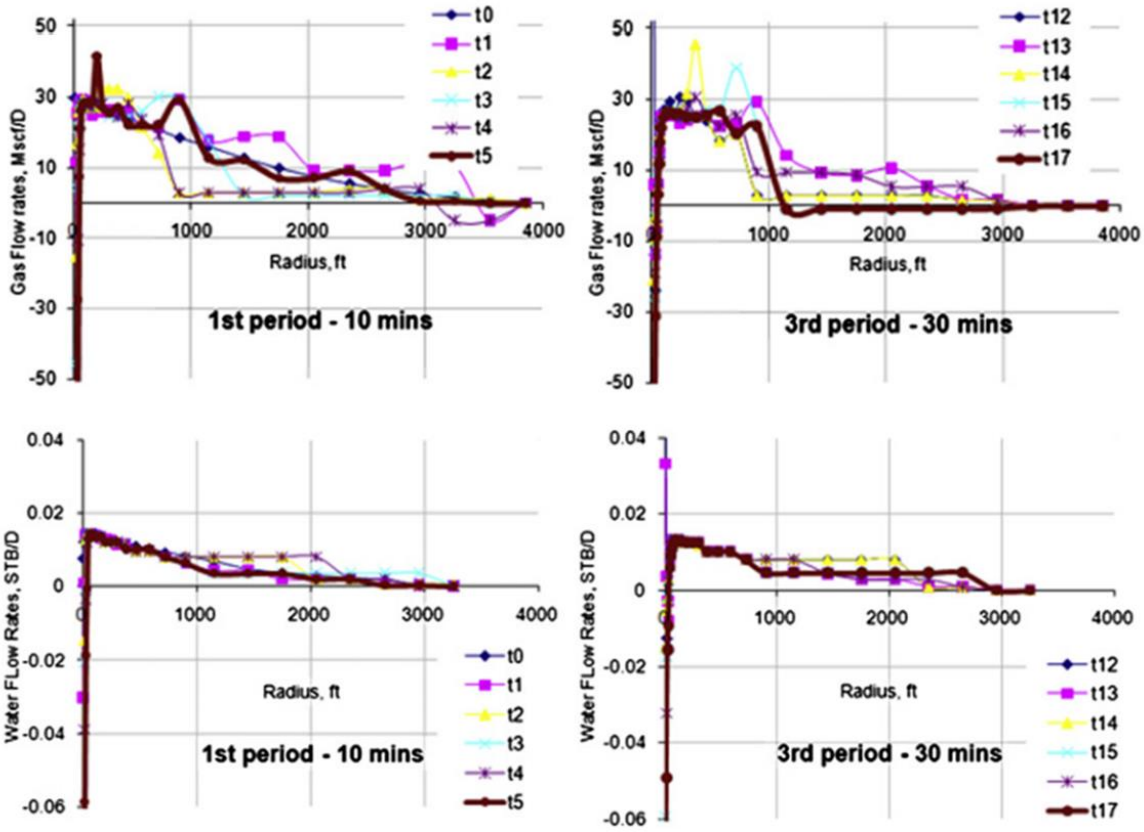

Fig. 4.5 – The inter-gridblock water and gas rates during two cycles of imposed backpressure from the wellbore (top – water, bottom – gas) (after Zhang et al., 2010)

From our model, the U-shaped pressure profile in the near-wellbore region is not observed during the pressure oscillation period because the reinjection cannot take place by increasing bottomhole pressure by only 5 psi. Pressure from the far-region reservoir can push the flow from one side, thus making it insensitive to small amounts of pressure oscillation in the wellbore. We suspect that the numerical errors in the Zhang et al. model are caused by incorrect wellbore boundary conditions embedded in the sink/source term.

Comparison Simulation Results from the Developed Numerical Simulator against Commercial Reservoir Package

We also verified our code development by evaluating the simulation results with those generated by a commercial software package. The commercial software ECLIPSE100, developed by Schlumberger, was selected for this evaluation. ECLIPSE100, which is generally applied in a wide-range of reservoir problems, is mostly suitable for solving large, complex reservoir problems. For the problem associated with well flow modeling, the vertical lift pressure tables are often included in the model specification to avoid lengthy multiphase flow calculation in the wellbore.

A simple synthetic case based on field data was chosen for this comparison. We refer to our model as Sim2 and the ECLIPSE100 as ECL. The radial geometry is described on one layer. The external radius is 6,000 ft. Equal-grid spacing is assigned on 600 blocks; each block has the length of 10 ft. The reservoir thickness is 400 ft. The reservoir is assumed to be homogenous in porosity and permeability. **Table 4.2** summarizes the key parameters used in this comparison exercise. Relative permeability and capillary pressure curves are shown in **Fig. 4.6**.

Table 4.2 – Key simulation parameters used in comparison of simulation results against ECLIPSE100

Reservoir Parameters	
Fluid type in the reservoir	Gas (C1) and Water
porosity	11%
Absolute permeability	6.5 md
Initial reservoir pressure	8000 psia
Reservoir temperature	260 deg F
Initial water saturation	35%
Well Parameters	
Well radius	0.25 ft

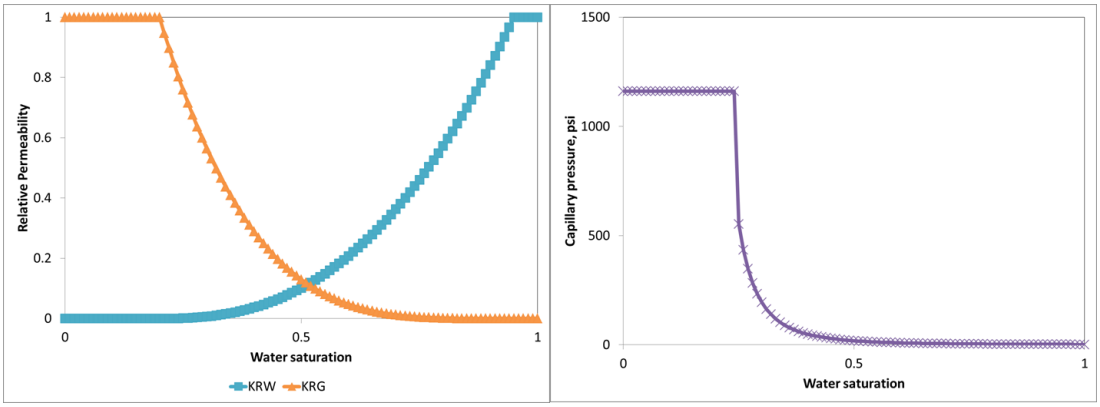

Fig. 4.6 – The relative permeability curves (left) and the capillary pressure curve (right) used in comparison of simulation results against ECLIPSE100

We investigated simulation solutions for the following three cases:

- **Case 1 – *One-layer model without capillary pressure***
    - Increase bottomhole pressure slightly more than the pressure at the well block, after production has stabilized.
    - Increase bottomhole pressure much more than the pressure at the well block, after production has stabilized.
- **Case 2 – *One-layer model with capillary pressure***
    - Increase bottomhole pressure slightly more than the pressure at the well block, after production has stabilized.
    - Increase bottomhole pressure much more than the pressure at the well block, after production has stabilized.
- **Case 3 – *Two-layer model with capillary pressure***
    - Increase bottomhole pressure slightly more than the pressure at the well block, after production has stabilized.
    - Increase bottomhole pressure much more than the pressure at the well block, after production has stabilized.

Our focus is to investigate changes in the flow direction of the phases around switching conditions: the wellbore pressure is slightly more/less than the current pressure in the near-wellbore region. We expected that the ECL model could not identify change in flow direction in these sensitive zones because it requires a predetermination of flow direction by the user in the schedule setup. On the other hand, our simulation,

associated with the new wellbore boundary condition, was expected to detect those changes in flow directions according to the pressure differences at the connection.

The initial reservoir condition corresponds to vertical equilibrium. The reservoir can contribute to gas and water production during the first stabilization, at which the constant bottomhole pressure is imposed. Depending on the pressure difference between the bottomhole and the well block, the reservoir can take water injection after we increase bottomhole pressure.

We compared simulation results at the well block during the first stabilization and after increasing the bottomhole pressure. **Fig. 4.7** shows gas-phase pressure, water rate, and gas rate during the first stabilization for Case 1. Both Sim2 and ECL models predict similar results in this period. However, once the wellbore pressure increased, the two models respond differently.

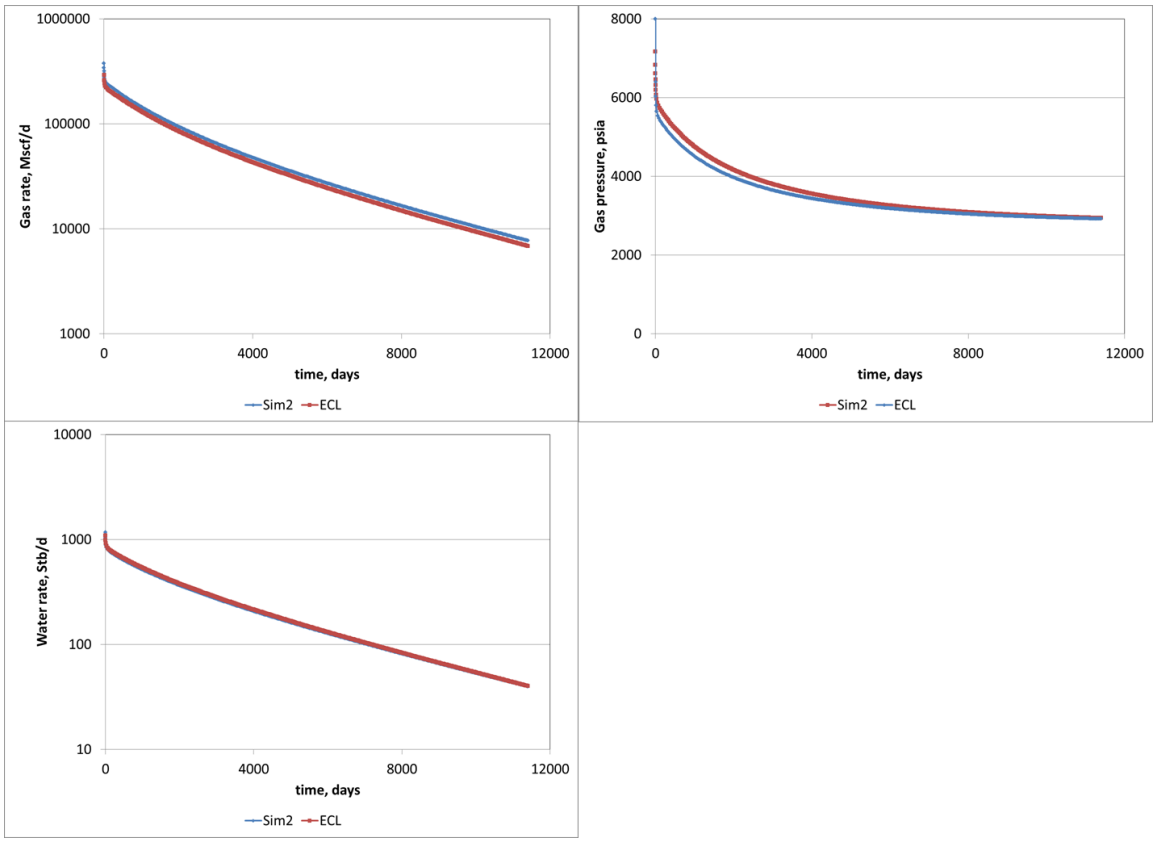

Fig. 4.7 – Comparison of simulation results of gas rate (top left), water rate (bottom left), and gas pressure (top right) at the well block versus time during the first stabilization period in Case 1

When the wellbore pressure is slightly increased from the first stabilization period, as described in Case 1.a, the solutions from the ECL model indicate that the well is shut in because the bottomhole pressure is insufficient to reinject water to the reservoir. However, the solutions from the Sim2 model show that less flow rate is produced from the reservoir, corresponding to the increased wellbore pressure. **Fig. 4.8** shows wellbore pressure, pressure at the wellbore and the water rate solutions during this period.

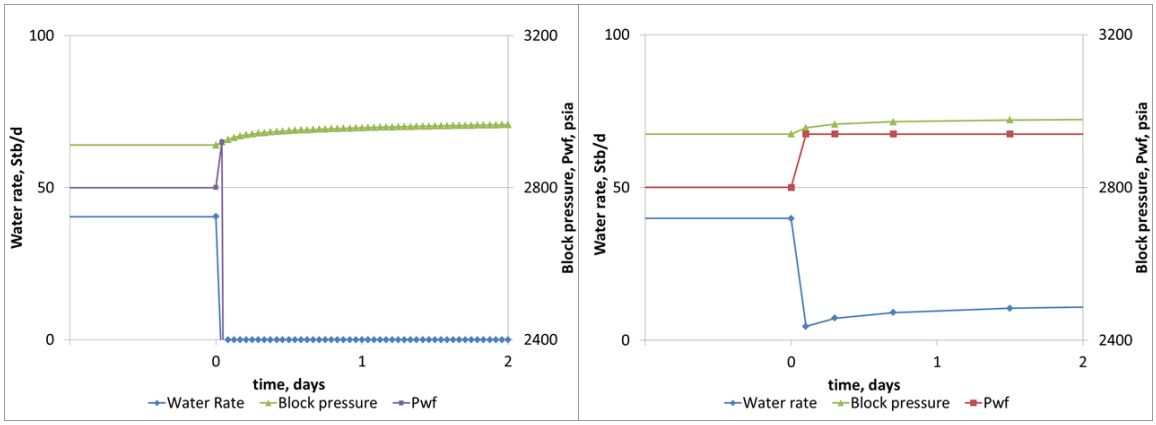

Fig. 4.8– Comparison of simulation results of water rate, well block pressure, and wellbore pressure solutions in Case1.a after increasing wellbore pressure slightly (left - ECL model, right – Sim2 model).

When the increase in the wellbore pressure was large, both simulators indicated water reinjection to the reservoir, which consequently increased pressure at the near-wellbore region. If this near-wellbore pressure is increased until it is impossible to reinject the water phase, the well is shut-in as given by the ECL model, while the well is switching back to produce again as predicted by the Sim2 model. **Fig. 4.9** illustrates wellbore pressure, pressure at the wellbore, and the water rate solutions in Case 1.b during this period. The injection used a simple relation: $\left(\frac{k_r}{\mu}\right)_{eq} = \left[\left(\frac{k_r}{\mu}\right)_g (1 - S_{wwf}) + \left(\frac{k_r}{\mu}\right)_w S_{wwf}\right]$, where the local volumetric ratio of the liquid phase inside the wellbore, S_{wwf}, is assumed to be 1.0 .

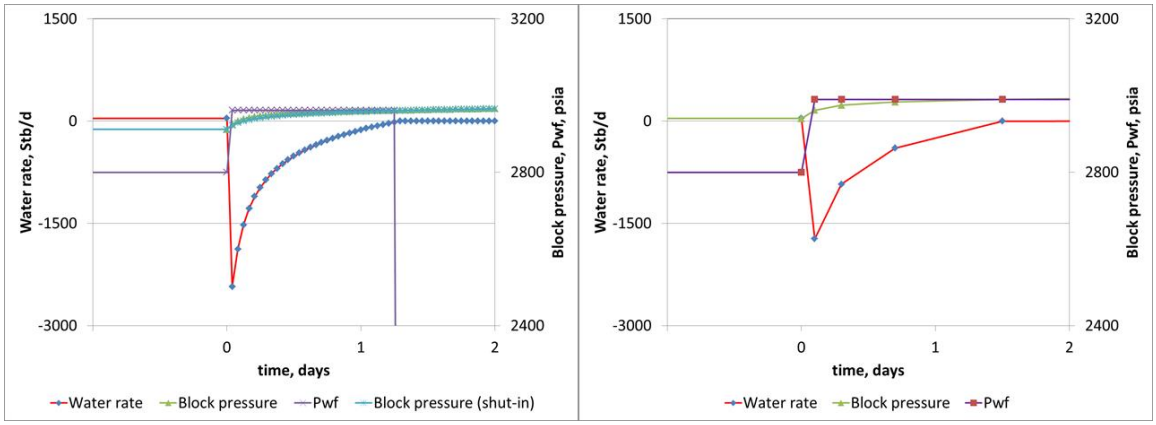

Fig. 4.9 – Comparison of simulation results of water rate, wellblock pressure, and bottomhole flowing pressure solutions in Case1.b after increasing wellbore pressure (left – ECL model, right – Sim2 model)

For Case 2, we considered capillary pressure in the one-layer model. In this case, the ECL model determines the gas as the reference phase pressure; thus the water reinjection can take place only when the wellbore pressure is larger than the gas-phase pressure in the well block. In the Sim2 model, the reinjection can take place if the wellbore pressure is greater than p^0 in the well block; otherwise, production corresponds to our wellbore boundary condition.

In Case 2.a, even though the increased wellbore pressure is larger than the water phase pressure in the well block, it is still less than the gas phase pressure. Therefore, the solution from the ECL model indicates that the well is shut in. On the other hand, the solution from the Sim2 model shows that the well still flows (albeit with reduced water rates) corresponding to the increased wellbore pressure. We note that the p^0 is very close

to gas phase pressure in this case.. **Fig. 4.10** shows wellbore pressure, reservoir pressure at the wellbore, and the water rate solutions during this period.

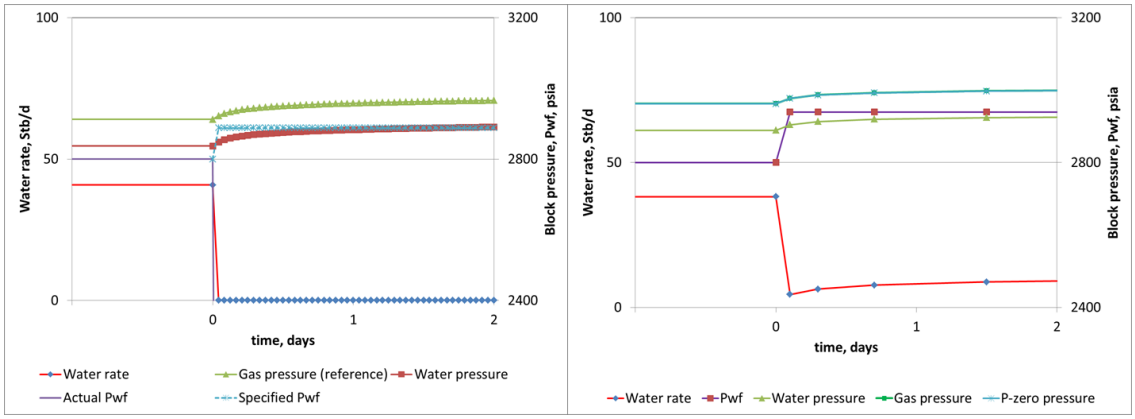

Fig. 4.10 – Comparison of simulation results of water rate, wellblock pressure, and bottomhole flowing pressure solutions in Case2.a after increasing wellbore pressure slightly (left – ECL model, right – Sim2 model)

A similar explanation to Case 1.b applies to the simulation results from Case 2.b. The water reinjection occurs because the wellbore pressure is greater than the current gas-phase pressure and the p^0, as indicated by ECL and the Sim2 models, respectively. Then, once the reservoir is built up such that the reference pressure is higher than the imposed wellbore pressure, the well is shut in as suggested by the ECL model, or is switched back to production suggested by the others. **Fig. 4.11** illustrates wellbore pressure, pressure at the wellbore, and the water rate solutions in Case 2.b during this period.

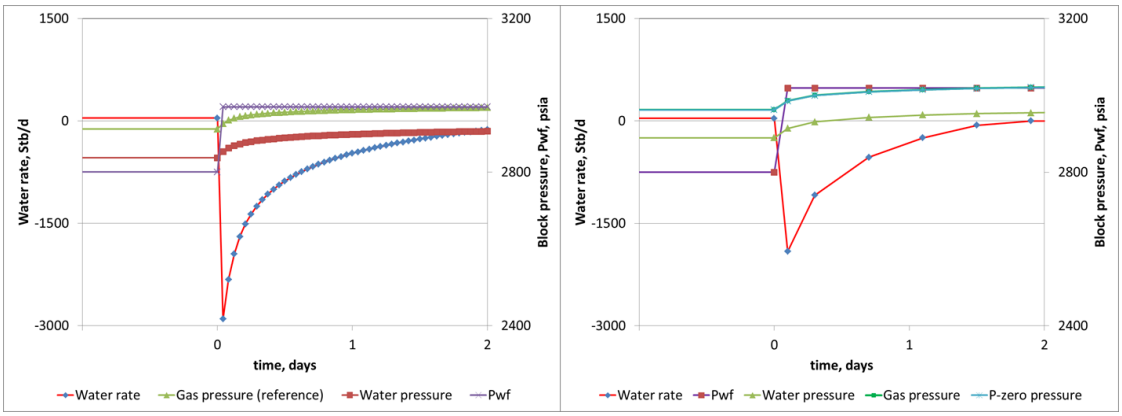

Fig. 4.11 – Comparison of simulation results of water rate, well block pressure, and bottomhole flowing pressure solutions in Case2.b after increasing wellbore pressure (left – ECL model, right – Sim2 model)

In Case 3, the two-layer model with equal original gas in place (OGIP) was constructed using a 600x1x2 grid system. Only one connection between the reservoir and the wellbore is located at the mid-depth of the upper well block. **Fig. 4.12** compares the initial pressure and water saturation in each layer for the ECL and Sim2 models. The pressure differences between layers are 84 psi for water and and 19 psi for gas phases. In the ECL model, we adjusted the depth of the gas/water contact in the initialization setup in order to obtain a match of vertical equilibrium conditions with the Sim2 model.

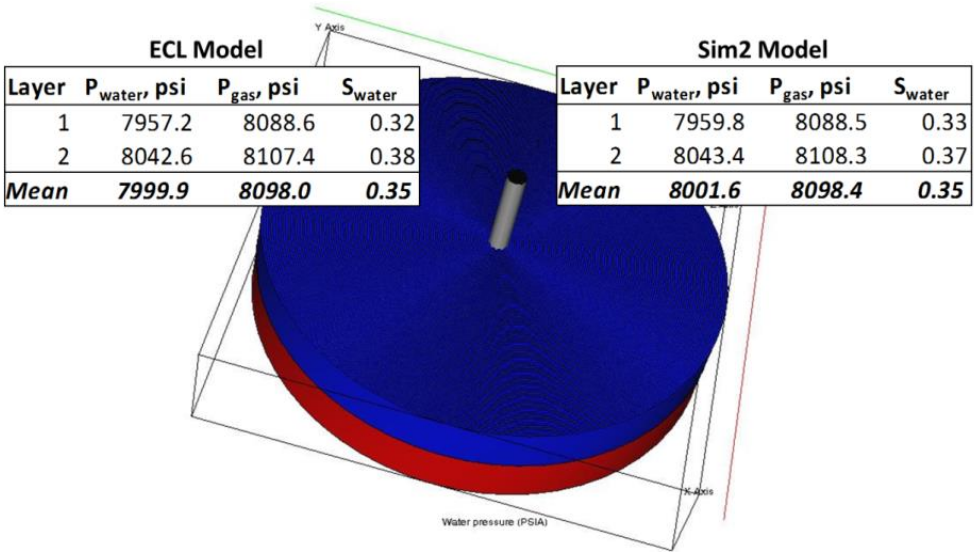

Fig. 4.12 – Water, gas phase pressures, and water saturation distribution at initial conditions in the two-layer model

Similar to the one-layer model, **Fig. 4.13** illustrates gas-phase pressure, water rate, and gas rate during the first stabilization in the two-layer model. The simulation results generated from ECL and Sim2 models are almost identical in this stabilization period.

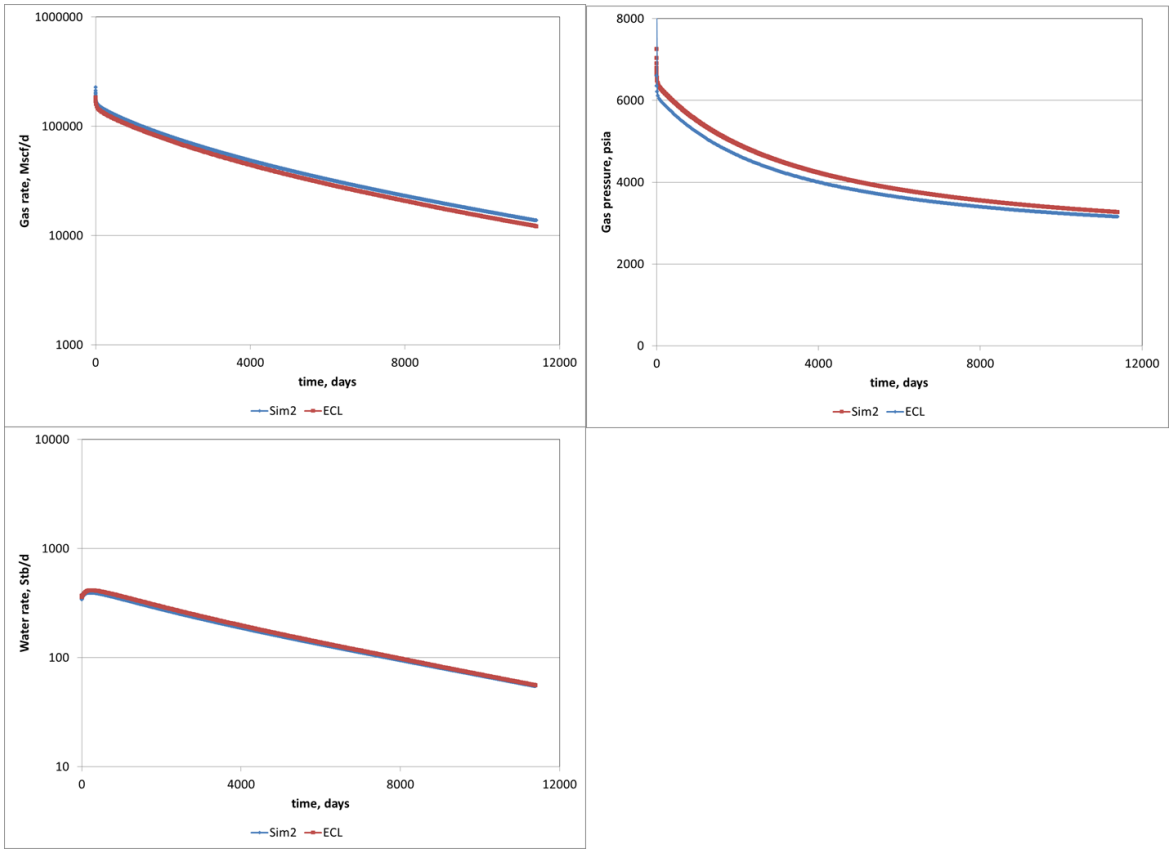

Fig. 4.13 – Comparison of simulation results of gas rate (top left), water rate (bottom left), and gas pressure (top right) at the well block versus time during the first stabilization period in Case 3

In addition, in Case 3.a, the imposed wellbore pressure is less than the reference pressure at the well block. Therefore, the well is shut in, as suggested by the ECL model, while lower flow rates are predicted by the Sim2 model. **Fig. 4.14** shows wellbore pressure, pressure at the wellbore, and water rate solutions during this period.

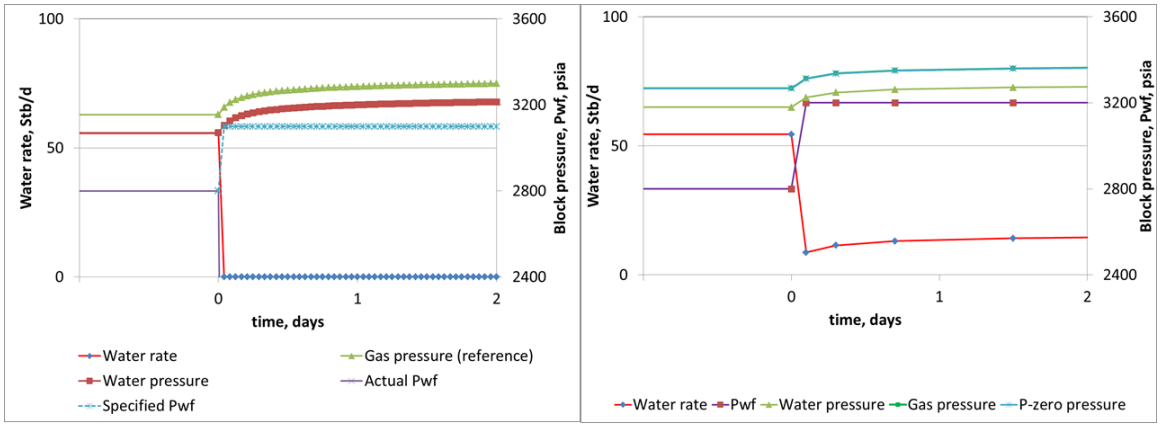

Fig. 4.14 – Comparison of simulation results of water rate, well block pressure, and bottomhole flowing pressure solutions in Case 3.a after increasing wellbore pressure slightly (left – ECL model, right – Sim2 model)

In Case 3.b, the increased wellbore pressure is greater than the current gas-phase pressure and p^0; thus, the water reinjection can take place as suggested by both models. **Fig. 4.15** shows wellbore pressure, pressure at the wellbore, and water rate solutions for Case 3.b.

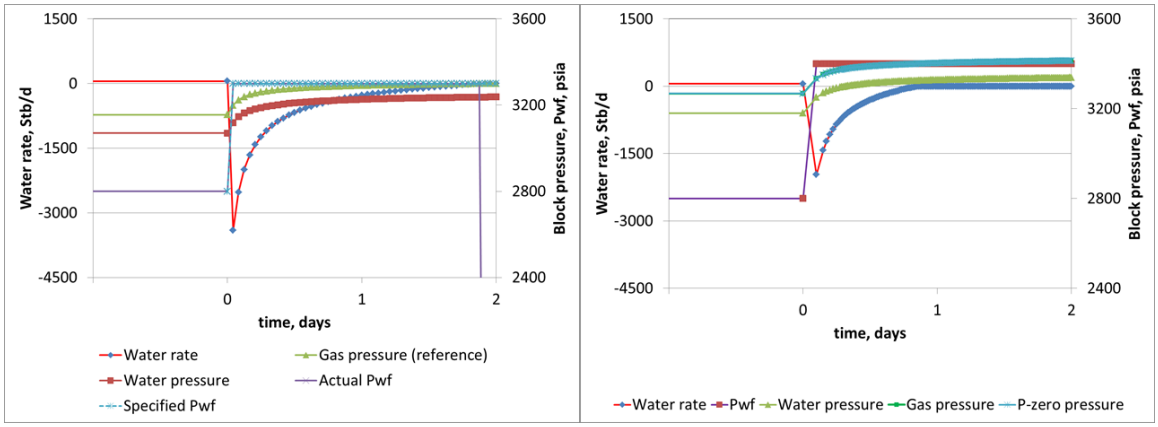

Fig. 4.15 – Comparison of simulation results of water rate, well block pressure, and bottomhole flowing pressure solutions in Case 3.a after increasing wellbore pressure (left - ECL model, right – Sim2 model)

Effect of Liquid Reinjection to the Near-Wellbore Region

In this section, we used our reservoir simulator to investigate effects in the near-wellbore region under liquid loading. The bottomhole pressure can undergo high-frequency fluctuations caused by the liquid column. If the immediate bottomhole pressure is higher than the pressure near the wellbore, the liquid can reinject back to the reservoir. This results in a U-shaped pressure profile in the near-wellbore region, as presented by Zhang et al. (2009). This U-shaped pressure profile will exist temporarily during the reinjection, and will disappear once the flow of gas and water phases towards the wellbore becomes steady again.

To illustrate this behavior, we simply imposed increasing bottomhole pressure on the reservoir initially in steady-state. We constructed the one-dimensional reservoir model using a 10x1x1 Cartesian-grid system. Each grid block has a dimension of

10x10x10 ft^3. A constant boundary pressure is assumed at the last grid block to represent the effect of the far region. The well model was placed at the first grid block with a constant bottomhole pressure. **Fig 4.16** is a schematic of this synthetic reservoir model.

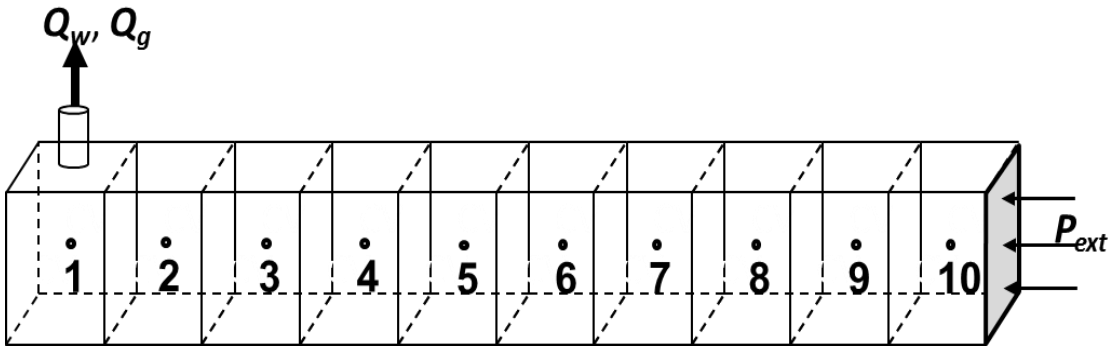

Fig.4.16 –Schematics of the linear reservoir model to generate the U-shaped pressure profiles

Reservoir parameters obtained from **Table 4.1** are used in this model. The relative permeability and capillary pressure curves from **Fig. 4.1** are also applied in this reservoir model. **Fig. 4.17** presents simulation results of pressure drawdown, reservoir pressure, and water saturation at the well block while imposing increased bottomhole pressure. With the new wellbore boundary condition, the water reinjection takes place for a short moment, only when the wellbore pressure is larger than the p^0 at the near-wellbore region. As a consequence, the water saturation around the wellbore increases. Once the reservoir pressure has built up higher than the bottomhole pressure, the water

and gas phases flow back into the wellbore. Only water phase is reinjected to the reservoir, corresponding to the liquid column that accumulates at the bottomhole of the loading well.

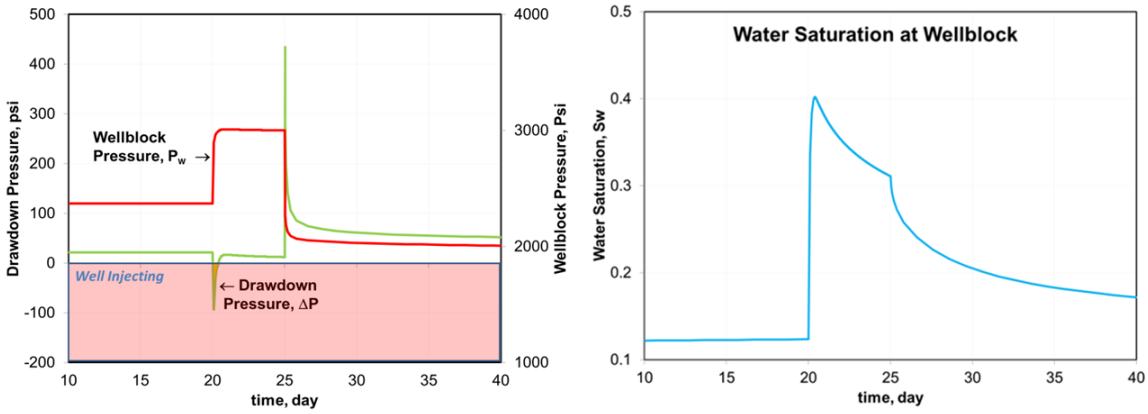

Fig. 4.17 – Simulation results of reservoir pressure, pressure drawdown, and water saturation at the wellblock over time in the one-layer Cartesian-grid system as a result of pressure-specified wellbore boundary conditions.

The water and gas phase pressure profiles during the reinjection period are illustrated in **Fig. 4.18**. The U-shaped pressure profile is observed in both the water and gas phases, as a result of water reinjection. In the U-shaped pressure profiles, the location of the minimum corresponds to the gridblock encountering inflow of the given phase from both directions. The water reinjection distance can be identified as the distance between the wellbore and the occurrence of the minimum. This U-shaped pressure profile gradually dissipates as new phase flows become steady in the near-well reservoir.

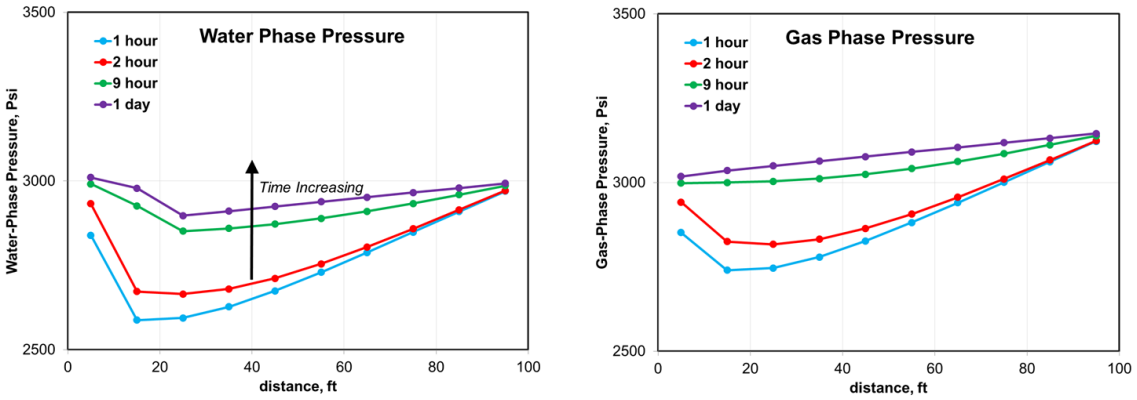

Fig. 4.18 – Simulation results of water and gas pressure profiles in the reservoir in the one-layer Cartesian-grid system during the liquid reinjection

The same reservoir model was used to investigate the impact of oscillating bottomhole pressure. We assumed that the fluctuation at the bottomhole caused by slug flow in the well could be represented by a sinusoidal pattern. **Fig. 4.19** illustrates the bottomhole pressure oscillation characterized by a sine function.

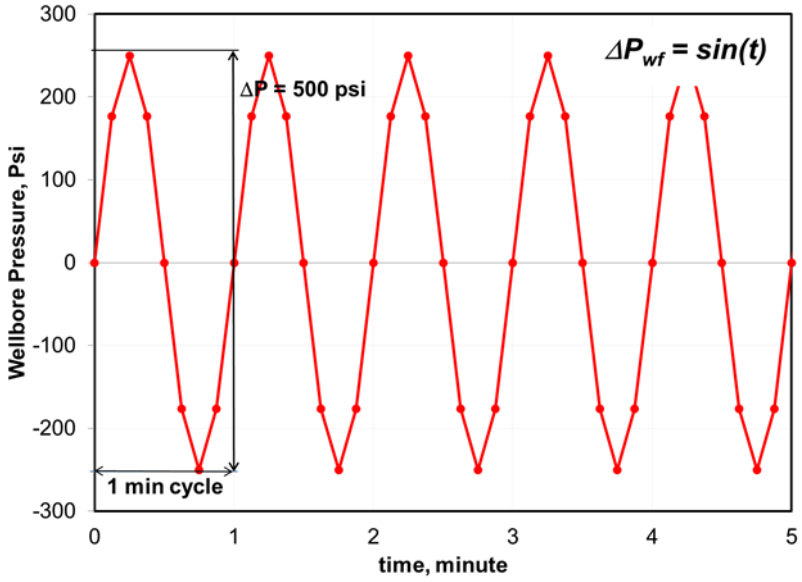

Fig. 4.19 – A sinusoidal function representing bottomhole pressure as a function of time, representing impact of liquid loading phenomena to the near-well reservoir

We performed a simulation of the reservoir under oscillating bottomhole pressure for 5 days. The simulation result of the cumulative gas production is compared with the case with a constant bottomhole pressure as shown in **Fig. 4.20**. When the bottomhole pressure is oscillating, less gas can be produced from the reservoir because the water reinjection increases the water saturation in the near-wellbore region, at least temporarily. This increase in saturation reduces the gas mobility around the wellbore; hence, less gas flows.

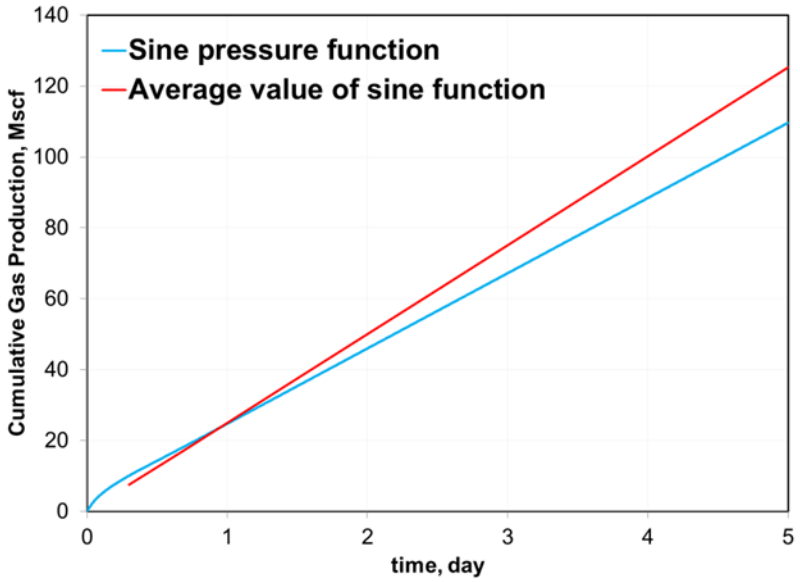

Fig. 4.20 – Comparison of cumulative gas production over the period of 5 days demonstrated the effect of oscillating pressure to reservoir production.

Use of Reservoir Simulation to Investigate Backpressure Effect on Gas Flow in Porous Media

Our reservoir simulator was also applied to validate results of the experimental investigation on the backpressure effects in gas flow through porous medium. This experimental study is a part of the same JIP project on the liquid loading problem. The experiment was conducted at Clausthal University of Technology, Germany. The main objective for this experiment was to verify the U-shaped pressure profile that exists in multiphase flow in the near-wellbore region during liquid loading, as presented by Zhang et al. (2009). The current verification targeted the single-phase compressible flow to avoid complexity in multiphase measurement.

Y. Wang (2012) modified the standard Hassler cell permeameter to investigate pressure responses during transient conditions and named it the Institut für Tiefbohrkunde und Erdölgewinnung Closed Loop Circulating System (ITE CLCS). The pressure taps were installed in the ITE CLCS in order to monitor pressure distribution along the core sample during the experiment. The nitrogen gas storage was also attached at the downstream end of the ITE CLCS to simulate effect of backpressure. **Fig. 4.21** outlines the main components of the ITE CLCS.

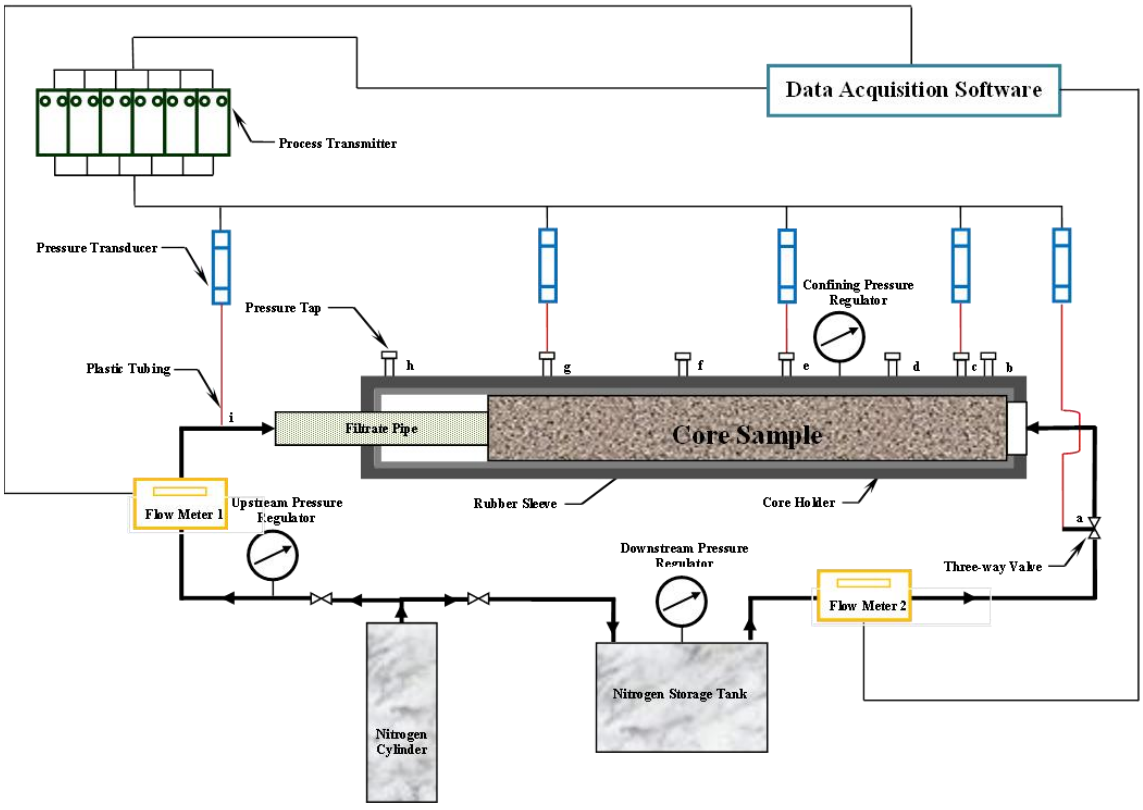

Fig. 4.21 – Schematic of the ITE CLCS

The test procedure to develop the U-shaped pressure profile in the core sample can be described as follows. Initially, the nitrogen gas was flowed through the core sample with the inlet pressure of 5 barg and the outlet pressure of zero barg until the steady-state flow condition was reached. Then, the three-way valve was switched to immediately connect the core sample to the nitrogen storage tank. This was to impose backpressure onto the core sample. The U-shaped pressure profiles were recorded until the new steady state condition was reached. The location of pressure taps and mass flow meters as shown in the schematic were interpreted and reported by the data acquisition software.

In this experiment, the upstream pressure of the core sample was always maintained at 5 barg. The imposed downstream pressures were varied at 1, 3, and 4.8 barg.

To validate accuracy in the experiment, our reservoir simulation was modified to gas flow modelling. The numerical formulation for the water/gas simulation described in Chapter III was embedded into this single-phase gas flow model.

We incorporated the Klingkenberg effect on the low-pressure gas flow system to correct for slippage of gas molecules in determining effective permeability in this experiment. The resulting effective permeability is given by:

$$k_{\text{eff}} = k_{\text{abs}}\left(1 + \frac{b}{p}\right) \tag{4.1}$$

where b is the Klingkenberg correction parameter; k_{abs} is the average absolute permeability; $p_g$is the gas pressure; and k_{eff} is the effective permeability.

Table 4.3 summarizes the parameters used in the simulation as reported by Liu et al.(2013). Based on the available grid-geometry system, the cylindrical core sample was discretized into 52 rectangular grids with the equivalent surface flow area and volume. Isothermal system and homogeneity properties were assumed in all cases. Constant pressures at the inlet and outlet boundaries were defined as boundary conditions in both stages of simulation.

Table 4.3 – Key parameters for simulation to validate the experiment

Core Parameters	**Values**	**Unit**
Length	20.765	cm
Cross-sectional area	5.212	cm^2
Porosity	0.18	
Intrinsic Permeability	5.51E-15 (5.6)	m^2 (md)
Inlet pressure	5	barg
Klinkenberg parameter	4.04E+5	Pa
Atmospheric pressure	0.951	bara
Atmospheric temperature	18	°C

The same sequence of boundary pressures as in the experiment was followed in our simulation. The simulation results were compared with experimental data through time histories of pressure profiles. During the first stead-state flow condition, the

pressure profiles between the experiment and the simulation were within reasonable agreement, as shown in **Fig. 4.22**.

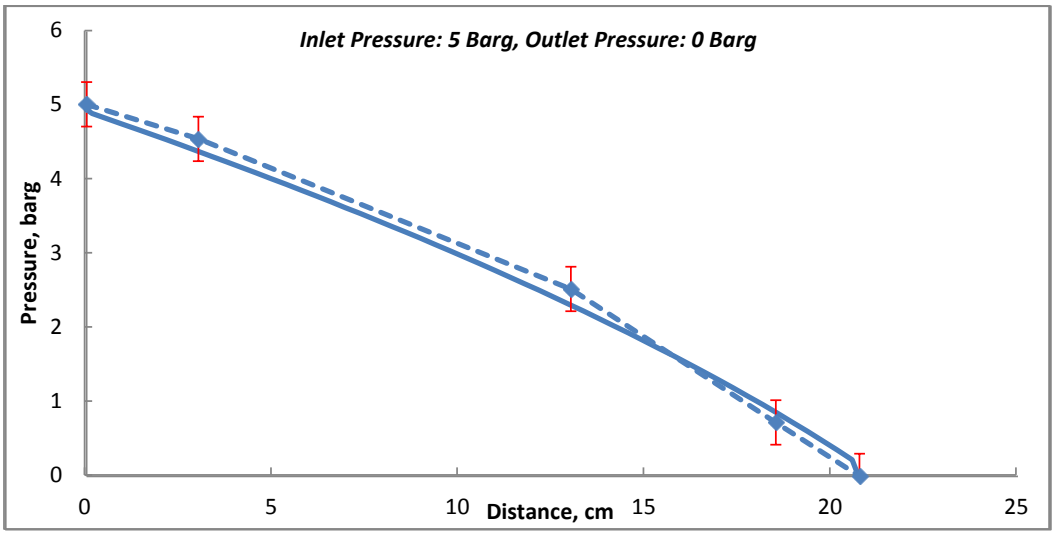

Fig. 4.22 – Comparison of pressure profiles between experimental data (dotted line) and simulated results (solid line) under steady-state condition

The U-shaped pressure profiles were developed once the outlet pressure was suddenly increased similar both in the experiment and the simulation. However, in the simulation, these pressure profiles occurred immediately after imposing new outlet pressures and dissipated within a minute after, while in the experiment, the U-shaped pressure profiles seem to occur immediately and last a longer time. In essence, the transient pressure response from the simulation is faster than that from the experiment. **Fig. 4.23** compares the U-shaped pressure profiles of the experiment with the outlet pressure of 3 barg.

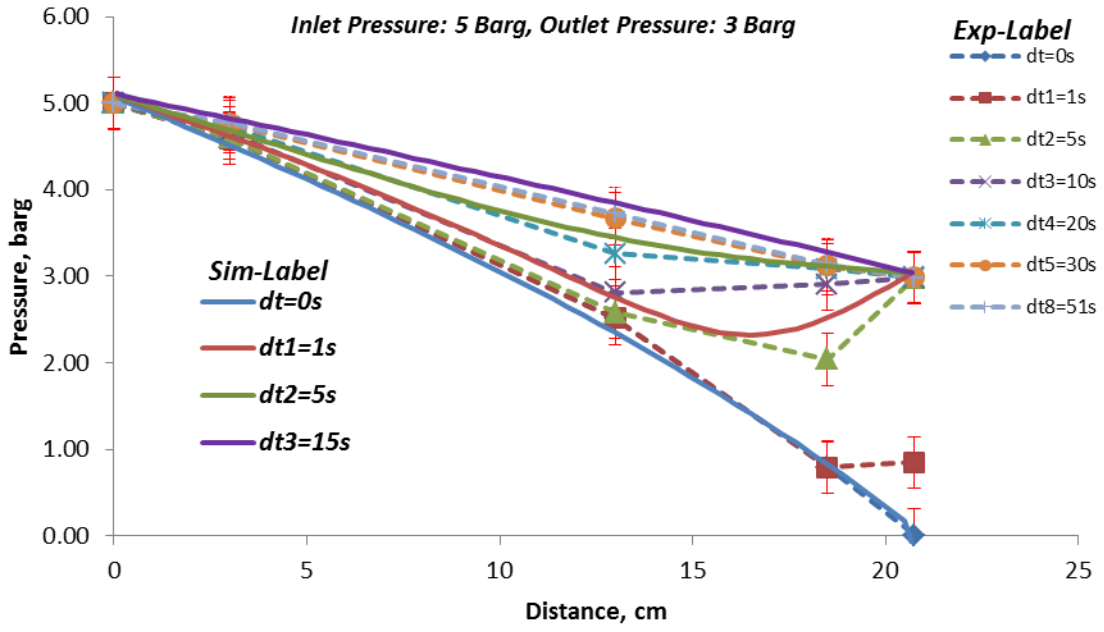

Fig. 4.23 – Comparison of pressure profiles between experimental data (dotted line) and simulated results (solid line) during transient period at the outlet pressure of 3 barg. Note that the simulations were performed by assuming that the outlet pressure switches instantaneously from 0 barg to 3 barg; the experiments show a delay time (>1 s) due to the slow response of control valves and pressure transducers.

The slow transient responses in the experiment was analysed by incorporating error propagation in the data measurement. Several factors in the experimental set-up contribute to the mismatch between simulation results and the experimental data. The major contributed factor is believed to be associated with the time required in processing the measurement signal in the current data acquisition system. Moreover, switching the three-way valve by hand required a time delay in transient response in the experiment. The equipment upgrade should improve accuracy in this experiment.

In addition, the sensitivity analysis on the measured rock parameters was conducted to understand the impact of measurement accuracy in the transient response. The measured rock parameters are the porosity and the absolute permeability.
The sensitivity analysis was carried out for the experiment result with the outlet pressure of 3 barg. Two values of porosity and permeability were arbitrarily selected to represent extreme variations in this rock sample. Output data were outlet flow rates at the first steady-state condition and transient time required to reach the new steady-state flows. When reaching steady state condition, inlet rate must equal the outlet rate. **Tables 4.4** and **4.5** summarize simulation results from the sensitivity analyses.

Table 4.4 – Simulation results from sensitivity to porosity variations

Output parameters	**Low** **10%**	**Base** **18%**	**High** **25%**
Flow Rate (ml/min)	96	96	96
Transient time (sec)	19	38	51

Table 4.4 shows that porosity is insensitive to flow rate calculation, according to Darcy's law. At steady-state flow, there was no accumulation of gas in the core sample; therefore, the flow rate of all cases with varying porosities must be similar. However, the low-porosity case took less transient time to reach the new steady-state condition as the gas had less pore space to compress/expand than in the base case, and vice versa.

Table 4.5 – Simulation result from sensitivity on permeability variations

Output parameters	**Low** **1 md**	**Base** **5.6 md**	**High** **20 md**
Flow Rate (ml/min)	17	96	344
Transient time (sec)	204	38	11

According to Darcy's law, flow rate is proportional to the permeability of the rock. From **Table 4.5,** simulation results show the same agreement, in that the low-permeability case has less flow rate, and vice versa. Moreover, the low-permeability case takes more transient time to stabilize to the new steady-state condition, while the high-permeability case takes slightly less time than the base case. This relationship is not linear; however, it is clear from this table that in low-permeability rock, stabilization will take a lot more time during transient conditions than in high permeability rock.

The simulation results also show that the permeability variation is more sensitive to both transient time and flow rate than to porosity variation. Thus, it is important that the measurement of the permeability must be precise to accurately analyze transient flow conditions in the experiment.

Conclusion

The simulation results generated from the new reservoir simulation were compared with those from the Zhang et al. (2010) simulator. The discrepancy in the

solution at the boundary indicated numerical errors generated in the Zhang et al. model while imposing bottomhole pressure oscillation. This numerical problem was caused by incorrect wellbore boundary conditions embedded in the sink/source term.

Our reservoir simulation was also evaluated against the commercial package, ECLIPSE100. The simulation run concerning the near-switching in the flow direction was investigated. Our simulation was always able to predict flow directions without demanding shut-in (depending on the instantaneous state on the two sides of the connections), while ECLIPSE100 will indicate that the well should be shut in if the upstream pressure of the boundary is insufficient to continue flowing at the predetermined direction defined by users. Thus, our numerical simulation is more appropriate for modeling of the liquid loading phenomena.

The investigation of the U-shaped pressure profiles in the near-wellbore region shows that, during the liquid reinjection to the near-wellbore region, our reservoir simulation can indicate the U-shaped pressure profile, similar to that presented by Zhang et al. (2009). The reservoir simulation under the oscillating bottomhole pressure indicated that the cumulative gas production will more likely be lost due to worse gas mobility in the near-wellbore region than in conditions with constant bottomhole pressure.

Our numerical simulation was adjusted for the gas flow through porous media to mimic the experimental investigation of the U-shaped pressure profile under backpressure. The simulation results show that the with the same pressure condition, the U-shaped pressure profiles generated from the simulation dissipate much faster than that

in the experiment. In the experiment, the inlet flow rates were not equal to the outlet ones, which probably indicated leakage in some parts of the testing apparatus or the inaccuracy in the measuring system. Further modification of the experimental setup is required to improve experiment accuracy. Sensitivity on porosities and permeabilities was conducted to identify the uncertainty in those parameters to the response during the transient condition.

CHAPTER V

COUPLED RESERVOIR/WELLBORE SIMULATION TO INVESTIGATE METASTABLE FLOW CONDITIONS IN LIQUID LOADED GAS WELLS

Introduction

The complexity in modeling the liquid loading problem associates with the dynamic interaction between the wellbore and the near-wellbore region. Metastable flow is one of the production behaviors found in liquid-loaded wells. It is strongly related to the dynamic interaction between the two subsystems. The modeling of metastable flow was initially presented by Dousi et al. (2006) by simple steady-state IPRs combined with an empirical wellbore model.

This chapter presents an application of dynamic modeling for the metastable flow condition. The simplified steady-state IPRs, representing the reservoir, can be replaced by our numerical simulation. This can be beneficial in investigating the impact of reservoir depletion in triggering the onset of metastable flow, which is different from Dousi et al.'s (2006) hypothesis that the onset of metastable flow is when the flow is below critical flow rate values. With the new wellbore boundary, backflows can be easily predicted without numerical difficulty.

As an appropriate wellbore model was not readily available, we applied the empirical model used in the Dousi et al. approach in our dynamic modeling. This empirical wellbore model accounts for hydrostatic pressure and friction pressure losses in gas flow, but also the liquid accumulation at the bottomhole during liquid loading.

The coupling algorithm between the two submodels is implemented in an implicit scheme. During the simulation, the reservoir model assumes the bottomhole pressure to calculate the flow rate of each phase at the interface. The wellbore model then calculates liquid accumulation, pressure loss in the tubing, and the flow rates at surface. An iterative procedure is continued to minimize appropriate objective functions, depending on specifications of the wellbore boundary at the wellhead. This iterative process is carried out by a simple bisection scheme.

Analysis of the Dynamic Modeling Approach from Dousi et al. (2006)

Dousi et al. (2006) developed their numerical approach to explain the mechanism behind producing gas wells that were able to flow at a stable gas velocity below that corresponding to Turner's (1967) criteria. This particular type of stable flow was referred to as *metastable.* In the rest of this chapter, the Dousi et al. approach will be referred to as the Dousi model.

The Dousi model can describe the metastable condition by a simple wellbore model and a single reservoir with two connection points as shown in **Fig. 5.1**.

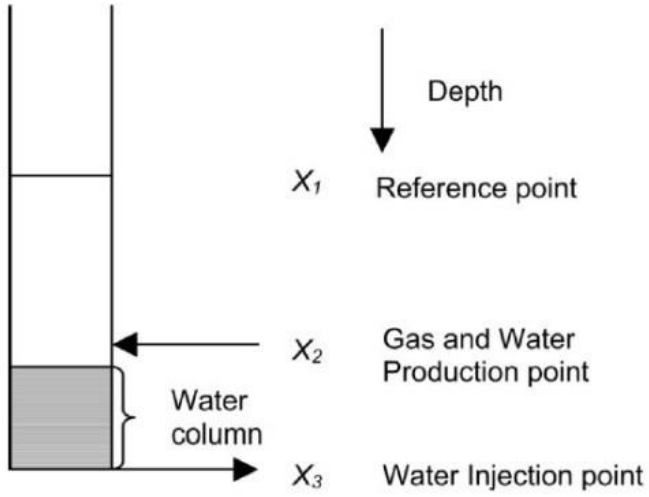

Fig. 5.1–Schematic of the Dousi model describing the metastable flow condition

The wellbore model can be described in two parts. The upper part considers the hydrostatic and friction effects of a gas flow at a given flowing bottomhole pressure following the Cullender-Smith (1956) relation as given by:

$$\left(p_{fbh1}\right)^2 = B\left(p_{fth}\right)^2 + C\left(q_g\right)^2 \tag{5.1}$$

where *B* and *C* are outflow constants reflecting hydrostatic head and friction effects, respectively; p_{fth} is the flowing wellhead pressure; q_g is the surface gas flow rate; and p_{fbh1} is the flowing bottomhole pressure at the reference point x_1 in **Fig. 5.1**.

Below the reference point x_1, the well model calculates the hydrostatic gradient of the water and gas, assuming that frictional effects in this part can be neglected. Thus, the bottomhole pressure at the production point x_2 can be evaluated by:

$$p_{fbh2} = p + G_w h_{wc1} + G_g h_{gc1} \tag{5.2}$$

where h_{wc1} and h_{gc1} are water and gas heights between the reference point x_1 and the production point x_2, respectively; and G_w, and G_g are the hydrostatic gradient of the water and the gas, respectively.

Similarly, the flowing bottomhole pressure at the injection point x_3 is evaluated by:

$$p_{fbh2} = p_{fbh1} + G_w h_{wc2} + G_g h_{gc2} \tag{5.3}$$

where h_{wc2} and h_{gc2} are water and gas heights between the production point x_2 and the injection point x_3, respectively.

In the Dousi model, there are two reservoirs. Gas and water are produced from the upper reservoir while water can be reinjected at the lower reservoir. The pressure difference between the reservoirs correspond to the gas gradient:

$$p_{res,w} = p_{res,g} + G_g h_{gc} \tag{5.4}$$

where h_{gc} is the distance between the injection and the production point; $p_{res,g}$ is the reservoir pressure at the production point x_2; and $p_{res,w}$ is the reservoir pressure at the injection point x_3.

The inflow gas rate at the production point is calculated from a simple quadratic equation given by:

$$\left(p_{res,g}\right)^2 - \left(p_{fbh2}\right)^2 = A_g q_g \tag{5.5}$$

where A_g is the gas inflow factor and q_g is the gas flow rate. The model neglects possible reinjection at the production point x_2.

The coproduced water is evaluated by:

$$q_{w,prod} = F_{wg} q_g \tag{5.6}$$

where F_{wg} is the water/gas ratio.

Similarly, the injection of water at the injection point x_3 is calculated by a linear inflow performance relation expressed as:

$$p_{fbh3} - p_{res,w} = A_w q_{w,inj} \tag{5.7}$$

where A_g is the water resistance factor and $q_{w,inj}$ is the water injection rate. The model neglects possible production at the injection point x_3.

In Turner's criteria, the critical rate is evaluated by a simplified formula as:

$$q_c = C_{st}\sqrt{P_{fth}} \tag{5.8}$$

where C_{st} is a constant including the impacts of relevant parameters in the equation for evaluating the Turner criteria; q_c is the critical Turner rate.

In the iterative numerical scheme, the Turner rate is compared with the calculated gas flow rate. If the gas flow rate is greater than the Turner rate, all water is produced to surface and the water column will not rise. If the flow rate is less than the Turner rate, all produced water in that time step will accumulate at the bottom of the well. The numerical schemes iterate with the new calculated gas flow rate, according to the new flowing bottomhole pressure, until the change in calculated flow rates is less than the preset criteria. After that, it moves to the next time-step. **Fig. 5. 2** depicts a flow chart for the numerical scheme of the Dousi model.

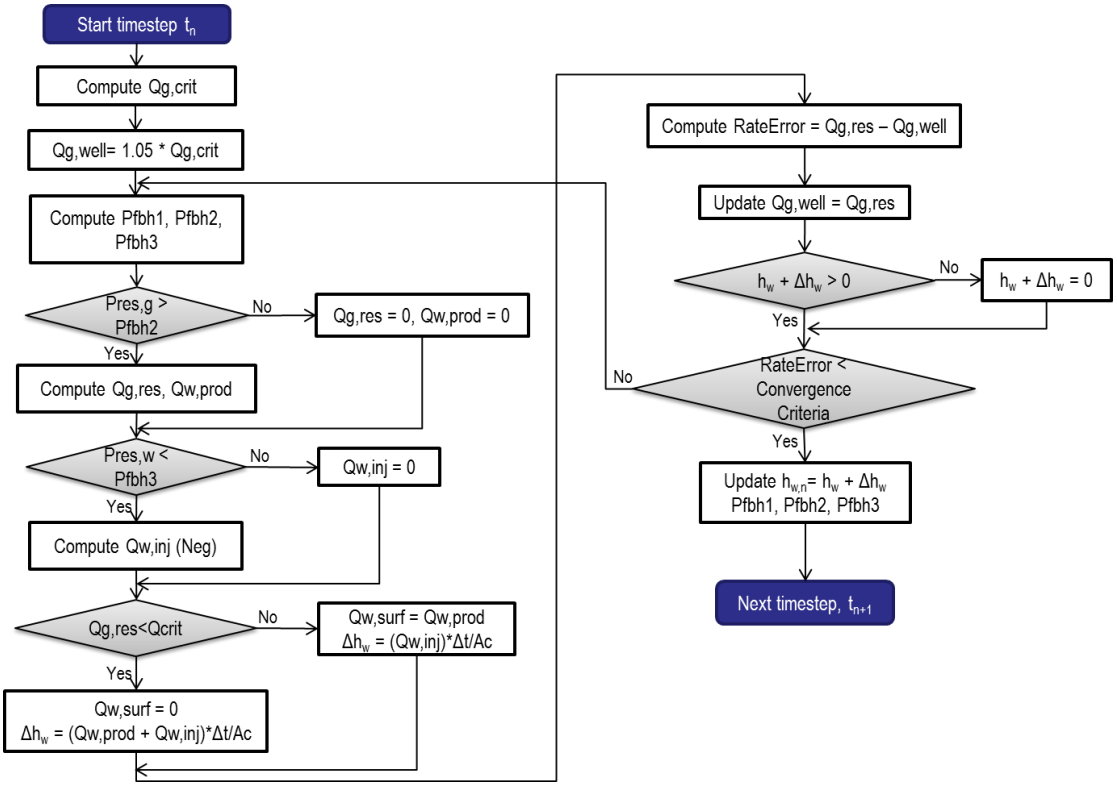

Fig. 5.2–A flowchart summarizing a numerical procedure in the Dousi model

From the Dousi model, the main mechanism to trigger the metastable regime is a larger hydrostatic pressure difference inside the wellbore than in the reservoir between the two level called the production and the injection points. In this model the flow directions are pre-defined, the model does not allow backflow with respect to the original direction. Moreover, the accumulated water is limited by the location of the reference point. To make this algorithm work, the distance between the production and injection levels must be sufficient to create a large hydrostatic pressure difference during the liquid loading regime. In spite of these limitations, the Dousi concept is able to describe dynamic interaction between the reservoir and the wellbore and hence

represents a significant step toward understanding the liquid loading phenomenon. In our work we replicate the basic concept but with a more detailed reservoir and wellbore model.

To follow this logic, we developed a simple program following **Fig.5.2**. The program is written in VBA. We used the input parameters illustrated in a demonstration example shown by Gool and Currie (2007). **Table 5.1** summarizes their parameters.

Table 5.1 – Simulation parameters for the validation of the Dousi's model

Reservoir Parameters	
$\rho_{g,sc}$	0.8 kg/m^3
ρ_g	52.8 kg/m^3
ρ_w	1000 kg/m^3
F_{wg}	50 m^3/(10^6·m^3)
$P_{res,g}$	66 bar
h_{gc}	dx_{23} m
Well Parameters	
A_g	10 (bar^2·d)/(10^3·m^3)
A_w	5 (bar·d)/(m^3)
B	2.2
C	0.015 [(bar·d)/(10^3·m^3)]^2
C_{st}	32 (10^3·m^3)/(d·√bar)
dx_{23}	200 m
x_1	0
x_2	170
x_3	$x_2 + dx_{23}$
D_{lin}	0.127 m

Fig. 5.3 shows the comparison of simulation results generated by our program and that shown by Gool and Currie (2007). The liquid loading condition is initiated once the critical Turner rate becomes larger than the gas flow rate as a consequence of increase in tubinghead pressure in Day 2. After that, the water column begins to rise at the bottom of the well, resulting in a decrease in inflow gas rate and coproduced water. As soon as the bottomhole pressure at the injection point x_3 is higher than the reservoir pressure, the reinjection can take place at the bottom point, and the water level decreases. The metastable regime is developed at the end of day 2 when the water production rate equals the water injection rate. After day 3, the increase in tubinghead pressure results in higher bottomhole pressure at the production point, $x_{2;}$ hence, the production ceases. The reinjection continues until there is no water column left at the bottom of the well.

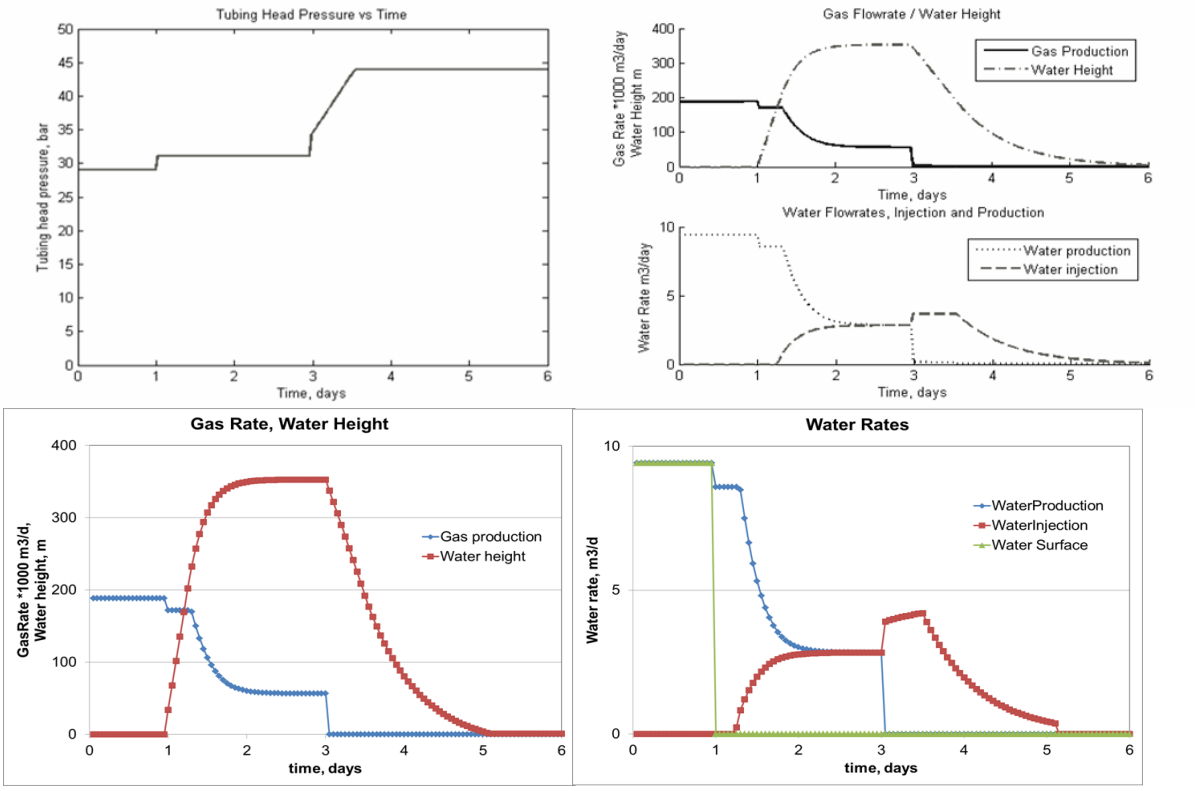

Fig. 5.3–Simulation results generated from our program are compared with those shown by Gool and Currie (2007). The tubinghead pressure (top left) is used as input to calculate gas flow rates and water rates shown by Gool and Currie (top right) and in the new program (bottom left and right).

From the demonstration result, the factor that triggers the loading condition is the increase in tubinghead pressure. From the Dousi model, the critical Turner rate is evaluated with respect to the tubinghead pressure and then compared with the calculated gas flow rates, assuming that the reservoir pressure is constant within 6 days of prediction.

A more realistic set of conditions would consider that the reservoir pressure declines if the well is flowing for a longer period of time (depletion). Here we show that

depletion can also trigger liquid loading without artificially impose a large increase in the tubinghead pressure. The simulation result shown in **Fig. 5.4** illustrates effect of depletion.

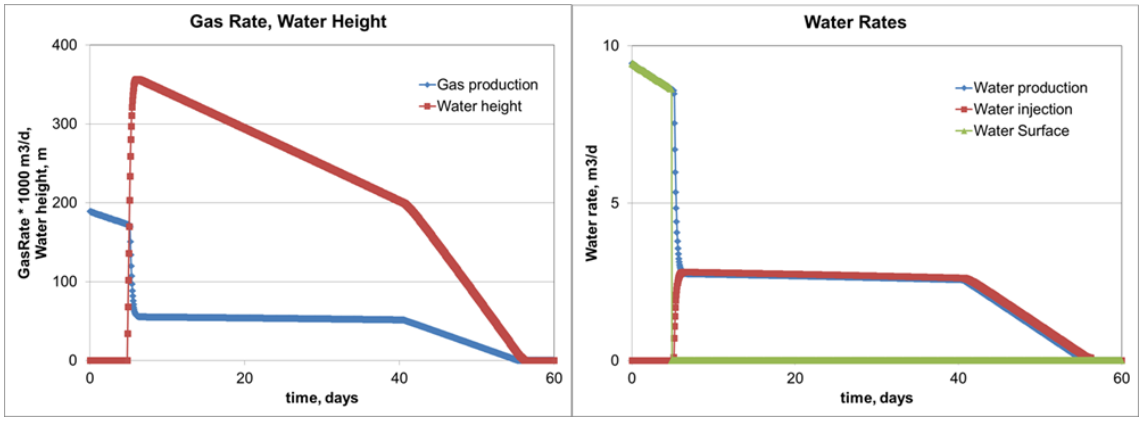

Fig. 5.4 – Simulation results generated from the new program for a specific case showing that the metastable regime is developed as the reservoir pressure declines.

From **Fig. 5.4**, the input parameters are taken from **Table 5.3**, but the flowing tubinghead pressure is held constant at 29 bar (426 psi). The reservoir pressure declines with 0.4 bar/D (6 psi/D). In this run we applied the depletion at both connection points. As the reservoir pressure decreases, the gas flow rate reduces over time. As soon as the gas flow rate falls below the Turner value (corresponding to the tubinghead pressure of 29 bar (426 psi)), the coproduced water accumulates in the well and develops a water column at the bottom of the well very rapidly. As a result, the reinjection can take place at the injection point. The metastable regime establishes for a long period of time (albeit with gradually declinin gas production rate). The simulation results confirm that not only

the constraints from the wellbore but also those from the reservoir can contribute to the onset of liquid loading. These dynamic interactions between the two subsystems make the phenomena complex to analyze.

Model Replication for the Metastable Flow Conditions with Our Numerical Simulation

As previously mentioned, the Dousi model is not able to reproduce changes in flow direction at the connection points. In addition, the model neglects the capillary pressure effect in the reservoir. These assumptions can be eliminated by applying our numerical reservoir model instead of the original Inflow Performance Relationship.

In our simulation, the bisection algorithm is applied in coupling the numerical solution of the two subsystems. The iterative coupling is done as follows. Initially the reservoir model is run with a guessed wellbore flowing pressure at the nodal (reference) point. Using the calculated phase flow rates at the connections, the wellbore model calculates the wellbore pressure loss and liquid holdup in the tubing, using imposed conditions at the wellhead (e.g. wellhead pressure or rate of one of the phases). Then the algorithm updates the bottomhole pressure and evaluates the mismatch between the guessed and the calculated wellbore pressure. If the residual error of this mismatch reduces below the preset threshold, the simulation advances to next time step.

To show that our numerical reservoir simulator can replace the reservoir model described in the Dousi approach, the input parameters in **Table 5.1** were converted to describe an equivalent reservoir in our numerical model. In the rest of this chapter, we

refer to it as the "numerical model". **Table 5.2** compares input parameters in the Dousi model and our model. **Fig. 5.5** shows the relative permeability and capillary pressure curves in the numerical model.

Table 5.2 – Input parameters in the Dousi model and the numerical model used in the simulation study

Modeling Approach					
Dousi Model			**Numerical Model**		
Reservoir Parameters			**Reservoir Parameters**		
$\rho_{g,sc}$	0.8	kg/m^3	Layer thickness	600	ft
ρ_g	52.8	kg/m^3	Reservoir radius	1000	ft
ρ_w	1000	kg/m^3	Porosity	10	%
F_{wg}	47.6	$m^3/(10^6 \cdot m^3)$	Absolute permeability	1.5	md
$P_{res,g}$	65.64	bar	Initial pressure, upper layer	944	psi
$P_{res,w}$	66.34	bar	Initial pressure, lower layer	997	psi
			Initial water saturation	30	%
			Reservoir temperature	260	deg F
			Pressure depletion rate	2	psi/D
Well Parameters			**Well Parameters**		
A_g	10	$(bar^2 \cdot D)/(10^3 \cdot m^3)$	Openhole diameter	7	in
A_w	5	$(bar \cdot D)/(m^3)$	Tubing diameter	5	in
B	2.2		Total depth	7700	ft
C	0.015	$[(bar \cdot d)/(10^3 \cdot m^3)]^2$	Wellhead pressure	430	psi
C_{st}	32	$(10^3 \cdot m^3)/(d \cdot \sqrt{bar})$	Wellhead temperature	60	deg F
dx_{23}	200	m			
x_1	0				
x_2	170				
x_3	$x_2 + dx_{23}$				
D_{lin}	0.127	m			

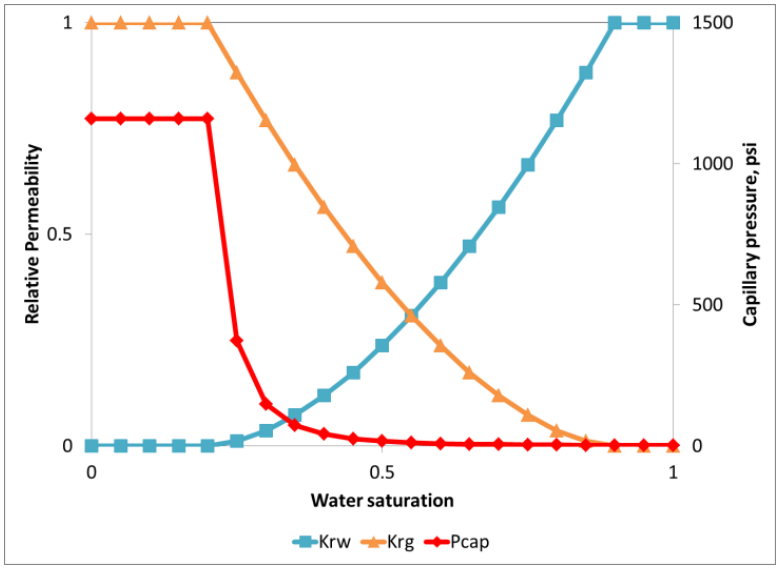

Fig. 5.5 – The relative permeability and capillary pressure curves used in our numerical model

The two-layer radial reservoir with equal grid spacing had a total of 10x1x2 gridblocks. Each layer is 600 ft in thickness. An external boundary pressure with decline rate of 2 psi/day was applied at the external boundary to represent impact from the far region. The vertical well was 7700 ft in depth. The perforations were at 7100 and 7700 ft, which corresponds to the bottom of the reservoir gridblocks.

In the numerical model, we used the similar wellbore model to reproduce the Dousi concept. For the purpose of comparison, the Dousi assumptions were also applied without change in the numerical model: the production took place at the upper perforation while the injection took place at the lower perforation. Possible backflow from these specified flow directions was excluded from calculation. The capillary pressure was also excluded.

The simulation results generated from the Dousi model and the numerical model are compared in **Fig. 5.6**.

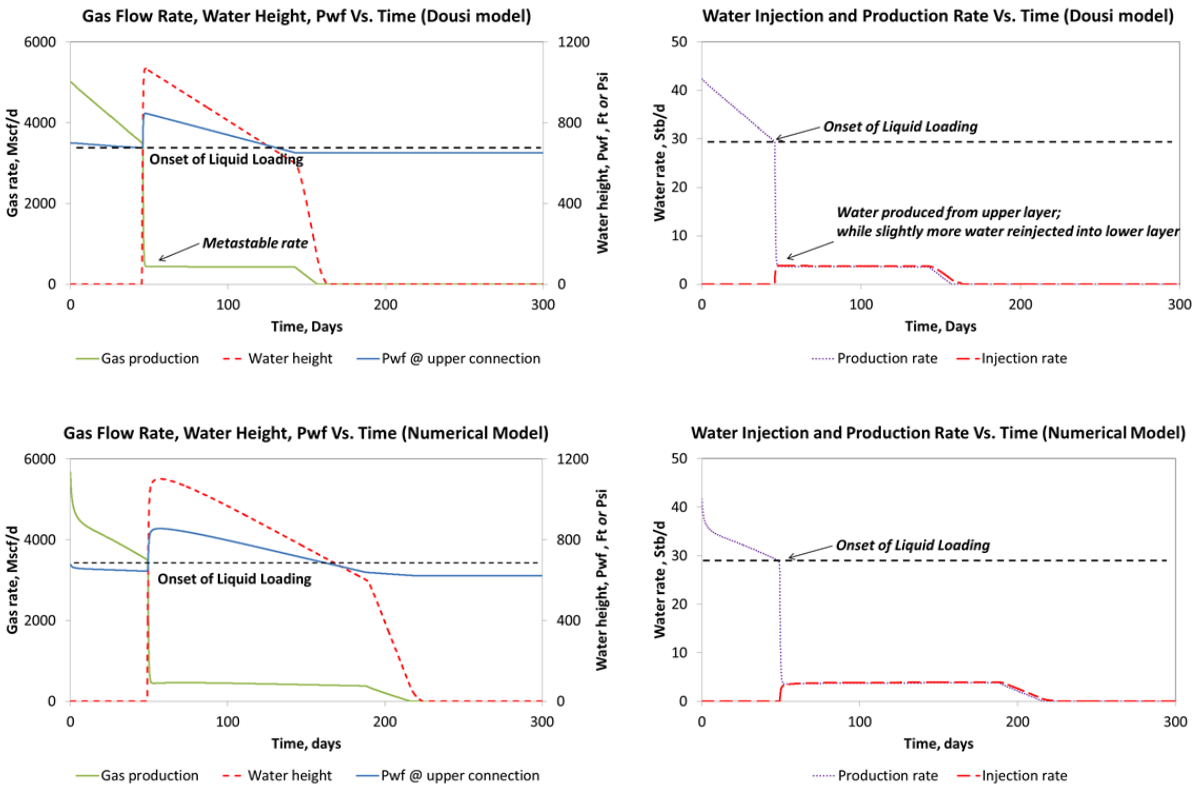

Fig. 5.6 – Comparison of simulation results generated from the Dousi model (top) (the program described on pages 80-81) and the numerical model (bottom)

From the comparison, the numerical model was able to replicate the results from the Dousi model. The metastable regime was rapidly established once the gas flow rate was lower than the Turner rate, which was set at 3.5 MMscf/d. However, the duration for the metastable regime in the numerical model was longer than that in the Dousi model

because of the effect of reservoir pressure depletion. In the Dousi model, the pressure decline rate was applied to the reservoir pressure at the connection points; hence, the effect of reservoir depletion takes place abruptly in calculating inflow gas rate. However, in the numerical model, the pressure depletion was applied at the outer boundary; hence, it took longer before the gas rate started its final, steep decline

With the new wellbore boundary condition implemented in the numerical model, it was not necessary to specify flow directions at the connections between the two subsystems, as previously implemented in the Dousi model. Depending on the immediate pressure difference between the bottomhole and the near-wellbore region, the coupling algorithm will identify the solution of the flows at all connections. A similar model specification was used to generate the numerical solution for this case, as shown in **Fig. 5.7**. For this case, the perforations were set at 6800 and 7400 ft, corresponding to the center of the gridblock .

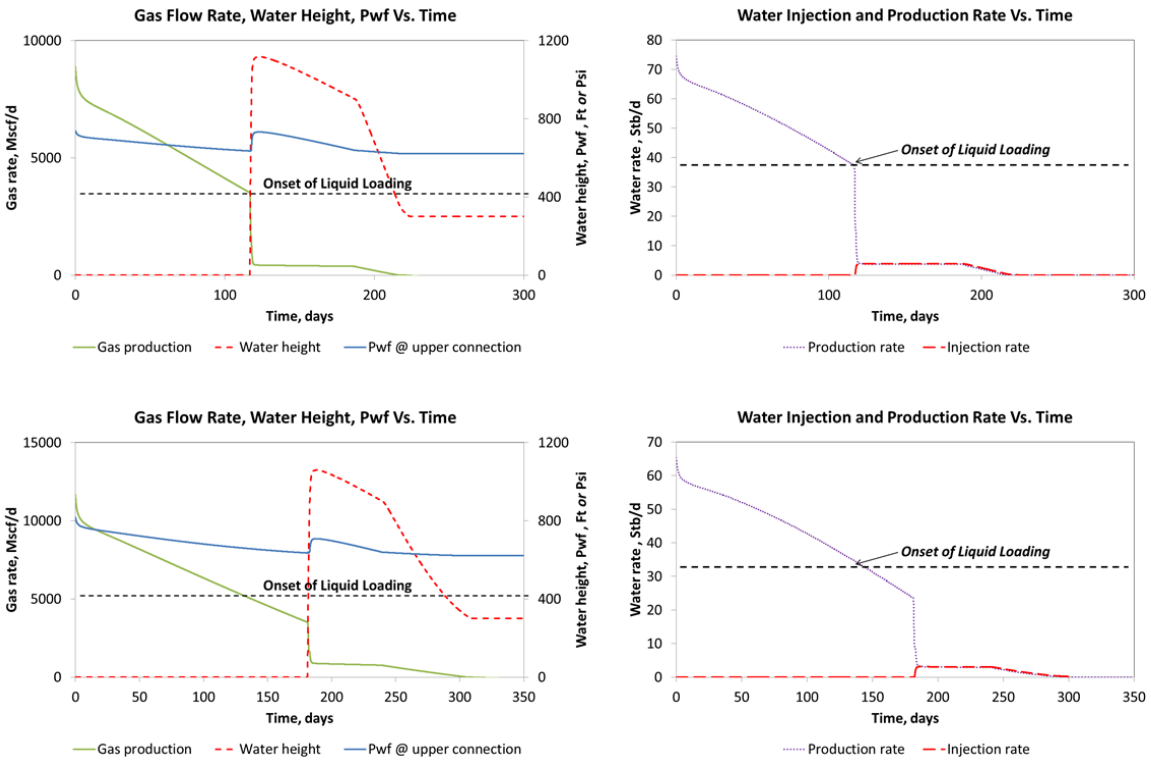

Fig. 5.7– Simulation results are generated from the numerical model when letting the simulator predict the flow directions. Upper plots are generated without the capillary pressure effect. Lower plots are generated with the capillary pressure effect.

Fig. 5.7 presents the results for two cases: without and with capillary pressure effects. In both cases, the Turner rate was set at 3.5 MMscf/d. Since both layers contributed production before reaching the loading condition, the well flowed longer than in the simulation results shown in **Fig. 5.6**. However, the periods in the metastable regime were shorter because the reservoir pressure declined at the same declined rate, resulting in the same total period of production. When the capillary pressure was taken into account in the simulation, the production period before the onset of the liquid

loading was about 30 days longer than that without the capillary effect, as shown in the upper left and the lower left plots. This implies that the capillary pressure should always be incorporated in the modeling for the liquid loading problem to explain physical driving forces between the two systems during the liquid loading regime.

All demonstration examples shown above follow the original Dousi et al. assumptions that the reservoir and the wellbore model are connected by two perforations. Gool and Currie (2007) also investigated the more realistic scenario with multiple perforations. To reproduce their case, we discretized the reservoir into 10 layers. The layer thickness was 120 ft and the perforations were placed at the center of the gridblocks. Capillary pressure was also incorporated in the model. The simulation results are shown in **Fig. 5.8**. In this case, the Turner critical rate was set at 7 MMscf/d.

Similar to previous cases, the metastable regime established very quickly once the gas flow rate fell below the Turner rate. The highest water column was around 1500 ft, which means that all perforations were covered by the water column at the beginning of the metastable regime. Four layers at the bottom part of the reservoir were taking water while the rest still contributed to production, as seen in the bottom plot in **Fig. 5.8**. As the height of the water column in the wellbore decreased, gradually more layers contributed to production. However, even the increased number of layers could not provide enough gas inflow, and the well died within a year.

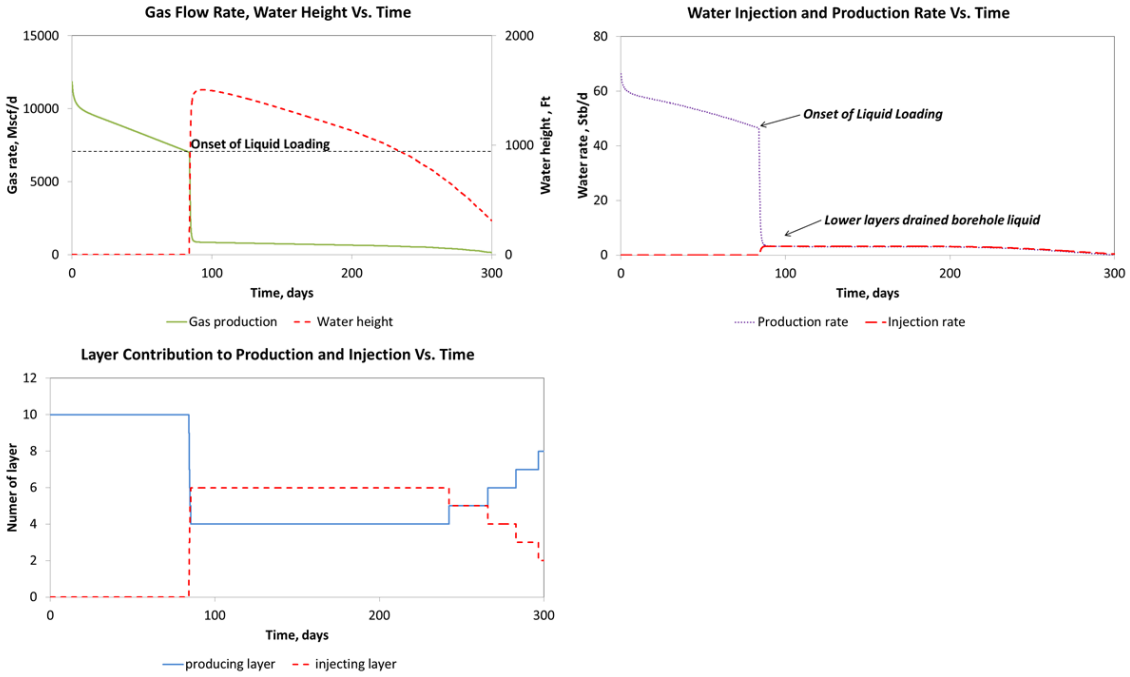

Fig. 5.8 – Simulation result of a 10-layer case generated from the numerical model

It should be noted that in the Dousi model, the metastable condition is caused by the interplay of a larger vertical pressure gradient in the wellbore and a smaller gradient in the reservoir. In addition, the assumptions implied in the Cullender-Smith equation for calculating the pressure gradient in the upper wellbore section are suitable only for the steady-state flow of dry gas. The method does not take into account the hydrostatic contribution of the liquid hold-up.

It is interesting to note that numerical difficulties were not observed during the course of simulation, even when the flow direction was determined automatically and capillary pressure was incorporated.

Simulation Results of the Metastable Flow Condition to Compare with Chupin et al. (2007)

Chupin et al. (2007) presented a coupling wellbore/reservoir model for prediction of liquid loading problems. The numerical reservoir model solves fluid flow through porous media in three dimensions. At a given time step, the wellbore boundary condition must be given by the wellbore flow model. The wellbore model simulates transient multiphase flow in pipes according to momentum and energy balance equations incorporated in the commercial software OLGA.

The coupling scheme considers the reservoir model as a plug-in to the wellbore model. It requests the reservoir model to calculate (temporarily valid, linearized) inflow performance relationships for each individual fluid, and those relationships are used in the wellbore model for the given time-step. Then the wellbore model is solved, resulting in pressure and mass rates at the interface. Then the reservoir model is solved with the mass rates as boundary condition (The above description is our best interpretation, but not stated explicitly in Chopin's work. The reservoir simulator cannot be given both mass rates and the wellbore flowing pressure simultaneously, so one of the three must have been not used. Unfortunately, it is not quite clear what was "sacrificed").

Chupin et al. (2007) used this integrated model to simulate the metastable conditions, similar to what was presented by Dousi et al. (2006). Chupin et al. found that the coupling scheme could simulate liquid backflow into the reservoir during the metastable regime.

It is interesting to compare their results and our numerical solution, especially at the interface between the reservoir and the wellbore.

Even though our reservoir model equipped with the p^0 concept was able to simulate backflow, we still required a coupled wellbore model that also allowed for automatic detection of the flow direction at the interface.

In this simulation, we used a standard Gray's correlation procedure (1974) to compute frictional pressure loss and liquid holdup in the upper section of the well. The details of Grays's correlation are given in **Appendix B**. In the lower section the frictional losses were neglected, and the gas gradient was used to calculate wellbore pressure difference between two connections.

The bisection algorithm is applied to minimize the objective function, which is the mismatch in the value of the pressure at the reference point, one guessed for the purpose of running the simulator and the other calculated by the wellbore model using all the phase rates at the interface, in addition to the tubinghead pressure.

In this simulation, a closed, two-layer reservoir is modeled with no vertical communication between the layers. The radial geometry was described using a 20x1x2 grid with an external radius of 1640 ft. **Table 5.3** summarizes the key parameters. We used the relative permeability curves from **Fig. 5.5** as there was no information provided by Chupin et al. (2007). Capillary pressure was neglected in this simulation.

Table 5.3 – Key simulation parameters presented in Chupin et al. (2007)

Reservoir Parameters		
Layer thickness	164	ft
Reservoir radius	1640	ft
Porosity	25	%
Absolute permeability top layer	1.25	md
Absolute permeability bottom layer	0.25	md
Initial pressure top layer	711	psi
Initial pressure bottom layer	747	psi
Initial water saturation top layer	28	%
Initial water saturation bottom layer	70	%
Reservoir temperature	260	deg F
Well Parameters		
Openhole diameter	7	in.
Tubing diameter	3.5	in.
Total depth	5577	ft
Wellhead pressure	261	psi
Wellhead Temperature	100	deg F

In the Chupin et al. example, an openhole well was considered at the bottomhole; while in our simulation the constant-diameter tubing reached the bottom.

The results are shown in **Fig. 5.9**. Unlike the previous case, the Turner criterion *was not* used. Surprisingly, the metastable regime could be still observed, starting at day 2000. This is caused by a sudden increase in the liquid holdup in the upper section of the well, as calculated by Gray's correlation. The increase in the liquid holdup resulted in larger hydrostatic pressure in the tubing, which consequently reduced the inflow gas rate

from the reservoir. In late time, liquid holdup decreased as less water flowed into the wellbore. No reinjection took place in both reservoir layers, which maybe associated with the specified gas gradient between layer1 and 2. No reinjection took place in either layers, which may associate with the gas gradient specified in the bottom layer.

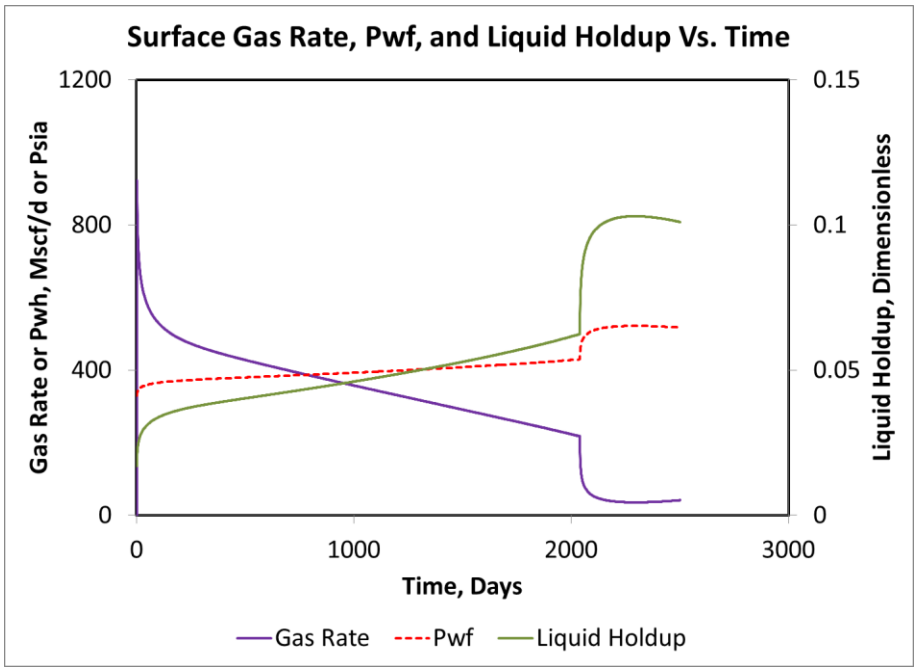

Fig. 5.9 – Surface gas rates, wellbore flowing pressure, and liquid holdup generated from our coupled simulation

As seen in **Fig. 5.9**, there was no oscillation in the simulation results.. This is different from the solutions presented by Chupin et al. (2007), as shown in **Fig. 5.10**. We believe that the high-frequency oscillation in the Chupin et al. results were caused by numerical difficulties and are not related to the physics of the problem. Additional

investigation should be carried out with the more rigorous wellbore model to predict transient flow conditions in the wellbore.

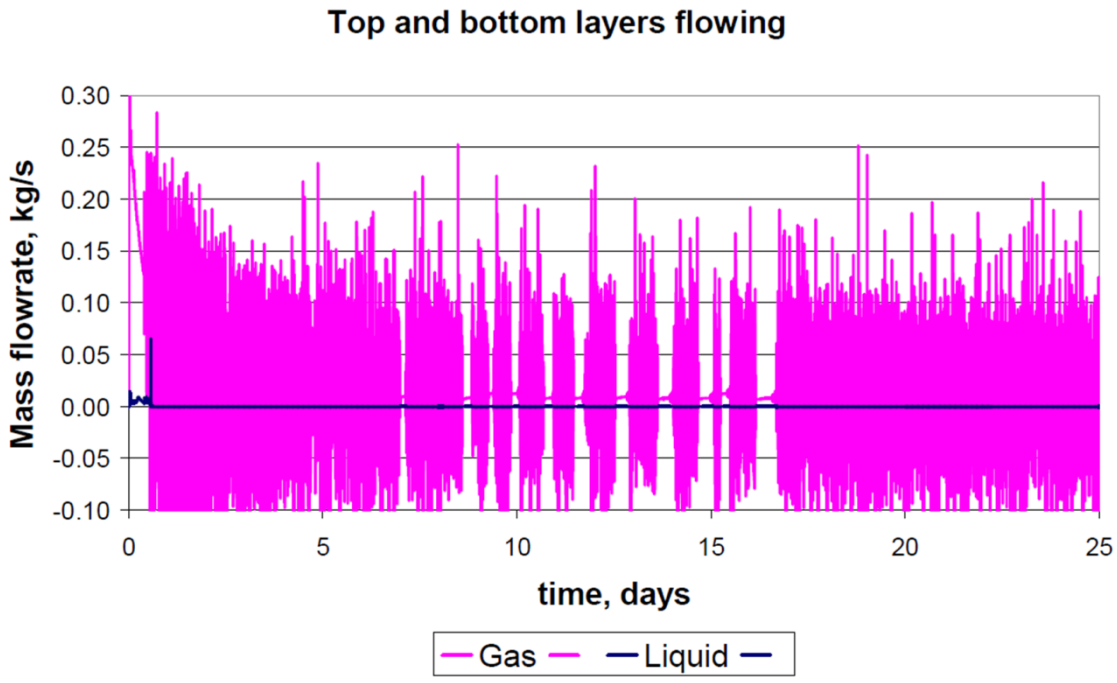

Fig. 5.10 – Simulation results of gas and liquid flow rates at wellhead as presented by Chupin et al. (2007)

The impact of capillary pressure was investigated in this simulation. **Fig. 5.11** compares the surface gas production when applying the capillary pressure curve from **Fig. 5.5** in the simulation. It shows that the capillary forces in tight formations can extend the stable production regime before reaching the liquid loading condition in the wellbore. The accuracy in prediction of the integration modeling will be reduced if the capillary pressure is neglected, similar to most previous studies in this concern.

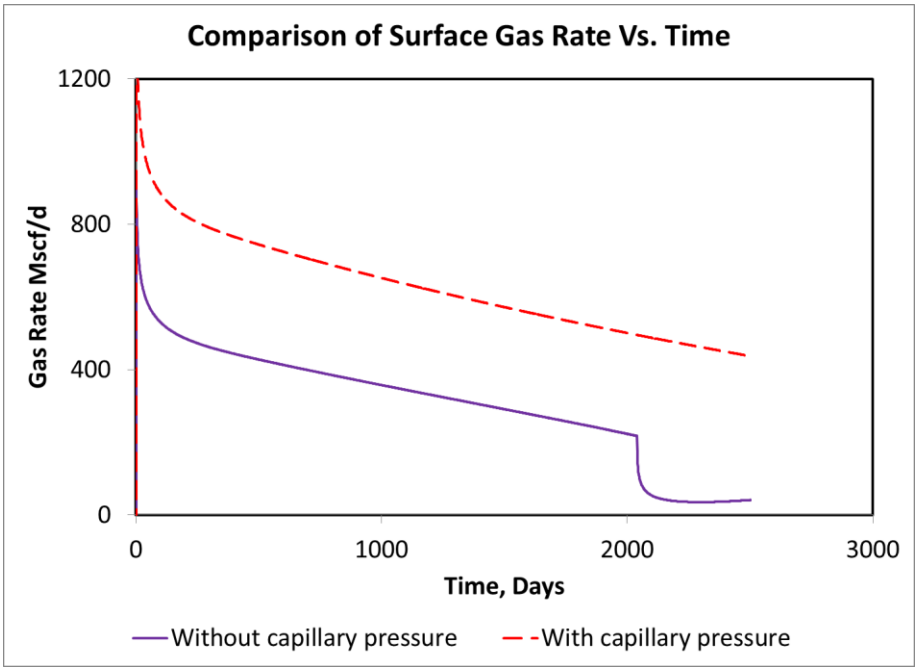

Fig. 5.11 – Comparison of the gas rate solutions when considering the capillary pressure in the simulation

Conclusion

The metastable production regime during liquid loading can be analyzed by integrated reservoir/wellbore modeling. Dousi et al. (2006) presented a model to understand some aspects of the metastable condition: it is caused by the larger vertical pressure gradient in the wellbore and the smaller gradient in the reservoirs. The larger pressure difference in the wellbore results in liquid reinjection into the lower-reservoir layer; while at the upper-reservoir layer, the coproduced liquid is still flowing and

accumulating in the wellbore. The metastable flow rate happens when the rate of injection equals the rate of production.

By replacing the IPR reservoir model with our reservoir simulation, the metastable condition can be obtained in a straightforward manner. The coupled simulation does not need additional restrictions built infor the flow direction and does not need two sets of reservoir parameters, as embedded in the Dousi et al. model.

CHAPTER VI

APPLICATION OF THE NEW WELLBORE BOUNDARY CONDITION IN HISTORY MATCHING OF THE LIQUID-LOADED GAS WELL*

Introduction

In this chapter, we present another application of our simulator in history matching data from a liquid-loaded of the liquid-loaded gas well.

The well data consisted of surface production rates of gas and water and the corresponding tubinghead pressure (THP) history. The gas well had been experiencing the usual symptoms of liquid loading from the start. A strategy of intermittent production cycles had been followed for over 25 years. Such a strategy can result in near optimal recovery as discussed, for instance, by Whitson et al. (2012).

Even though the reservoir model equipped with the p^0 concept was able to simulate backflow, we still required a wellbore model that also allows automatic detection of the flow direction at the connections.

---

* Part of this chapter is reprinted with permission from "A New Concept of Wellbore Boundary Condition for Modeling Liquid Loading in Gas Wells" by Limpasurat et al., 2013. Paper SPE 166199MS accepted for the 2013 SPE Annual Technical Conference and Exhibition. New Orleans, LA, USA. 30 September – 2 October. Copyright 2013 by the Society of Petroleum Engineers.

Since an appropriate wellbore model was not readily available, for this study we developed a simple model to describe multiphase flow and liquid accumulation/drainage during both the production and shut-in parts of a cycle, also satisfying the material balance for both phases during the switching between operation modes.

This model is overly simplified for the case of one wellbore/reservoir connection (as we refer to it, the one-layer model), but becomes quite sophisticated for the two-layer case because the new boundary conditions are fully implemented for each connection and can result in opposite flow directions in any time step.

Our main goal was to reproduce the main characteristics of the tubinghead pressure (THP) behavior in terms of how the well and the reservoir interact. The history matching process was carried out in two steps. First, we considered a one-layer model of the reservoir to understand the overall (net) inflow and outflow of the phases during the production/shut-in cycles. Then we repeated the history match using a two-layer representation of the reservoir and the corresponding two-perforation wellbore model in such a way that the previously identified net flows were automatically provided by the physics involved; this can be accomplished to a satisfactory degree for the shut-in periods, but we still needed some assumptions during the production periods, because currently there is no physics-based model available for modeling long-term liquid accumulation in the wellbore under typical liquid-loading conditions.

One-Layer Model

For modeling proposes, we represented the history by 34 cycles, each consisting of a production and a shut-in period. Zooming in on the production history, we found that the surface gas production rate had been nearly constant for numerous production periods, as shown in **Fig. 6.1**. Thus, we imposed the average gas surface rate as the prescribed rate during the production period, while the surface rate was specified as zero during the shut-in period. **Fig. 6.2** summarizes the imposed surface gas flow rates. During the data filtering process we kept all shut-in intervals longer than 2 months, but we agglomerated the shorter periods into the surrounding production period. The actual number of production/shut-in cycles could have been much larger than 34; this choice was the result of a compromise to keep the data handling manageable. Also, each cycle had to have numerous days in it to be sure the available data were of daily resolution.

To match the surface water rate, we adjusted the relative permeability curves and initial water saturation.

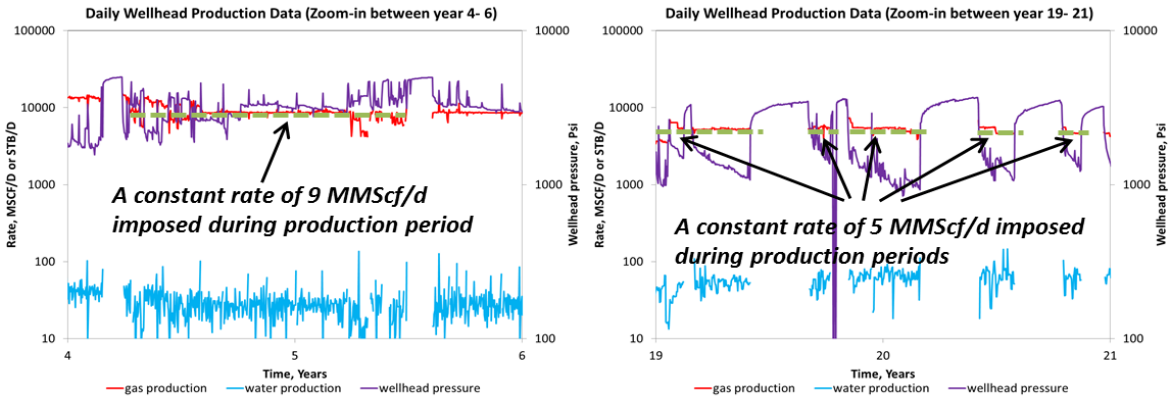

Fig. 6.1 – Plot of wellhead production history at the early time interval (left) and the late time interval (right). The surface gas production rate is nearly constant during the production period.

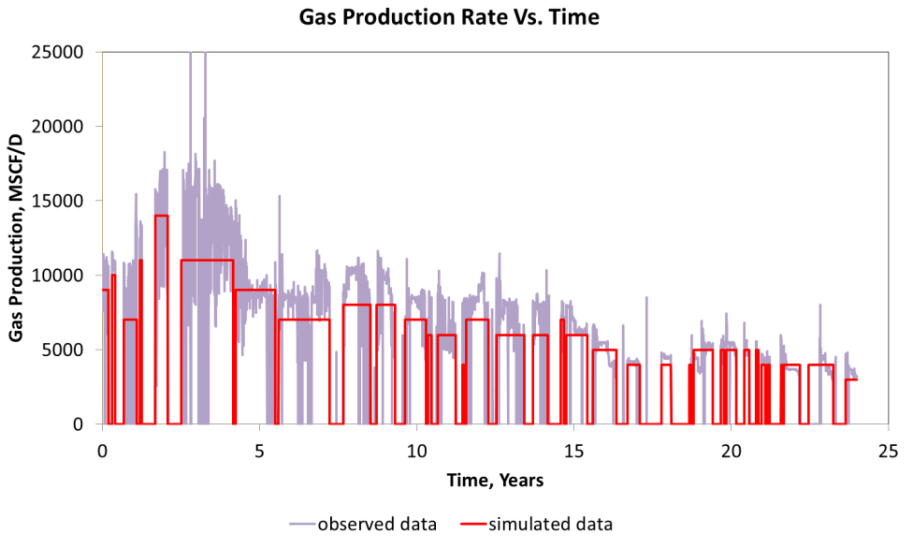

Fig. 6.2 – Recorded and assumed surface gas production in the simulation

From the overall decline in the THP trend, we identified a substantial overall depletion. Accordingly, we adjusted the net/gross ratio and saturation. After these

adjustments, we had an overly simplified but consistent description of the reservoir, as summarized in **Table 6.1** and **Fig. 6.3**.

Table 6.1 – Key simulation parameters

Reservoir Parameters		
Drainage radius	5476	ft
Gross thickness	400	ft
Net/Gross ratio	15	%
Fluid type in the reservoir	Gas (C1) and Water	
Porosity	11	%
Absolute permeability	6.5	md
Initial reservoir pressure	8000	psia
Reservoir temperature	260	deg F
Initial water saturation	50	%
Openhole diameter	7 7/8	in

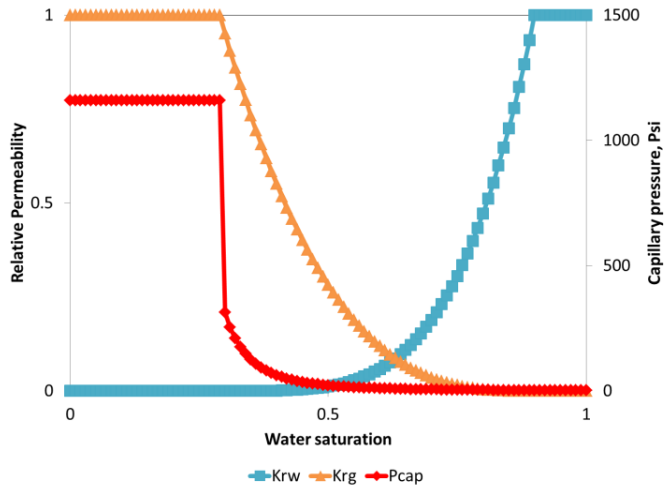

Fig. 6.3 – The relative permeability and capillary pressure curves

The net/gross parameter can be incorporated in our simulator by multiplying porosity and horizontal permeability by the net/gross ratio (see **Eqs. 3.3**, **3.4**, and **3.16**) to obtain effective values to be used in the model. From the decline trend of the THP peaks, we estimated that the well had produced about 40% of the original gas in place. There is no information about aquifer influx, but the data support the simplifying hypothesis of no-flow outer boundary.

The basic data for the well are shown in **Table 6.2**.

Table 6.2 – Well parameters

Well Parameters		
Total well depth	15,400	ft
Perforation depth	15,200	ft
Tubing ID	3 1/2	in
Wellhead temperature	100	deg F
Interfacial tension	60	dyne/cm

Technically, the wellbore model is a transient model with respect to material balance, since it keeps track of storage of the gas and liquid phases, but it is quasisteady with respect to momentum balance. At the wellhead, the gas mass rate is specified. At the connection, the p_{wf} and both the gas and water rates are known. (In accordance to our boundary condition, the rates must have the same sign, but the actual direction of the flow is determined by the difference of p_{wf} and the p^0 of the connection grid-block.) The wellbore model includes a standard Gray's (1974) correlation procedure to compute frictional pressure loss and liquid holdup in the upper section, when there is positive surface gas rate.

While the surface gas rate is imposed, the gas rate through the connection is not necessarily the same. When the wellhead is shut-in, there is no frictional pressure loss and the two phases are completely segregated due to gravity. In either case, however, the wellhead and bottom gas rates differ from each other. The actual pressures and phase accumulations for the given time step are calculated from the common algorithm shown in **Fig. 6.4**, valid both for the production and the shut-in period.

The implicit coupling algorithm can be summarized as follows. In any time step, we have 3 key unknowns: the p_{wf} and the mass flow rates of the gas and water phases through the connection. If we assume a p_{wf}, the boundary conditions and the reservoir model together provide the mass flow rates, but volume balance (material balance + equation of state) inside the wellbore will be satisfied only at one particular p_{wf}. That value is determined by a bisection algorithm, driving the "objective function" to zero.

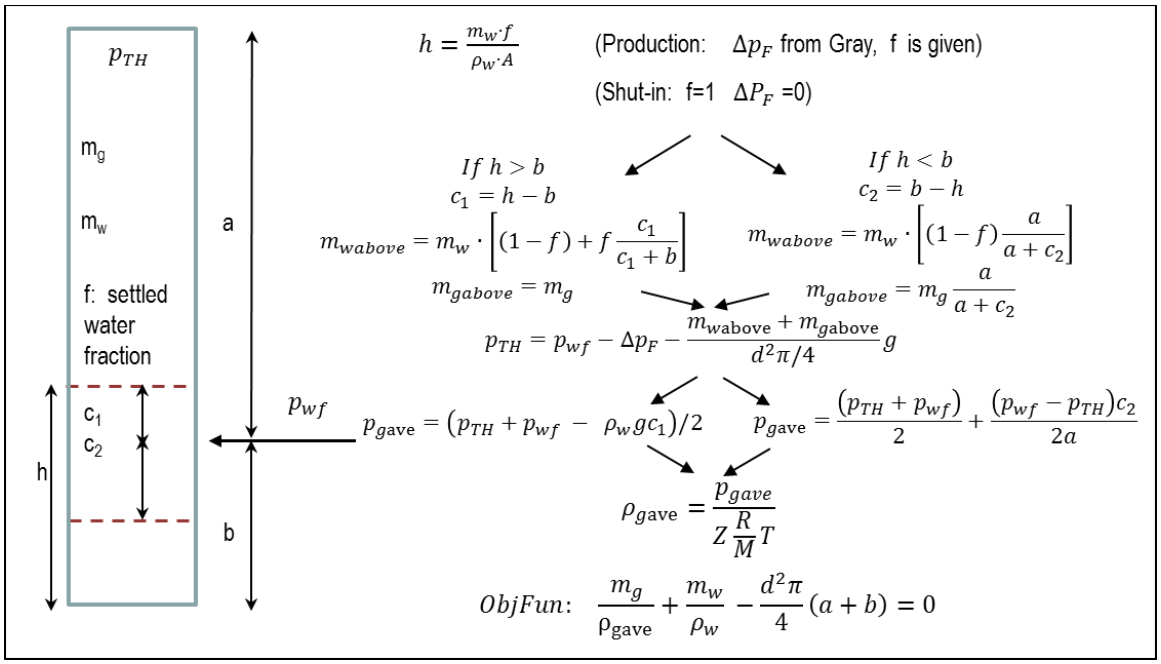

Fig.6.4 - Common logic for the determination of wellbore flowing pressure p_{wf} (and tubinghead pressure p_{TH}) from the volume balance (material balance plus equation of state). The reservoir simulator is run "to convergence" at each assumed p_{wf} , when m_w and m_g are updated with the rates calculated from the boundary conditions (**Fig. 3.2**) Ultimately, that p_{wf} is accepted that drives the "objective function" to zero.

The wellbore model keeps track of water in two forms: holdup within the gas and settled water. The settled water occupies the lowest part of the wellbore. Accumulation can happen in both forms, and the hydrostatic pressure difference between two vertical levels is calculated from the total mass of water (in either of the two possible forms) and the total mass of gas between them. (Future extension may incorporate the empirical S-shaped saturation distribution identified by Rowlan et al. (2004), instead of complete separation of the two types of water.)

The accumulation of water in the holdup form is easy to keep track of (comparing two values obtained from the Gray correlation). Keeping track of the accumulation of water in the settled form is more difficult. In Case Study 1 (based on the Dousi et al. 2006 concept), either the settled water was zero (if the gas rate was above the Turner rate) or all water was in settled form (if the gas rate was below the Turner rate). Such simplifying assumptions could not be used in this case. The data indicate that water is coming to the surface (though in a somewhat more erratic manner than gas) even when the gas velocity is already bellow critical (whatever specific form we use for V_{gc}).

In the one-layer model, we imposed a constant accumulation rate of the settled water during each production period. In other words, after the onset of liquid-loading, a certain fraction of the water entering the wellbore through the connection is not carried to the surface, but instead accumulates at the bottom in the form of "settled water." There is no available correlation to determine the *accumulation rate of the settled water*. We noticed that a useful correlation would ultimately describe the accumulation rate in

terms of the ratio of actual superficial gas velocity to the V_{gc}, whatever specific form is used for the latter.

In this work we simply identified the accumulation rate from the slope of the THP during the production periods. This was done during the one-layer history matching, with the help of the single-connection wellbore model. **Fig. 6.5** illustrates the process.

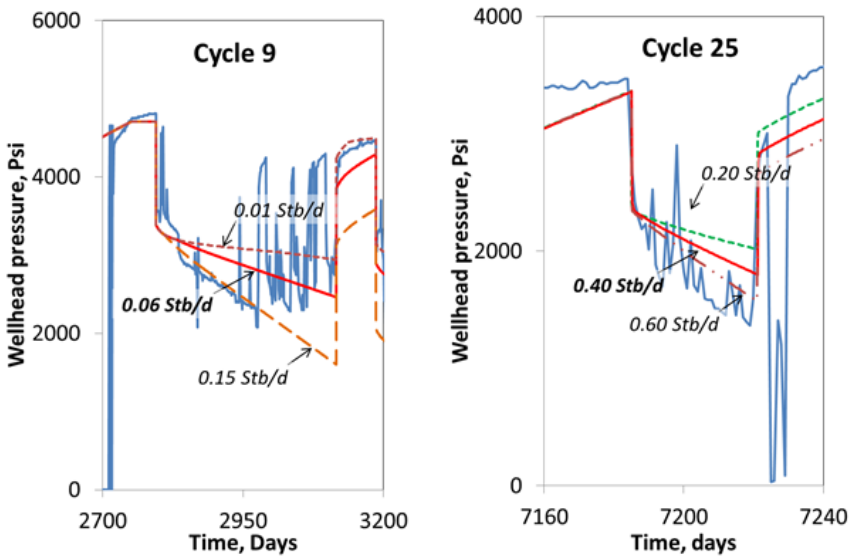

Fig. 6.5 - Matching the accumulation rate of settled water during a production period.

The history matching of the THP curve results in a surprisingly consistent set of accumulation rates, as shown in **Table 6.3.**

Table 6.3 - Accumulation and leakage rates necessary for the one-layer model

	Cycles	Rate (Stb/day)
Accumulation during production period	1-8	0.01
	9-11	0.06
	12-17	0.05
	18-20	0.1
	21	0.3
	22-23	0.4
	24	0.2
	25	0.4
	26	0.3
	27	0.6
	28-29	0.8
	30-31	0.6
	32	0.3
	33	0.2
	34	0.4
Leakage during shut-in period	1-7	-0.05
	8-12	-0.15
	13-20	-0.2
	21-23	-0.3
	24-27	-0.5
	28	-0.4
	29	-0.9
	30-32	-0.6
	33	-0.5

We modeled the "after-flow" during the shut-in periods by solving the wellbore-reservoir model still coupled by the boundary conditions. However, we assumed that at the start of the shut-in period, the water existing in the form of holdup settles out instantaneously. In the one-layer model, we imposed a constant water leakage rate for the water, because in the single available connection, gas is flowing in (after-flow). Therefore we determined the leakage rate (assumed constant) from the positive slope of

the THP curve. The leakage will continue as far as settled water is available in the wellbore. This history matching process is illustrated in **Fig. 6.6**.

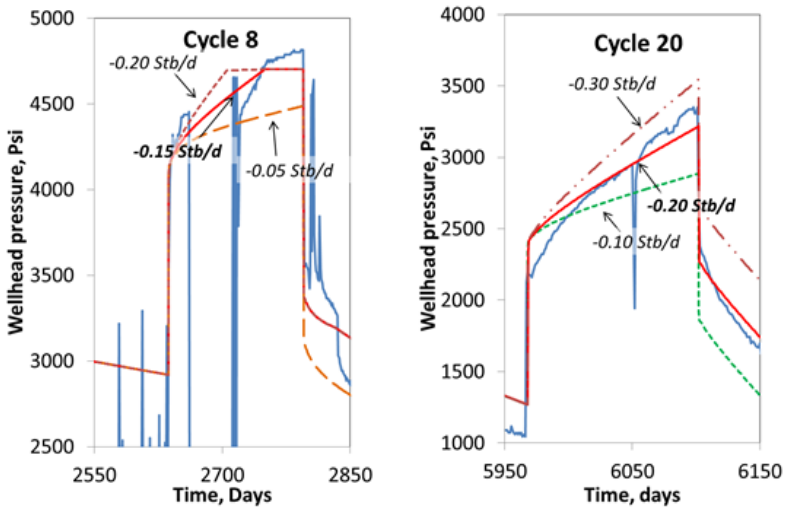

Fig. 6.6 - Matching the leakage rate of settled water during a shut-in period

We noticed that sometimes a "cap-off" appeared in the calculated curve, because all the available settled water leaked off.

The history matching result of the THP is shown in **Fig 6.7**. Obviously, the one-layer model is capable of reproducing the basic trends in the THP, but this is still done by imposing a non-physical "leakage" during shut-in.

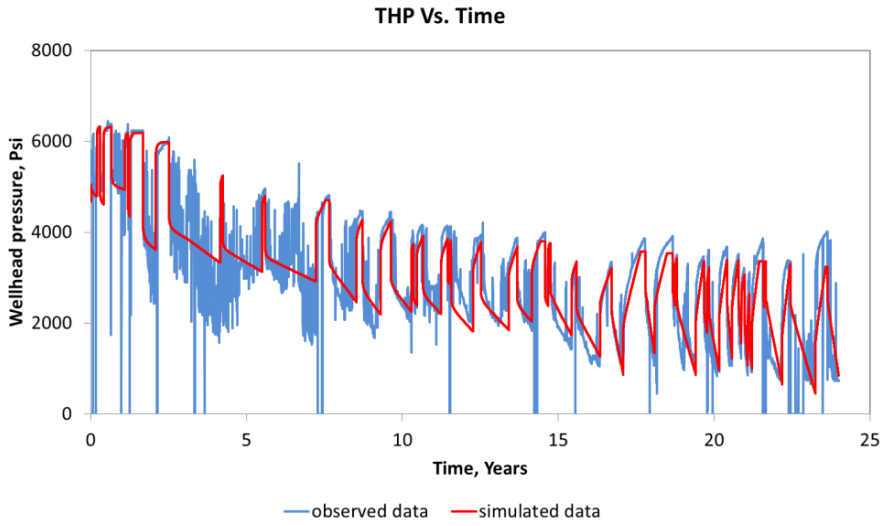

Fig. 6.7 – Matching wellhead pressure history with the one-layer model

Fig. 6.8 shows the settled water and total water content in the wellbore. The sharp drop/rise sections of the THP curve are associated with the accumulation and leakage of the settled water.

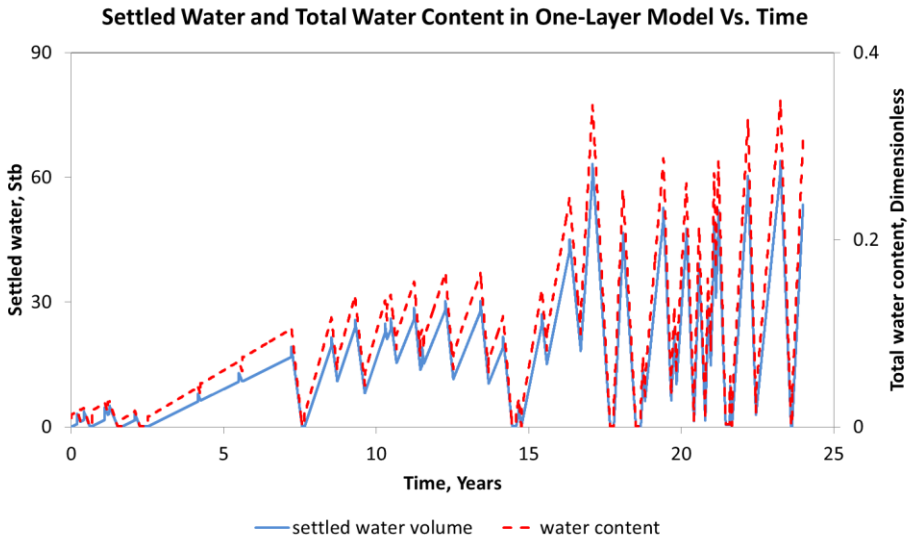

Fig. 6.8 - Settled water volume and total water content in the wellbore over time in the one-layer model

Two-Layer Model

The two-layer model preserves the OGIP of the one-layer model, using a 100x1x2 grid system. The perforations were now placed at depths of 15,100 and 15,300 ft.

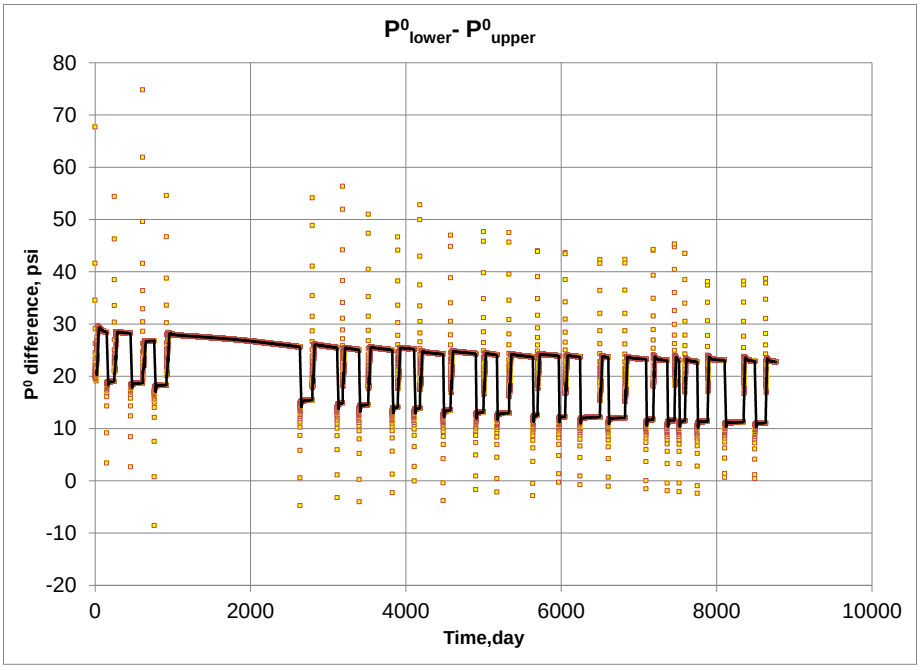

Fig. 6.9 - The p^0 difference between the two layers as a function of time. The solid line is smoothed (moving average).

The difference in p^0 is 17 psi between the upper and the lower layers in the vertical equilibrium state. This is the starting value in **Fig. 6.9**. Production periods start with a peak in the difference, but on average the value is about 25-30 psi. In shut-in periods the average is about 15-20 psi. The implications can be understood in the light of the pressure difference between the lower and upper perforations in the wellbore, which varies between a couple of psi (only gas is present) and a maximum of 87 psi (hydrostatic pressure of a 200-ft water column).

The wellbore model had now two connections, and the algorithm depicted on **Fig. 6.4** had to be augmented, because two p_{wf} values had to be determined. To preserve simplicity, we used the implicit scheme only for the upper connection p_{wf} —as shown in

Fig. 6.4—while the difference between the two p_{wf} values was handled explicitly, taken as known from the previous time-step.

In the production periods, the calculation procedure still involved the constant water accumulation rates determined previously by history matching the one-layer model. However, when running the two-layer model, we did not use the previously determined leakage rates in **Table 6.3**; we simply let the boundary conditions determine the "leakage". The parameter $\left(\frac{k_r}{\mu B}\right)_{eq}$ was set to 0.046/cp, indicating that even if only water is injected, still there are significant relative permeability effects. **Fig. 6.10** to **Fig. 6.14** illustrate results from the history match of the two-layer model.

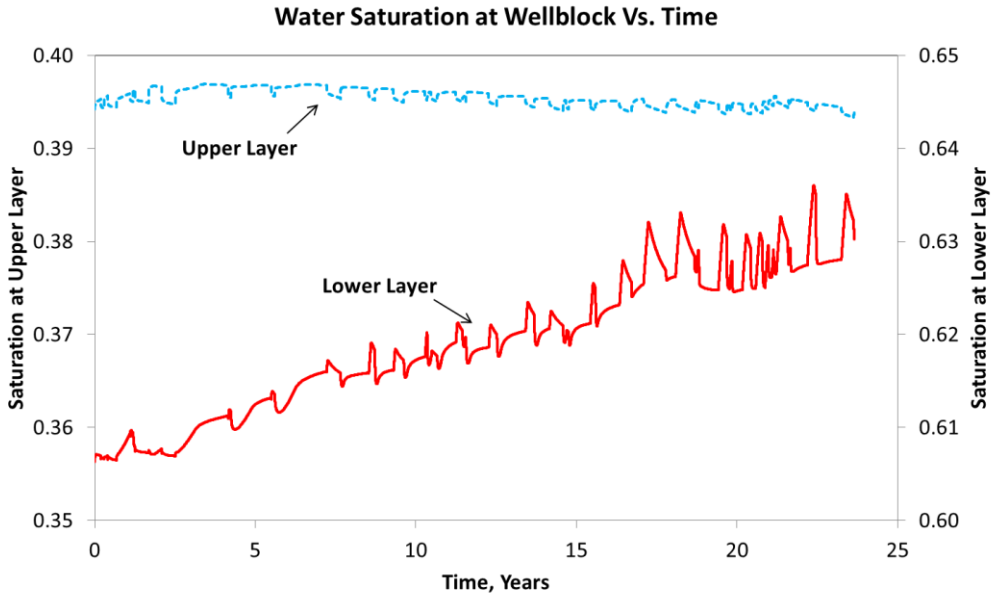

Fig. 6.10 - Water saturation at wellblocks over time shows the water has been re-injected to the lower layer for 25 years.

Fig. 6.10 shows the water saturation at the wellbore over time; the water saturation in the lower layer increased in the near-wellbore region, while the opposite was happening in the upper layer. **Fig. 6.11** shows that the lower layer produces water during the production periods, but also receives water during the shut-in periods (until the settled water level falls below the perforation level, and the corresponding S_{wwf} changes from one to zero.)

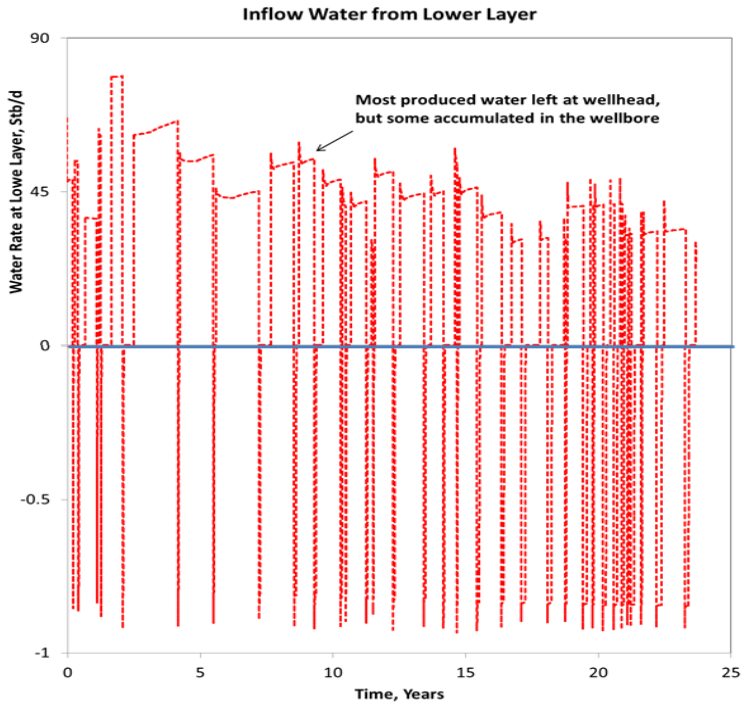

Fig. 6.11 – The lower layer produces water during production periods, but drains water during shut-ins.

Fig. 6.12 shows the match of the THP with the two-layer model. The calculated THP curve traces well the overall trends, but for a more rigorous match the number of cycles should be increased substantially. At some points, for instance at years 17 and 18, the calculated THP curve is cut off. The reason is that all the available water was pushed back to the lower layer (see also **Fig. 6.13**). Some of the discrepancy could be eliminated with better resolution and by refining the water accumulation rate during the last production cycles.

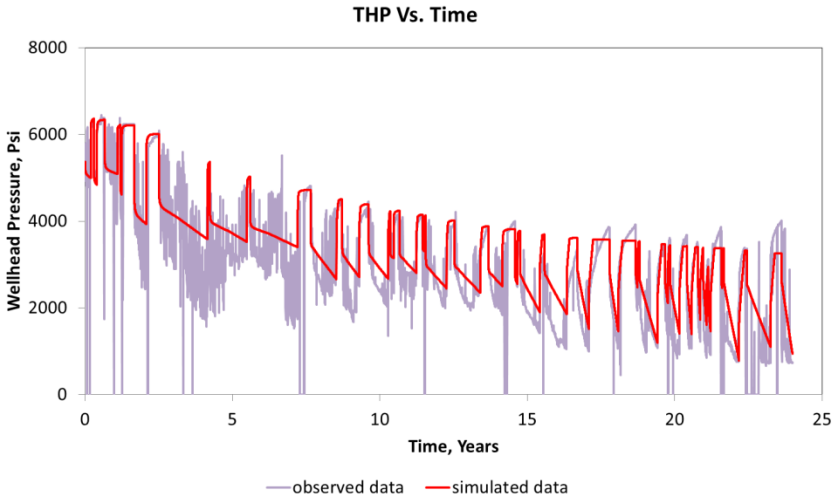

Fig. 6.12 – Field and simulated wellhead pressure over time in the two-layer model

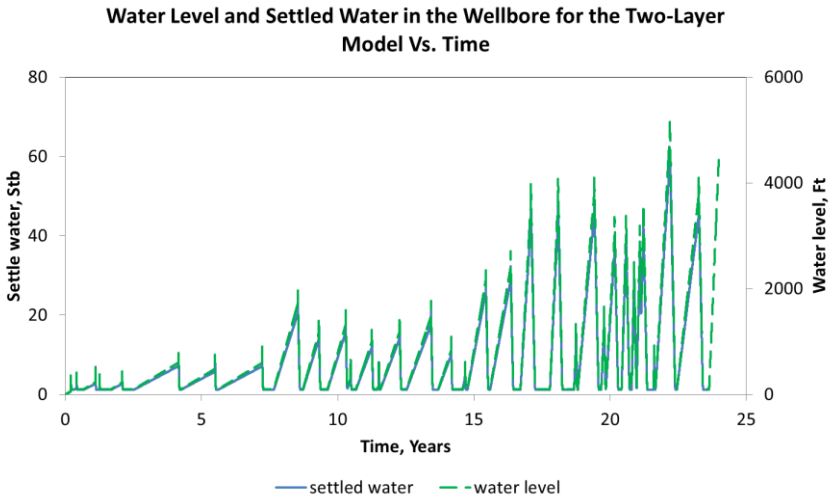

Fig. 6.13 – Settled water volume and water level inside the wellbore over time in the two-layer model

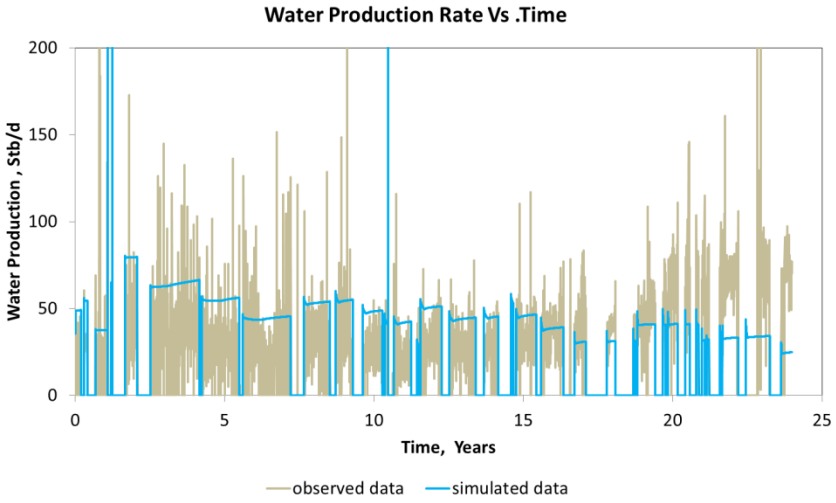

Fig. 6.14– Field and simulated surface water production over time in the two-layer model

The current two-layer model seems to lack the resolution necessary to reproduce yet another trend: the steady increase in the surface water production rates in the last 5 years, as indicated by **Fig. 6.14**. We decided not to pursue a better match by adjusting individual water accumulation rates, because we consider such "history matched" accumulation rates only as an intermediate result. Ultimately, a correlation is needed for predicting the actual water accumulation rates during the production periods under liquid-loading conditions. Nevertheless, the two-layer model in its present form is already suitable for investigating various production strategies in order to achieve specific goals (cash-flow, NPV, EUR, contractual obligations, etc.)

Conclusion

The integrated reservoir/wellbore modeling was applied for history matching of the gas well operated in the liquid loading regime. The strategy of intermittent production cycles resulted in sustaining the gas production for 25 years; the production history was represented by 34 production/shut-in cycles. During the production period, average gas production rate were imposed. We modeled the after-flow effect during the shut-in at wellhead.

As there is no appropriate wellbore model to model the long-term liquid loading, the simple transient well model with respect to material balance was developed. The well model keeps track of water accumulation in both in the holdup and settled water form, which is at the bottom of the well.

The one-layer radial reservoir was modeled to understand basic trends associated with sharp tubinghead pressure drop and buildup during the production and the shut-in periods. These trends can be simply and consistently traced by accumulation rates and leakage rates in the production and the shut-in periods, respectively.

The two-layer model was then modeled to eliminate artificial leakage rates applied in the one-layer models. With two connections between the reservoir and the wellbore models, the THP history can be replicated by our approach.

CHAPTER VII

CONCLUSIONS AND FUTURE WORK

Conclusions

This study addressed the importance of the wellbore boundary condition for describing dynamic interaction in the reservoir and the wellbore model in modeling liquid loading problems. Due to wellbore phase-redistribution and potential phase reinjection into the reservoir, the boundary condition must be able to handle changing flow directions through the connection between the two subsystems.

We developed a new reservoir simulator able to model gas/water flows through isothermal systems. The alternative wellbore boundary condition was formulated and used in this reservoir simulator. The new formulation uses a new state variable, the multiphase zero flow pressure (*MPZFP, p^0*) instead of individual phase pressures. Consequently, the sink/source terms are zero in the connection grid block if the wellbore pressure equals the p^0. If the wellbore pressure is less than the p^0, the connection is producing; otherwise, it is injecting. Phase composition is always determined by the upstream side.

The simulation results were verified against the commercial package, ECLIPSE100. The results showed that changes in flow direction are automatically predicted thanks to the wellbore boundary condition. This makes our simulation more suitable to modeling of this liquid loading problem.

The U-shaped pressure profiles in the near-wellbore region were also simulated using our reservoir simulator. The U-shaped pressure curves develop because of reinjection of the liquid phase from the wellbore boundary. In addition, the simulation was modified to handle gas flows through porous media in order to verify the accuracy of the U-shaped pressure profiles in the experimental study. We found that the flowing gas was leaked from the testing apparatus during the transient condition, making the U-shaped pressure profiles dissipate much slower than predicted by the simulation.

With our coupled reservoir wellbore model the metastable production regime was found in a straightforward manner. The assumptions of restricted flow directions at the connections and two sets of reservoir parameters could be eliminated.

We used our coupled model to history match long-term behavior of a gas well under liquid-loading conditions. A simplified—but already genuinely transient—wellbore model was developed for this purpose. Local trends in THP history could be traced by keeping track of settled water in the wellbore. Our simulation showed that the water reinjection takes place in the lower-layer during the shut-in periods.

Future Work

To continue developing dynamic reservoir/wellbore modeling, the following developments should be incorporated into the reservoir model:

1. In the history matching problem with the two-layer model, we used the combined implicit-explicit coupling to determine p_{wf} at the upper and the lower connections. The improved version of the simulation results should be

incorporating the implicit approach to determine the p_{wf} at the lower connection at the new time level instead of taking the difference between two p_{wf} values from the previous time step to calculate the p_{wf} of the lower connection explicitly.

2. We experienced that for the history matching problem, it took a long time to complete the simulation run. Most computational times were used to solve the reservoir model in each coupled iteration step. Since the radius of the reservoir is huge (The drainage radius is 5,476 ft discretized by 100 gridblocks in radial direction), the simulation time was wasted to compute the intermediate solution of the far-region reservoir, which is nearly insensitive to the change from the wellbore model. The more effective way to reduce the simulation time is to represent the effect of the far-region reservoir by the external boundary condition. The pressure and saturation at the external boundary will be computed regularly by the simulation of the far-reservoir model, but less often than the near-wellbore model. The near-wellbore model will be calculated in every iteration level; while, the far-region reservoir may be updated in the time level. There should be a criterion to identify the required times step that the external boundary condition should be updated and the simulation of the far-reservoir model should be advance to the next time step.

REFERENCES

Alves, M.V.C., Falcone, G., Barbosa, J. R. (2012). Modeling the Transient Behaviour of Churn-Annular Flow in a Vertical Pipe, 3rd EBECEM (3º Encontro Brasileiro sobre Ebulição, Condensação e Escoamentos Multifásicos), Curitiba, Brazil. 7 - 8 May. http://www.jem2012.com.br/EBECEM_Program_vFINAL.pdf.

Belfroid, S., Schiferli, W., Alberts, G. et al. (2008). Predicting Onset and Dynamic Behaviour of Liquid Loading Gas Wells. Paper SPE 115567 presented at the SPE Annual Technical Conference and Exhibition, Denver, Colorado, USA. 21-24 September.

Cullender, M.H., and Smith, R.V. (1956). Practical Solution of Gas Flow Equation of Wells and Pipelines with Large Temperature Gradients. Trans, AIME 207. SPE 000696-G.

Chupin, G., Hu, B. Haugset, T., and Claudel, M. (2007). Integrated Wellbore/Reservoir Model Predicts Flow Transients in Liquid-Loaded Gas Wells. Paper SPE 110461 presented at the SPE Annual Technical Conference and Exhibition. Anaheim, California, 11 -14 November.

Coats, B.K., Fleming, G.C., Watts, J.W., Rame, M., and Shiralkar, G.S. (2003). A Generalized Wellbore and Surface Facility Model, Fully Coupled to a Reservoir Simulator. Paper SPE 79704 presented at the SPE Reservoir Simulation Symposium. Houston, Texas, 3-5 February.

Coleman, S. B., Clay, H.B., McCurdy, D.G., and Lee Norris, H. III (1991). A New Look at Predicting Gas-Well Load-Up. Journal of Petroleum Technology, **43**(3): 329-333.

Dake, L.P. (1978). Fundamental of Reservoir Engineering. Elsevier. Amsterdam and New York.

Daas, M., Golczynki, T., Harry, J. (2012). Minimum Flowrate to Unload Gas Wells: Dynamic Multiphase Modeling to Validate Exisitng Correlations. Paper SPE 152597 presented at the SPE Latin American and Caribbean Petroleum Engineering Conference. Mexico City, Mexico. 16 – 18 April.

Dousi, N., Veeken, C.A.M., Currie, P.K. (2006). Numerical and Analytical Modeling of the Gas-Well Liquid-Loading Process. SPE Production & Operations **21**(4): 475-482. SPE 95282-PA.

Dunham, C., Lea., J.F., and Stephenson, G. (2008). Guidelines Help Operators Select Artificial Lift Systems for Deliquifying Gas Wells. American Oil and Gas Reporter, **51**(6).

Ertekin, T., Abou-Kassem, J.H., and King, G.R. (2001). Basic Applied Reservoir Simulation. Richardson, Texas.

Fernandez, J., Falcone, G., Teodoriu, C. (2010). Design of a High-Pressure Research Flow Loop for the Experimental Investigation of Liquid Loading in Gas Wells. SPE Projects, Facilities & Construction **5** (2), 76-88. SPE 122786-PA.

Gool, F.V., Currie P.K. (2007). An Improved Model for the Liquid-Loading Process in Gas Wells. Paper SPE 106699 presented at the 2007 SPE Production and Operations Symposium. Oklahoma City, Oklahoma, 31 March – 3 April.

Gray, H.E. (1974). Vertical Flow Correlation in Gas Wells. User Manual for API14B, Subsurface Controlled Safety Valve Sizing Computer Program. App. B, June.

Guo, B., Ghalambor, A., Xu, C. (2006). A systematic approach to predicting liquid loading in gas wells. SPE Production and Operations, **21** (1):81-88. SPE-94081-PA.

Hewitt,G.F., Roberts, D.N. (1969). Study of Two-Phase Flow Patterns by Simultaneous X-Ray and Flash Photography. UKAEFA Report AERE- M2159. Atomic Energy Research Establishment, Berkshire, UK.

Holmes, J.A., Barkve, T., Lund, ∅. (1998). Application of a Multisegment Well Model to Simulate Flow in Advanced Wells. Paper SPE 50646 presented at the 1998 European Petroleum Conference. The Hague, Netherlands. 20-22 October.

Hu, B., Veeken, K., Yusuf, R. and Holmas, H. (2010). Use of Wellbore-Reservoir Coupled Dynamic Simulation to Evaluate the Cycling Capability of Liquid-Loaded Gas Wells. Paper SPE 134948 presented at the SPE Annual Technical Conference and Exhibition. Florence, Italy, 19-22 September.

Huber, M.L., Perkins, R.A., Laesecke, A., et al. (2009). New International formulation for the Viscosity of H2O. Journal of Physical and Chemical Reference Data. **38** (2): 101-125.

Lea, J.F., Nickens, H.V., and Wells, M. (2003). Gas Well Deliquification - Solution to Gas Well Liquid Loading Problems, Houston, Texas: Gulf Professional Publishing.

Liu, X., Limpasurat, A., Falcone, G., and Teodoriu, C. (2013). Experimental and Numerical Investigation of Transient Gas Flow through Porous Media – Back Pressure Effects. Manuscript in preparation for publication in 2013.

Meyer, C.A., McClintock R.B., Silvestri, G.J., et al. (1979). ASME Steam Tables. fourth edition. American Society of Mechanical Engineers, New York, NY.

Moridis, G.J. (2009). Class notes "Models for Simulation of Advanced Coupled Processes in Geologic Media" offered at Dept. of Petroleum Engineering, Texas A&M University.

Moridis, G.J., Kowalsky, M. and Pruess, K. (2008). TOUGH+HYDRATE v1.0 User's Manual. Report LBNL-0149E, Lawrence Berkeley National Laboratory, Berkeley, CA.

Oyewole, P. O., Lea, J. F. (2008). Artificial Lift Selection Strategy for the life of a Gas Well with some Liquid Production. Paper SPE 115950 presented at the SPE Annual Technical Conference and Exhibition. Denver, Corolado, USA. 21 – 24 September.

Peaceman, D.W. (1977). Fundamentals of Numerical Reservoir Simulation. Elsevier. Amsterdam and New York.

Peaceman, D.W. (1983). Interpretation of Well-Block Pressures in Numerical Reservoir Simulation with Nonsquare Grid Blocks and Anisotropic Permeability. Society of Petroleum Engineers Journal **23**(3): 531-543. SPE 10528-PA.

Pourafshary, P., Podio, A.L. and Sepehrnoori, K. (2009). Application of a Coupled Wellbore/Reservoir Simulator to Estimate Accumulated Liquid Phase in Gas Wells. Petroleum Science and Technology, **27**(11): 1175-1184.

Rowlan, O.L., McCoy, J.N., and A.L. Podio (2004). Acoustic Liquid-LevelDetermination of Liquid Loading in Gas Wells. Paper SPE 100663 presented at the 2006 SPE Western Regional/AAPG Pacific Section/GSA Cordilleran Section Joint Meeting. Anchorage, Alaska, USA. 8-10 May.

Sagen, J., Sira, T., Ek, A., Selberg, S., Chaib, M., and Eidsmoen, H. (2007). A Coupled Dynamic Reservoir and Pipeline Model–Development and Initial Experience. Paper presented at the 13th International Multiphase Conference on Multiphase Production Technology, Edinburgh, UK, 13-15 June.

Selim, M.S., and Sloan, E.D. (1989). Heat and Mass Transfer during the Dissociation of Hydrates in Porous Media. AIChe J., **35**(6): 1049-1052.

Schiferli, W., Belfroid , S.P.C., Savenko, S., Veeken, C.A.M.,and Hu, B. (2010). Simulating Liquid Loading in Gas Wells. Paper presented at the 7th North American Conference on Multiphase Technology. Banff, Canada. 2-4 June.

Solomon, F.A., Falcone, G., and Teodoriu, C. (2008). Critical Review of Existing Solutions to Predict and Model Liquid Loading in Gas Wells. Paper SPE 115933

presented at the SPE Annual Technical Conference and Exhibition. Denver, Colorado, USA. 21-24 September.

Sutton, R. P., Cox, S.A., Williams, E.G., Stoltz, R.P., and Gilbert, J.V. (2003). Gas Well Performance at Subcritical Rates. Paper SPE 80887 presented at the SPE Production and Operations Symposium. Oklahoma City, Oklahoma, USA. 22-25 March.

Sutton, R.P., Cox, S.A., Lea, J.F., Rowlan, O.L. (2010). Guidelines for the Proper Application of Critical Velocity Calculations. SPE Production & Operations, **25**(2): 182-194. SPE 120625-PA

Turner, R.G., Hubbard, M.G., and Dukler, A.E. (1969). Analysis and Prediction of Minimum Flow Rate for the Continuous Removal of Liquids from Gas Wells. J. Pet. Tech., November: 1475-1482. SPE 2198-PA

Veeken, K., Hu, B., Schiferli, W. (2009). Transient Multiphase Flow Modeling of Gas Well Liquid Loading. Paper SPE 123657 presented at the 2009 Offshore Europe Oil & Gas Conference & Exhibition. Aberdeen, UK. 8-11 September.

Veeken, C.A.M. and Belfroid, S.P.C. (2011). New Perspective on Gas-Well Liquid Loading and Unloading. SPE Production and Operations, **26**(4): 343-356. SPE 134483-PA

Waltrich, P.J. (2012). Onset and Subsequent Transient Phenomena of Liquid Loading in Gas Wells: Experimental Investigation Using a Large Scale Flow Loop. PhD Dissertation, Department of Petroleum Engineering, Texas A&M University, College Station, Texas, USA.

Waltrich, P.J., Falcone, G., Barbosa Jr., J.R. (2011). Performance of Vertical Transient Two-Phase Flow Models Applied to Liquid Loading in Gas Wells. Paper SPE 147128 presented at the SPE Annual Technical Conference and Exhibition. Denver, CO, USA. 30 October – 2 November.

Wang, J.Y. (2012). Well Completion for Effective Deliquification of Natural Gas Wells. Journal of Energy Resources Tecnology. **134**(1).

Wang, Y. (2012). Investigation on the Near Wellbore Transient Flow under Liquid Loading Conditions in Gas Wells. Papierfieger Verlag GmbH, July 2012, ISBN: 978-86948-225-5. Doctoral Dissertation, Clausthal University of Technology, Germany.

Westende, J.M.C., Kemp, H.K., Belt, R.J. et al. (2007). On the Role of Droplets in Cocurrent Annular and Churn-Annular Pipe Flow. International Journal of Multiphase Flow **33** (6): 595-615.

Whitson, C.H., Rahmawati, S.D., Juell. A. (2012). Cyclic Shut-in Eliminates Liquid-Loading in Gas Wells. Paper SPE 153073 presented at the SPE/EAGE European Unconventional Resources Conference and Exhibition. Vienna, Austria. 20-22 March.

Wu, Y.S. (2000). A Virtual Node Method for Handling Wellbore Boundary Conditions in Modeling Multiphase Flow in Porous and Fractured Media. Water Resources Research, **36**(3): 807-814.

Yusuf, R., Veeken, K., Hu, B. (2010). Investigation of Gas Well Liquid Loading with a Transient Multiphase Flow Model. Paper SPE 128470 presented at the SPE Oil and Gas India Conference and Exhibition. Mumbai, India. 20-22 January.

Zhang, H., Falcone, G., Valko, P., and Teodoriu, C. (2009). Numerical Modeling of Fully-Transient Flow in the Near-Wellbore Region during Liquid Loading in Gas Wells. Paper SPE 122785 presented at the SPE Latin American and Caribbean Petroleum Engineering Conference. Cartagena, Colombia. 31 May–3 June.

Zhang, H., Falcone, G., Teodoriu, C. (2010). Modeling Fully-Transient Two-phase Flow in the Near-Wellbore Region During Liquid Loading in Gas Wells. Journal of Natural Gas Science & Engineering, **2**(2-3),. 122-131.

Zhou, D. and Yuan, H. (2009). New Model for Gas Well Loading Prediction. Paper SPE 120580 presented at the SPE Production and Operations Symposium. Oklahoma City, Oklahoma, USA. 4-8 April.

APPENDIX A

FORMULA FOR CALCULATION OF FLUID PVT PROPERTIES AND HYDRAULIC ROCK PROPERTIES IN THE RESERVOIR SIMULATION

Introduction

This appendix details the formula for calculating the fluid properties and hydraulic rock properties applied in the reservoir simulation.

Gas Properties

Gas Density

To describe thermodynamic properties of real gas, the Peng-Robinson equation of the state was used to determine gas compressibility at a given pressure and temperature condition. The derivation of the Peng- Robingson equation of state is given as:

$$P = \frac{RT}{V_m - b} - \frac{a\alpha}{V_m^2 + 2bV_m - b^2} \tag{A-1}$$

$$a = \frac{0.457235R^2T_c^2}{p_c} \tag{A-2}$$

$$b = \frac{0.077796RT_c}{p_c} \tag{A-3}$$

$$\alpha = (1 + \kappa(1 - T_r^{0.5}))^2 \tag{A-4}$$

$$\kappa = 0.37464 + 1.54226\omega - 0.26992\omega^2 \tag{A-5}$$

$$T_r = \frac{T}{T_c} \tag{A-6}$$

When it is rewritten as the form to be solved when T and p are specified and the compressibility Z can be found analytically, it is:

$$Z^3 - (1 - B)Z^2 + (A - 2B - 3B^2)Z - (AB - B^2 - B^3) = 0 \quad \text{(A-7)}$$

$$A = \frac{a\alpha p}{R^2T^2} \quad \text{(A-8)}$$

$$B = \frac{bp}{RT} \quad \text{(A-9)}$$

While Eq. A-7 is in a cubic form, the maximum real-valued root of the cubic equation gives the compressibility factor Z.

The gas density is determined from the real-gas law, given as:

$$\rho_g = \frac{pM_g}{ZRT} \quad \text{(A-9)}$$

where M_g is the molecular weight of the gas; R is the universal gas constant; and Z is the compressibility factor.

Gas Viscosity

Gas viscosity follows the correlation presented by Selim and Sloan (1989). The equation describes the gas viscosity as a function of temperature and density as expressed by:

$$\mu_g = 2.4504 \times 10^{-3} + 2.8764 \times 10^{-5}T + 3.279 \times 10^{-9}T^2 - 3.7838 \times 10^{-12}T^3 + 2.0891 \times 10^{-5}\rho_g + 2.5127 \times 10^{-7}\rho_g^2 - 5.822 \times 10^{-10}\rho_g^3 + 1.8378 \times 10^{-13}\rho_g^4 \quad \text{(A-10)}$$

where T is in K and ρ_g is in kg/m^3; μ_g is in cp.

Gas Formation Volume Factor

The gas formation volume factor is a ratio of the gas volume at reservoir conditions and at standard conditions, defined as 14.7 psia and 60°F.

Water Properties

Liquid Water Densities

The formulae to calculate the liquid water densities follow standard formulae for steam tables used by American Society of Mechanical Engineers (Myer et. all, 1979). This formulation considers the densities of liquid water in the sub-regions 1 of water in the pressure-temperature diagram for water (**Fig. A-1**).

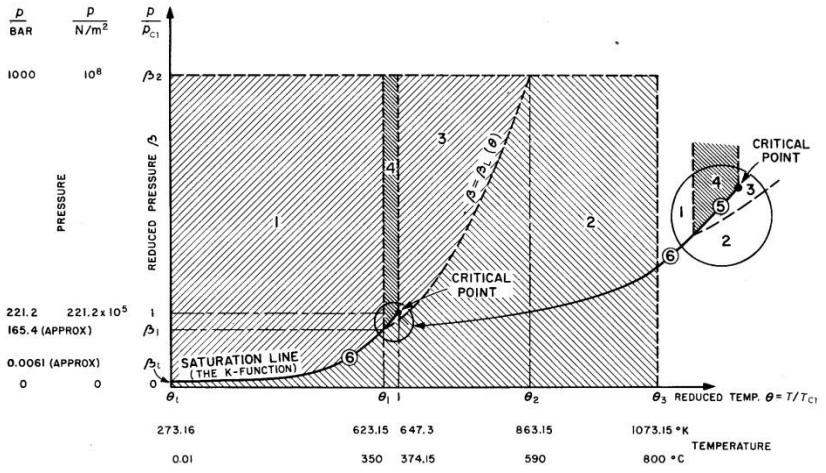

Fig. A-1 Pressure/temperature diagram for water substance

To calculate the water densities, the specific volume is first evaluated as given by:

$$\frac{v}{v_c} = \chi_1 \tag{A-1}$$

$$\chi_1 = A_{11}a_5 Z^{-\frac{5}{17}} + \{A_{12} + A_{13}\theta + A_{14}\theta^2 + A_{15}(a_6 - \theta)^{10} + A_{16}(a_7 + \theta^{19})^{-1}\} - (a_8 + \theta^{11})^{-1}(A_{17} + 2A_{18}\beta + 3A_{19}\beta^2) - A_{20}\theta^{18}(a_9 + \theta^2)\{-3(a_{10} + \beta)^{-4} + a_{11}\} + 3A_{21}(a_{12} - \theta)\beta^2 + 4A_{22}\theta^{-20}\beta^3 \quad \text{(A-2)}$$

where

$$Z = Y + (a_3 Y^2 - 2a_4\theta + 2a_5\beta)^{0.5} \quad \text{(A-3)}$$

$$Y = 1 - a_1\theta^2 - a_2\theta^{-5} \quad \text{(A-4)}$$

Then the water densities can be easily determined as:

$$\rho_w = 1/(\chi_1 * v_c) \quad \text{(A-5)}$$

β is the reduced pressure parameter given as $\beta = \frac{P}{P_c}$; θ is the reduced temperature parameter given as $\theta = \frac{T}{T_c}$; v_c is the critical volume constant = 0.00317 m^3/kg.

All constants in **Eq. A-2** to **Eq. A-4** are given as follows:

A_{11}	=	7.982692717	x	E0
A_{12}	=	-2.616571843	x	E-2
A_{13}	=	1.522411790	x	E-3
A_{14}	=	2.284279054	x	E-2
A_{15}	=	2.421647003	x	E2
A_{16}	=	1.269716088	x	E-10
A_{17}	=	2.074838328	x	E-7
A_{18}	=	2.174020350	x	E-8

A_{19} = 1.105710498 x E-9

A_{20} = 1.293441934 x E1

A_{21} = 1.308119072 x E-5

A_{22} = 6.047626338 x E-14

a_1 = 8.438375405 x E-1

a_2 = 5.362162162 x E-4

a_3 = 1.720000000 x E0

a_4 = 7.342278489 x E-2

a_5 = 4.975858870 x E-2

a_6 = 6.537154300 x E-1

a_7 = 1.150000000 x E-6

a_8 = 1.510800000 x E-5

a_9 = 1.418800000 x E-1

a_{10} = 7.002753165 x E0

a_{11} = 2.995284926 x E-4

a_{12} = 2.040000000 x E-1

Liquid Water Viscosities

We used the formula presented by Huber et al. (2009) to calculate the liquid water viscosities.

To calculate the water viscosities, first we determine the dimensionless variables given by:

$$\bar{\mu} = \bar{\mu}_0(\bar{T}) \cdot \bar{\mu}_1(\bar{T}, \bar{\rho}) \tag{A-6}$$

Where

$$\bar{\mu}_0(\bar{T}) = \frac{100\sqrt{\bar{T}}}{\sum_{i=0}^{3} \frac{H_i}{\bar{T}}} \tag{A-7}$$

$$\bar{\mu}_1(\bar{T}, \bar{\rho}) = \exp\left[\bar{\rho} \sum_{i=0}^{5} \left(\frac{1}{\bar{T}} - 1\right)^i \sum_{j=0}^{6} H_{ij} (\bar{\rho} - 1)^j\right] \tag{A-8}$$

Then the water viscosities can be determined as:

$$\mu = \bar{\mu} \cdot \mu^* \tag{A-8}$$

$\bar{T}$ is the dimensionless temperature given as $\bar{T} = \frac{T}{T^*}$; $\bar{\rho}$ is the dimensionless density given as $\bar{\rho} = \frac{\rho}{\rho^*}$.

The reference constants are: T^* = 647.096 K, ρ^* = 322.0 kg m^{-3} , μ^* = 1x10^{-6} Pas.

All constants in **Eq. A-7** and **Eq. A-8** are given below. The coefficients H_{ij}, not shown below, are identically equal to zero.

H_0	=	1.6775200	x	E0
H_1	=	2.2046200	x	E0
H_2	=	0.6366564	x	E0
H_3	=	-0.2416500	x	E0
H_{00}	=	5.20094	x	E-1
H_{10}	=	8.50895	x	E-2
H_{20}	=	-1.08374	x	E0
H_{30}	=	-2.89555	x	E-1

H_{01}	=	2.22531	x	E-1
H_{11}	=	9.99115	x	E-1
H_{21}	=	1.88797	x	E0
H_{31}	=	1.26613	x	E0
H_{51}	=	1.20573	x	E-1
H_{02}	=	-2.81378	x	E-1
H_{12}	=	-9.06851	x	E-1
H_{22}	=	-7.72479	x	E-1
H_{32}	=	-4.89837	x	E-1
H_{42}	=	-2.57040	x	E-1
H_{03}	=	1.61913	x	E-1
H_{13}	=	2.57399	x	E-1
H_{04}	=	-3.25372	x	E-2
H_{34}	=	6.98452	x	E-2
H_{45}	=	8.72102	x	E-3
H_{36}	=	-4.35673	x	E-3
H_{56}	=	-5.93264	x	E-4

Water Formation Volume Factor

The water formation volume factor is a volumetric ratio of the water at reservoir conditions to standard conditions, defined as 14.7 psia and 60°F.

Relative Permeability

The correlation for the two-phase relative permeability follows Brook and Corey's model. The relative permeability can be calculated by first determining the normalized wetting phase saturation:

$$S_w^* = \frac{(S_w - S_{wr})}{(S_{gr} - S_{wr})} \quad \text{(A-8)}$$

whereS_w is the water saturation; S_{wr} is the residual saturation of the water phase; and S_{gr} is the residual saturation of the gas phase. The following equations calculate the water and gas phase relative permeability:

$$k_{rw} = k_{rw,\text{end}}(S_w^*)^{nw} \quad \text{(A-9)}$$

$$k_{rg} = k_{rg,\text{end}}(1 - S_w^*)^{ng} \quad \text{(A-10)}$$

where $k_{rw,\text{end}}$, $k_{rg,\text{end}}$ are the water and gas phase relative permeability at endpoint, respectively; *nw* and *ng* are the water and gas phase exponents.

Capillary Pressure

We used the capillary pressure correlations from Brook and Corey. It is calculated by first evaluating the normal parameter:

$$S_w^* = \frac{(S_w - S_{wr})}{(1 - S_{wr})} \quad \text{(A-10)}$$

Then the capillary pressure is:

$$p_{\text{cap}} = p_{GE}(S_w^*)^{-\frac{1}{\lambda}} \quad \text{(A-10)}$$

where p_{GE} is the gas entry pressure; λ is the exponent.

APPENDIX B

GRAY CORRELATION

Gray (1974) developed an empirical correlation based on experimental work on 108 gas well data sets producing some liquids. The correlation considers liquid holdup, temperature gradient, and frictional flow effects to calculate the two-phase pressure drop in the well.

Gray's correlation is applicable for a vertical well with high gas fraction. No flow pattern is considered in the model. Thus, it is suitable for steady-state or pseudosteady-state flows.

To use Gray's correlation, in-situ liquid void fraction must first be evaluated as follows:

$$\lambda_l = \frac{u_{sl}}{u_m} \tag{B-1}$$

where λ_l is the in-situ liquid void fraction; u_l is the superficial liquid velocity; and u_m is the two-phase mixture velocity.

Mixture fluid density and viscosity are weighted by void fraction as:

$$\rho_m = \rho_l \lambda_l + \rho_g (1 - \lambda_l) \tag{B-2}$$

$$\mu_m = \mu_l \lambda_l + \mu_g (1 - \lambda_l) \tag{B-3}$$

where ρ_m is the in-situ mixture density; μ_m is the in-situ mixture viscosity; ρ_l and ρ_g are in-situ densities for the liquid and gas phases, respectively; and μ_l and μ_g are in-situ viscosities for the liquid and gas phases, respectively.

Three dimensionless parameters are needed to evaluate the liquid holdup parameters:

$$N_1 = \frac{\rho_m^2 u_m^4}{g\sigma(\rho_l - \rho_g)} \tag{B-4}$$

$$N_2 = \frac{gD^2(\rho_l - \rho_g)}{\sigma} \tag{B-5}$$

$$N_3 = 0.0814\left[1 - 0.0554 \ln\left(1 + \frac{730R_v}{R_v + 1}\right)\right] \tag{B-6}$$

Where

$$R_v = \frac{u_{sl}}{u_{sg}} \tag{B-7}$$

u_{sg} is the superficial gas velocity; σ is the two-phase interfacial tension; D is the tubing inside diameter ; and g is gravitational constant.

Then the liquid holdup can be evaluated as:

$$y_l = 1 - (1 - \lambda_l)(1 - \exp f_1) \tag{B-8}$$

Where

$$f_1 = -2.314\left[N_1\left(1 + \frac{205}{N_2}\right)\right]^{N_3} \tag{B-9}$$

The potential energy pressure gradient is then evaluated as:

$$\left(\frac{dp}{dZ}\right)_{PE} = \frac{g}{g_c}\left(\rho_l y_l + \rho_g(1 - y_l)\right) \tag{B-10}$$

To calculate the frictional pressure gradient, Gray's correlation uses an effective pipe roughness to account of entrained liquid along the pipe walls. The effective roughness can be evaluated as:

$$k_e = \begin{cases} k_o \; if \; R_v > 0.007 \\ k + R_v\left(\frac{k_0 - k}{0.007}\right) \; if \; R_v < 0.007 \end{cases} \tag{B-11}$$

where

$$k_o = \frac{0.285\sigma}{\rho_m u_m^2} \tag{B-12}$$

k is the absolute roughness of the pipe. The constant in Eq. B-12 is for all variables in oilfield units.

Reynold's number (in oilfield units) can be evaluated as:

$$N_{Re} = \frac{1488\rho_m u_m D}{\mu_m} \tag{B-13}$$

The relative roughness can be evaluated as:

$$\varepsilon = \frac{k_e}{D} \tag{B-14}$$

Then the friction factor can be evaluated by Chen's equation:

$$\frac{1}{\sqrt{f_f}} = -4\log\left[\frac{\varepsilon}{3.7065} - \frac{5.0454}{N_{Re}}\log\left(\frac{\varepsilon^{1.1098}}{2.8257} + \left(\frac{7.149}{N_{Re}}\right)^{0.8981}\right)\right] \tag{B-15}$$

The frictional pressure gradient can then be evaluated as:

$$\left(\frac{dp}{dZ}\right)_F = \frac{2f_f\rho_m u_m^2}{g_c D} \tag{B-16}$$

Finally, the total pressure drop in pipe can be evaluated as:

$$dp = \left(\frac{dp}{dZ}\right)_{PE} dh + \left(\frac{dp}{dZ}\right)_F dh \tag{B-17}$$

Gray's correlation was tested for well data with ranges of input parameters as follows:

- Flow velocities less than 50 ft/sec
- Tubing ID 1.049 to 2.992 in.
- Condensate ratio < 150 bbl/MMScf/D

- Water ratio , 10 bbl/MMscf/D